NUREG-0376

RESIDUAL STRESSES AT GIRTH-BUTT WELDS IN PIPES AND PRESSURE VESSELS

Final Report

April 1, 1976 - June 30, 1977

Battelle Columbus Laboratories
for
U. S. Nuclear Regulatory Commission

NUREG-0376
R5

RESIDUAL STRESSES AT GIRTH-BUTT WELDS IN PIPES AND PRESSURE VESSELS

Final Report
April 1, 1976 - June 30, 1977

E. F. Rybicki
J. J. Groom
M. M. Lemcoe
H. W. Mishler
E. C. Rodabaugh
D. W. Schmuester
R. B. Stonesifer
J. S. Strenkowski

Manuscript Completed: August 1977
Date Published: November 1977

Battelle Columbus Laboratories
505 King Avenue
Columbus, OH 43201

Prepared for
Division of Reactor Safety Research
Office of Nuclear Regulatory Research
U. S. Nuclear Regulatory Commission
Under Contract No. AT(49-24)-0293

TABLE OF CONTENTS

TABLE OF CONTENTS
(Continued)

TABLE OF CONTENTS
(Continued)

LIST OF TABLES

LIST OF FIGURES
(Continued)

LIST OF FIGURES
(Continued)

LIST OF FIGURES
(Continued)

LIST OF FIGURES
(Continued)

Page

I. INTRODUCTION

This section provides an introduction to the report contents. It begins with a statement of the objectives and an overall summary of accomplishments. This is followed by a brief description of each task and the interaction between tasks. Sections following the Introduction are devoted to the technical details of each task.

Objectives and Summary of Accomplishments

The objective of this research program is to develop mathematical model for calculating the magnitude, direction, and distribution of residual stresses at girth-butt welds. Models developed are to include parameters of the welding process and are to be evaluated by comparing experimental data with numerical computations obtained using the models. Only axisymmetric models are to be considered in this study.

In summary, a residual stress model for girth-butt welds in pressure vessels and pipes was developed and verified for welds ranging from 2 to 30 passes. The model also accurately predicts residual deformations. Results indicate that the model can be extended to represent weld repairs in pressure vessels. In addition, preliminary results directed at developing a simplified model of gir butt welds show good agreement with data for one and two-pass welds. Specif accomplishments toward the objectives are listed in the following:

- A critical review of the literature was made to evaluate analytical techniques for developing the model and identify residual stress data to be used in verifying the models.
- Experimental studies of two girth-butt welded pipes were conducted to provide temperature data and residual stress data for verifying the models. Data obtained from these experiments include residual stresses, temperatures during welding, strains during welding, and residual deflections of the welded pipe.
- Two experiments on girth-butt welded pipes were identified from the literature as test cases for the model.

- A description of the pipes for which data was obtained from the experimental study and through the literature is given in the following. All pipes are 304 stainless steel.

Pipe Identification	Outside Pipe Diameter (in.)	Pipe Wall Thickness (in.)	Number of Weld Passes
BCL Model No. 2	12.75	.180	2
BCL Model No. 3	12.75	.375	6
Argonne Pipe	4.50	.337	7
General Electric Pipe	28.00	1.300	30

- A model for predicting residual stresses in girth-butt welds of pressure vessels and pipes was developed. The model consists of two parts; a temperature model and a stress analysis model.
- The temperature model was developed through modification of a model described in the literature review. Good comparisons between temperature data and computations by the model were obtained for each pass of the two-pass and six-pass welds. The temperature model includes heat input, pipe thickness, location of weld pass, thermal properties of the pipe, torch speed, efficiency of the weld process, and time dependent effects.
- A finite element model for girth-butt welds was developed. The model includes temperature dependent material properties, elastic-plastic stress strain effects, the effects of changing geometry of the pipe as it is welded, and linear elastic unloading from an elastic-plastic state of stress. The weld geometry and number of weld passes are also represented by the model.
- Results of the residual stress model showed good agreement with residual stress data in the hoop and axial directions on the insides and outsides of the four pipes described above.

- Preliminary results were obtained using the residual stress model to represent a weld repair of the HSST Intermediate Vessel V-8. While the model needs further development before it can adequately represent the weld repair geometry, qualitative agreement between residual stress data and results of the model were obtained.
- The possibility of using a simplified model that is not based on a finite element representation was explored. Results showed good agreement for a one-pass girth-butt weld and the two-pass weld done in this study. While further development of this model is needed before it can handle more passes, results are encouraging that it can be an efficient useful model.
- Thus, an analytical model for predicting residual stresses in girth-butt welds has been developed and verified by comparison with experimentally obtained data for four pipes. It was demonstrated that with further development, the model can be applicable to other weld configurations such as weld repair of pressure vessels. Early developmental efforts on a simplified residual stress analysis model demonstrate the feasibility of obtaining an efficient useful simplified model.

Description of the Research Program

The program is divided into three tasks. Task 1 addresses current literature and available reports to obtain data and analytical techniques pertinent to residual stresses in girth-butt welds. Task 2 involves experimental determination of residual stresses from a series of girth-butt weld tests selected to provide maximum guidance for the development of the analytical models. Task 3 is the development of the analytical method or methods for calculation of residual stresses.

The purpose of Task 1, described in Section II, is to identify and critically review reports and papers concerned with mathematical models for predicting residual stresses, for evaluating residual stresses due to girth-butt welds, characterization of the temperature profiles associated with welding, analytical representations for these temperature profiles, and mathematical

models for predicting residual stresses. As a result of this task, an analytical model for predicting temperature distributions was selected and specific requirements for a finite element model of a girth-butt weld were identified. Residual stress data for two girth-butt welded pipes were also obtained and used in the verification of the model.

Task 2, described in Section III, involves experimental evaluations of residual stresses for girth-butt welds to provide guidance for the development of the analytical models. Two pipes with 12.75-inch outside diameters were welded. One pipe, BCL Model Number 2, has a wall thickness of .18 inch and required two weld passes. The other pipe, BCL Model No. 3, has a wall thickness of .375 inch and required six weld passes. Temperature data from both pipes and strains from one pipe, BCL Model Number 2, were measured during the experiment. Residual stresses and radial deflections for both pipes were determined from postweld measurements.

Task 3 is the development of analytical methods for predicting residual stresses. Two distinct mathematical models were needed. First, since residual stresses at butt welds are thermally induced, a model to represent the transient temperature distribution for each weld pass is needed. This is described in Section IV. Secondly, a stress analysis model that treats the temperature distributions as input and predicts stresses as a function of weld pass geometry, material properties, and the geometry of the pipe is needed. Temperature data obtained from BCL Model Numbers 2 and 3 have correlated well with the transient temperatures predicted by the mathematical temperature model. Section V contains a description of the mathematical stress analysis model that has been developed based on a finite element representation. A comparison of predicted results and the laboratory data for four pipes showed good agreement. Preliminary results obtained by applying the residual stress model to a weld repair of a pressure vessel are also presented in Section V. In Section VI, a simplified model is described and applications are made to one- and two-pass girth-butt welds.

Much of the discussion concerning the model and the results is included in sections where it is appropriate. The final section, Section VII, presents a technical summary with a discussion of points not included in other sections.

II. RELATED WORK

This section contains a review of available data and techniques pertinent to the determination of temperature distributions and residual stresses in girth-butt welds. Over 40 papers have been critically reviewed on the topics of analytical models and experimetal methods. Various analytical models have been utilized to predict temperature distributions, residual stresses, and distortions due to welding. Similarly, there are distinct experimental techniques for evaluating residual stresses. The review is not intended to be an exhaustive study, but rather to identify and describe analytical and experimental techniques that are representative of the activity in this area.

Analytical Modeling

Over the years, attempts have been made to establish empirical methods of investigating material behavior due to welding procedures. However, comparatively less effort has been directed toward the development of analytical models which predict the thermal mechanical response of welded structures. Much of the modeling has been focused on plates rather than pipes. For this reason, it was considered useful to examine work on butt-welds in plates as well as pipes and pressure vessels. Models for residual stresses due to welding must consist of two types: a temperature model and a stress analysis model. The temperature model provides a representation of the temperature distribution due to the weld torch. This information is then input to the stress analysis model which predicts the residual stress distributions. Two survey papers summarizing analysis methods have been published on temperature distributions due to welding[1] and welding stresses and distortions[2].

Temperature Models

Analytical formulations for temperature distributions during welding are frequently obtained by assuming that the thermal energy supplied by the weld process can be idealized as a point or line heat source. Early work done in this area focused on quasi-stationary, transient temperature distributions resulting from a point heat source traveling at a constant speed along a line on an infinitely

thick plate. Rosenthal[3] presented one of the early analytical treatments of this point source model in 1941.

Several researchers have used classical line heat source solutions to analyze different aspects of weld temperature distributions. Adams[4] has developed expressions for weld centerline cooling rates based on the line heat source solution, while Jhaveri, Moffet, and Adams[5] have used the moving point heat source solution to model the effects of plate thickness on cooling rates. Paley, Lynch, and Adams[6] have correlated peak temperatures calculated from the point heat source model with characteristic etching boundaries in HY-80 and T-1 steels. They found good correlations that were independent of cooling and heating rates over a range of conditions encountered in submerged-arc welding. In another approach, Paley and Hibbert[7] developed a computer program which solves the Laplace heat equation for heat flow by a finite difference scheme. The analysis assumes quasi-stationary thermal conditions and treated finite thickness plates. In concept, the method could also treat finite sized plates.

Several researchers have investigated temperature distributions during welding through experimental methods and analysis techniques not based on the classical point heat source equation. Rabkin[8] measured the temperature in aluminum weld pools by using chromel-alumel immersion thermocouples. He used these measurements to study the effects of welding speed, arc voltage, and parent metal temperature on the temperature distribution in the weld pool. Makhnenko[9] developed an analytical method for calculating the temperatures in hollow cylinders which were water-cooled from within and heated by depositing metal on their outer surface. Christensen, Davies, and Gjermundsen[10] made an extensive experimental examination of the temperature distribution in and outside the weld pool for single bead welds on thick sections of mild steel and aluminum. They also established average arc efficiencies for metal-arc, gas-metal arc, and submerged-arc processes. Pavelic[11] developed an analytical solution for calculating peak temperatures in gas tungsten-arc welding of thin plates. His solution procedure correlated the shape of the weld pool to welding variables and used the result as a boundary condition to the partial differential equation for heat conduction. Boughton[12] took a different approach to modeling quasi-stable heat flow situations in fusion welding by using an analog computer

Residual Stress Analysis Models

The classical line source solution to the heat equation was used by Tall[13] to develop an analytical model that calculates stresses parallel to the weld line direction. Tall's model is similar to an earlier model developed by Rodgers and Fletcher[14] in that it accounts for plastic deformations near the weld line. However, it differs from the Rodgers and Fletcher model in that it was applied to isotherms set up by a moving electrode. Masubuchi, Simmons, and Monroe[15] used Tall's analysis model to write a computer code to calculate temperatures and stresses in welded plates.

Although Gatovskii[16] has considered the effect of metal transformations during welding, and Makhnenko, Shekera, and Izbenko[17] have developed an analysis procedure that calculates linear deformations due to circumferential welding in thin cylindrical shells, little analytical work has been carried out that goes significantly beyond Tall's analytical model. The complexities inherent in performing analytical studies of welding stresses and distortions for various weld configurations--in particular, the complex effects of inelastic material response and material loading and unloading--suggest the use of numerical methods to evaluate residual stresses and distortions. The finite element method is one method which has been applied to problems of nonlinear, inelastic behavior of welded structures.

Fundamental aspects of the finite element method are discussed in a book by Hueber[18], and in a paper by Marcal[19]. Armen, Levine, and Pifko[20] present the development of various incremental solution procedures used in finite element solutions for plastic structural deformations. Thermal, nonlinear finite analysis of structures is discussed in a paper by Veda and Yamakawa[21].

One of the first applications of the finite element method to transient heat conduction in solids was presented by Wilson and Nickel[22]. Sagalevich and Mezentsevn[23] developed a method for calculating residual stresses and strains during welding of circular tubes. Their method recognized each weld pass as it was laid down. Kamichika, Yada, and Okamoto[24] applied the finite element method to determine residual stresses in low-alloy carbon steel plates for a case where a wide band of austenitic stainless steel was laid on top of the plate.

A report by Hibbitt and Marcal[25], which presents a thermomechanical model for the welding and loading of arbitrary fabricated structures, represents a first step in the development of numerical analysis techniques that simultaneously

account for many welding parameters. The model simulates gas-metal arc-welding process, and accounts for temperature dependent material properties, phase changes, and deposition of filler material, among others. A paper by Nickell and Hibbitt[26] presents thermal and mechanical analysis procedures for welded structures which take into account latent heat effects and weld metal deposition. Their paper also discusses methods for coping with possible floating solid regions during cooling. Friedman[27] developes finite element analysis procedures for calculating temperatures, stresses, and distortions in longitudinal butt welds. The analysis procedures presented by Friedman are applicable to planar or asix-symmetric welds under quasi-stationary conditions. Residual stresses obtained from his analysis were greater in the weld metal and heat-affected zones. Vaidyanathan, Todar, and Finnie[28] describe a model for single pass welds of pipes. The model uses a point heat source for the temperature analysis. The pipe solution is obtained by an energy formulation using a plate solution as the assumed deformation mode. Good correlation between predictions and data was obtained.

Iwamura and Rybicki[29] developed a mathematical model for calculating residual stresses and deformations due to a flame-forming process applied to a flat plate. This model predicts residual stresses through the plate thickness. The model consists of a simple finite element representation for deformations but contains constitutive relations that include material unloading and temperature-dependent properties. Rybicki, Ghadiali, and Schmueser [30] developed a mathematical model to predict deformations resulting from butt-welding of flat plates. The effect of changing the position of the base metal after each pass is included in the finite element model by relocating the finite element grid after each pass to include the distortions due to each weld pass. The results of this model show good agreement with experimentally obtained data.

Experimental Stress Analysis

Methods for measuring residual stresses due to welding can be classified into two main categories--methods which are destructive, such as the Sachs "boring out" method, and methods which are nondestructive, such as X-ray diffraction and ultrasonic methods. The following reviews various methods from each of these categories.

Experimental Methods

Descriptions of developments in nondestructive residual stress techniques through 1974 are summarized in the proceedings of a workshop[31] on nondestructive evaluation of residual stress. The proceedings of the workshop discuss x-ray diffraction, ultrasonic, and electromagnetic methods for measurement of residual stresses. K. Masubuchi authored a chapter of the proceedings on combining experimental strain gage measurements with analysis techniques to determine residual stresses in complex welded structures.

One of the early experimental techniques is the "boring-out method" developed by Sachs[32]. Later it was extended to the boring-out turning-off method[33]. These are methods of destructive testing which are used to determine the complete residual stress patterns in welded pipe. Weiss[34] developed equations for the determination of residual stresses in solid and hollow cylinders that are similar to the ones derived by Sachs.

A modification of the Sachs method was developed by Ceopolina and Cunonico[35]. This technique allows the determination of residual stress patterns over extremely short distances. In its most elementary form, the technique consists of removing portions of an experimental sample by machining, thereby releasing the residual stresses.

Experimental Data

Several papers in the literature present data from experimental investigations of residual stresses produced by welding plates and pipes. Nagaraja and Tall[36] describe stress patterns which result from multipass center and edge welding of ASTM A7 steel plates. The plates vary in thickness from 1/4 to 1 inch and in width from 4 to 20 inches. The test results show no great variation in residual stresses between successive passes, while the first pass caused the majority of the residual stress. Prokhorov[37] presents test results which illustrate the influence of the initial structure of hardenable steels on the magnitude and distribution of residual stresses in butt-welded pates. The results show that annealing of type 40Kh GSA steel at 650-720 C before welding alters the residual stress pattern significantly. Muraki, Bryan, and Masubuchi[38] conducted experiments on bead-on-plate and butt welds in 6061-T6 alloy plates, 1/4 of an inch thick. The butt-welded plates showed small strain changes through the plate thickness, while the bead-on-plate welds showed considerable differences in strain between the top and bottom plate surfaces.

Physical and geometrical aspects of TIG welding of aluminum pipe are presented in a paper by Spiller[39]. The paper reviews variable welding factors such as welding current amplitude, rate of travel, arc length, filler rod feeding techniques, gas flow rates, and torch angles. Welding characteristics of aluminum pipe, such as heat conductivity, preweld cleaning, and surface oxide buildup, are also presented in the paper.

The distribution of residual stresses in pipes welded with pulsating arcs is presented in a paper by Vagner[40]. Comparative investigations of welded butt-joints in pipes were made for continuous and pulsating arcs. The authors employ the method of x-radiography to determine the residual stress patterns. The results of the experiments show that the residual stresses in the pipe are lower with the pulsating arc than with the continuous arc.

General Electric has conducted numerous tests [41] which measure temperatures and residual stresses in Type 304 stainless steel pipe. The tests were conducted on 4-, 10-, and 26-inch-diameter pipe. During the welding tests, two temperature recorders monitored the inside and outside surface temperatures on the pipe. Residual stresses were determined by a stress relief technique. The technique consists of bonding strain gages to the pipe surface and sectioning the small element of material to which the gage is attached until it is stress free.

The General Electric experiments found that maximum temperatures on the pipe surfaces are experienced during the first few weld passes and that the maximum temperatures decrease with increasing pipe size. The welded pipes had both longitudinal and circumferential variance in tensile residual stresses on the pipe inside surface near the welds. The maximum tensile residual stress measured in the base material on the inside of the 26-inch diameter pipe was less than that for the 10-inch pipe, which in turn was less than that for the 4-inch pipe.

In summary, the critical review of the literature points out results and several techniques for predicting temperature distributions and residual stresses. As a result of this study, specific models for predicting temperature distributions and residual stresses in welded plates have been identified and are described in the section on mathematical models. Techniques for evaluating residual stress from laboratory tests similar to those found in the literature are described in the section on laboratory tests. In addition to identifying studies that have been completed, this review also identified researchers currently working on determining residual stresses due to welding.

III. LABORATORY TESTS FOR GIRTH-BUTT WELDS

The purpose of the laboratory tests is to provide data on temperature and residual stress distributions during welding. Welding conditions in pipes were selected to provide check cases for the mathematical models as well as data for different pipe thickness and heat inputs.

Two weld joints described in Table 1 were completed. These are denoted by BCL Model No. 2 and BCL Model No. 3. The following describes the experimental details and results for the two-pass girth-butt weld (BCL Model No. 2) and the six-pass girth-butt weld (BCL Model No. 3)

Experimental Details and Results for Two-Pass Girth-Butt Weld

Material

An 18-inch piece of 12-3/4-inch OD by 0.180-inch wall welded-seam 304 stainless steel pipe was cut in half and the cut edges were prepared for welding as illustrated in Figure 1. The Mill Test Report on the pipe material is contained in Table 2.

Weld Set-Up and Procedure

The weld on BCL Model No. 2 required two passes. The joint preparation is shown in Figure 2. A 5/32-inch Type 308L EB* insert ring was used to ensure that the root pass would have complete fusion and an underbead contour similar to a contour that would be obtained in a commercial weld. The insert ring was tack welded to one of the pipes at 14 locations approximately 2-7/8 inches apart. The two pieces of pipe then were mounted on the spider frame in a manner to maintain the joint alignment. The overall welding configuration is shown in Figure 3. The spider frame was attached to a rotary drive mechanism. The axis of the pipe was horizontal with the pipe being rotated under stationary welding heads. The welding heads were located so that welding was taking place at the 12:00 o'clock position.

---

* Name of insert marketed by Arcos Corporation of Philadelphia, Pennsylvania.

TABLE 1. COMPLETED TEST MODELS AND PARAMETERS

BCL Model No.	Outside Diameter, in.	Wall Thickness, in.	Material	Wall Thickness Variation	Passes	Welding Heat Input	Interpass Temperature
2	12.75	0.180	304	Straight Pipe	2	Medium	Room
3	12.75	0.375	304	Straight Pipe	6	Medium	Room

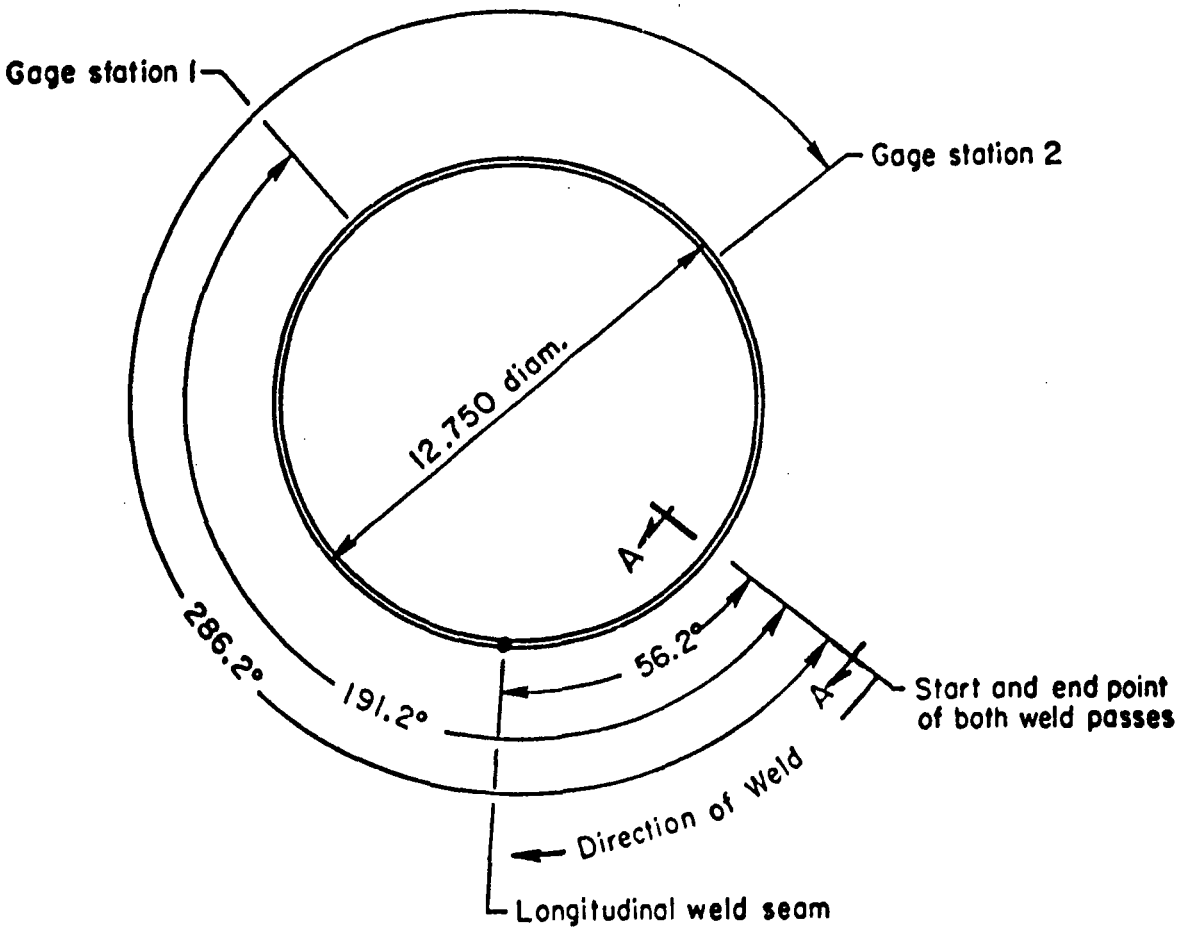

Note: All thermocouples are 28 gage chromel-alumel.
All dimensions are in inches.

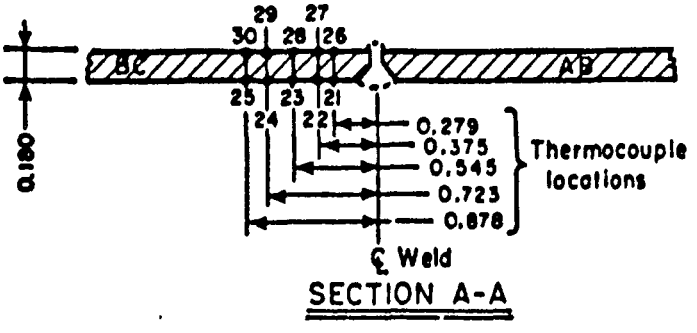

FIGURE 1. THERMOCOUPLE LOCATIONS FOR TWO-PASS WELD

TABLE 2. MILL TEST REPORT DATA FOR TYPE 304 PIPE USED IN BCL MODEL NO. 2

Size	Chemical Analysis										Yield Point Lbs. per sq. Inch	Tensile Strength Lbs. per sq. Inch	% Elong. in 2 Inches	Hard-ness
	C.	Mn.	P.	S.	Si.	Ni.	Cr.	Mo.	Co.	Cu.				
12" Sch 10s	.050	1.76	.027	.023	.59	9.03	18.03	.36	.17	.17	41900	82000	60.	B-81

Welded, annealed, and pickled; ASTM A-312, ASME SA-312
MIL-P-1144C
Hydrostatic tested at 425 psi; acidified copper sulphate test ok.

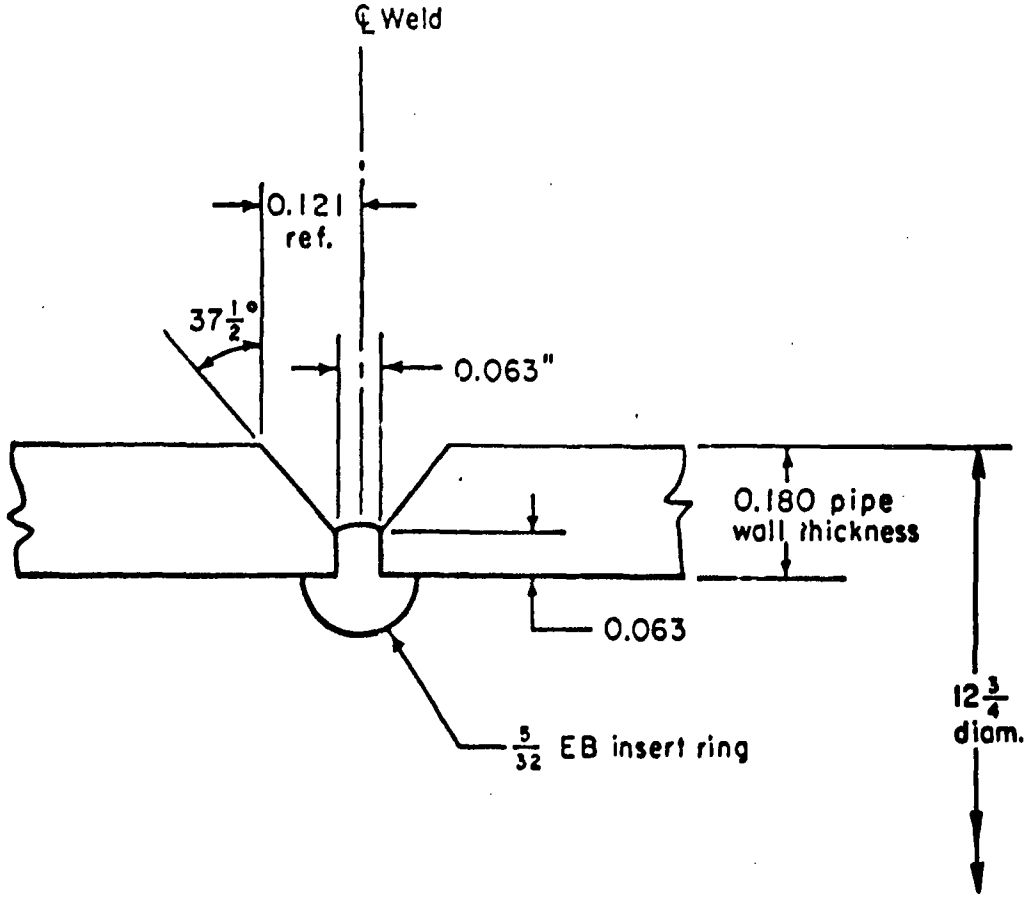

FIGURE 2. WELD JOINT GEOMETRY FOR BCL MODEL NO. 2

FIGURE 3. GENERAL ARRANGEMENT OF BCL MODEL NO. 2 IN WELDING FIXTURE

The root pass was made by gas tungsten arc (GTA) welding with the second pass being made by gas metal arc (GMA) welding.* No filler metal was added to the root pass. The necessary filler metal was provided by the EB insert. Prior to welding, the open ends of the pipe assembly were sealed and the interior of the assembly was purged with helium to prevent oxidation of the underside of the weld joint. The seals consisted of heavy wrapping paper attached to the pipe ends with masking tape. A slight flow of helium was maintained during the entire welding operation to prevent oxygen from entering the system. The shielding gas, which flowed through the welding torch, was helium for GTA welding and argon with 2 percent oxygen for the GMA welding. Welding conditions for BCL Model No. 2 are given in Table 3.

Both passes started at the same point, 6.25 inches before the longitudinal pipe seam, and proceeded in the same direction. An elapsed time of 30 minutes and 35 seconds occurred between the completion of the root pass and the start of the second pass. This time was necessary to make instrumentation changes, to remove the GTA torch from the mechanism, and to install and align the GMA torch.

Cross Sections of the Weld

A photomacrograph of an etched cross section of the two-pass girth-butt weld from BCL Model 2 is shown in Figure 4. The figure includes a schematic drawing of the section identifying various features of the weld. The pass subsequent to the root pass has a tear-drop shape at the root of the pass. In contrast, the root of a weld made by the manual shielded-metal arc process using covered electrode would be shallower and have a uniformly curved shape without the tear-drop extension.

At the location where the section shown in Figure 4 was taken, the insert ring had lifted from the inside surface of the joint. This lifting may have been caused by the shrinkage of a tack weld. For this reason, the insert ring was not completely fused at this location. Complete fusion of the insert ring would have resulted in a flatter root reinforcement that would have blended more smoothly into the inside circumference of the weld. This occurrence should have little effect on the magnitude of the residual stresses that were created in the weld joint since this material does not connect the weld bead to the base metal.

---

* These processes are also known as tungsten inert gas (TIG) welding and metal inert gas (MIG) welding.

TABLE 3. WELD CONDITIONS FOR BCL MODEL NO. 2

	First Pass GTA	Second Pass GMA
Travel speed, (ipm)	3	20
Welding current, (amps)	112-115	220
Arc voltage, (volts)	8-9	22
Polarity	Straight	Reverse
Contact tube-to-work distance, (inch)	Not Applicable	0.5
Electrode type	Thoriated Tungsten	Type 308 L
Electrode diameter, (inch)	.0625	0.045
Shielding gas	Helium	Argon + 2% oxygen
Shielding gas flow, (cfh)	15	40
Time for each pass, (min:sec)	10:41	1:55

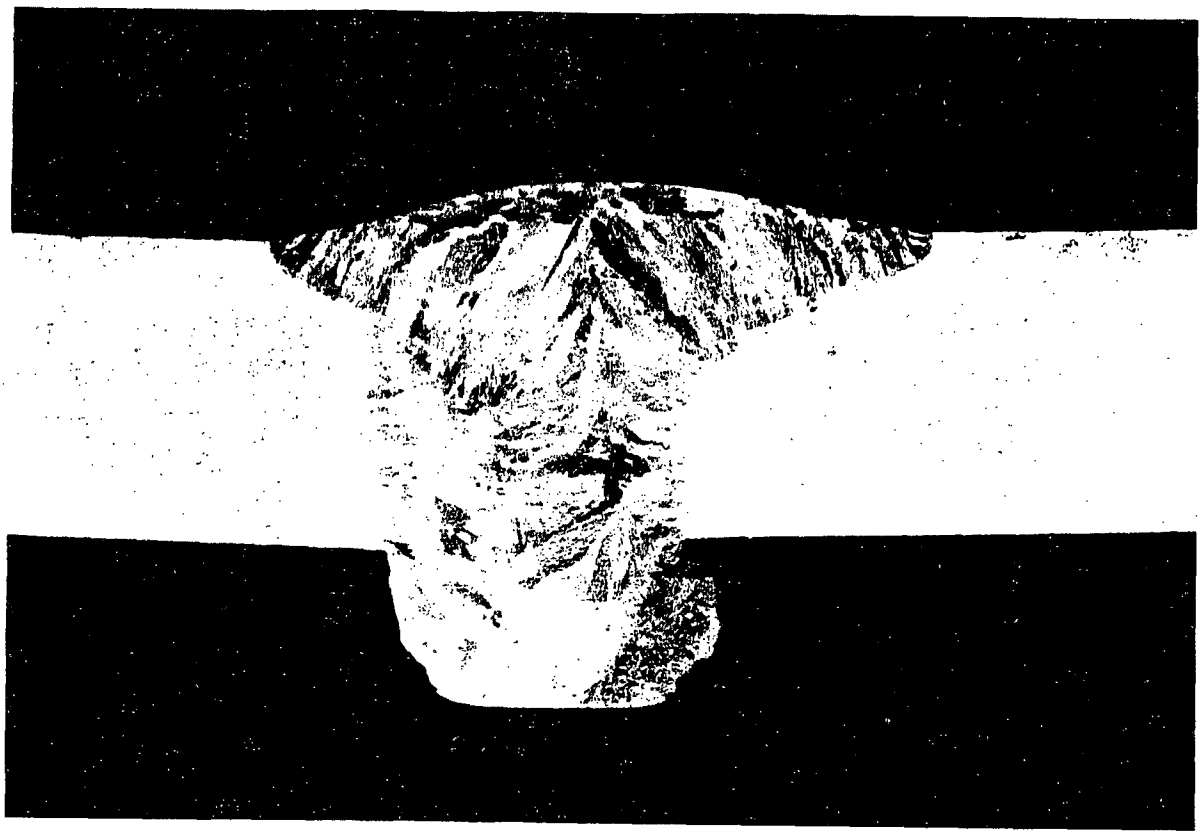

Photograph 10X Etchant: 97 HCl, 3HNO_3, 1/2 gm $CuCl_2$ 0.1769

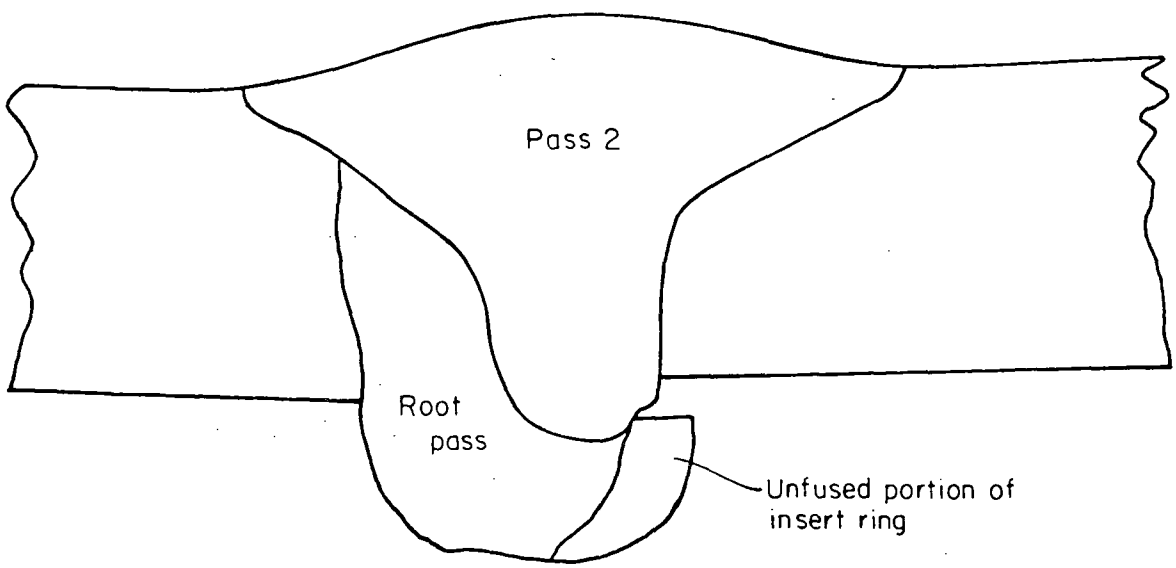

FIGURE 4. SECTION OF WELD MADE IN 12.75-INCH OD BY 0.180-INCH WALL STAINLESS PIPE (BCL MODEL NO. 2)

Temperature Measurements

A total of 20 thermocouples were spot welded to the pipe at various locations on BCL Model 2. Ten of these thermocouples were used to obtain dynamic temperature distribution recordings. These were located relative to the two high-temperature strain gage stations as shown in Figures 5 and 6. The remaining ten thermocouples were located along a longitudinal line on the inside and outside surfaces of the pipe near the starting position for welding. These latter ten thermocouples were recorded on a point thermocouple recorder and were used to obtain temperature distributions between and, to some extent, during weld passes.

Portions of the dynamic record of temperature versus time in the vicinity of the two high-temperature strain gage locations are shown in Figures 7 through 10. The temperature curves shown in these figures were obtained from the thermocouple data, but have been interpreted in a form that could be used to reduce the data from the high-temperature stain gages. For example, the thermocouples at Strain Gage Station I are distributed at varying circumferential distances off the longitudinal centerline of Strain Gage No. 12. In order to get a picture of the longitudinal distribution of temperatures at any instant in a time frame relative to Strain Gage No. 12, the actual recorded temperature data were shifted on their time axis to make them appear as if they were located on the longitudinal centerline of Strain Gage No. 12. The amount of each time shift is determined by the individual thermocouple's circumferential distance from the strain gage's centerline divided by the circumferential speed of the weld pass. Thermocouples that would see the effects of the weld torch sooner than Strain Gage No. 12 had a time increment added to their time scale. Thermocouples seeing effects of the weld torch later than the strain gage had a time increment deducted from their time scale. This latter procedure was also used to shift the strain readings from the axial gage in each strain gage pair. This was done in order to make the axial readings appear to have been taken in the same location frame as the circumferential gage.

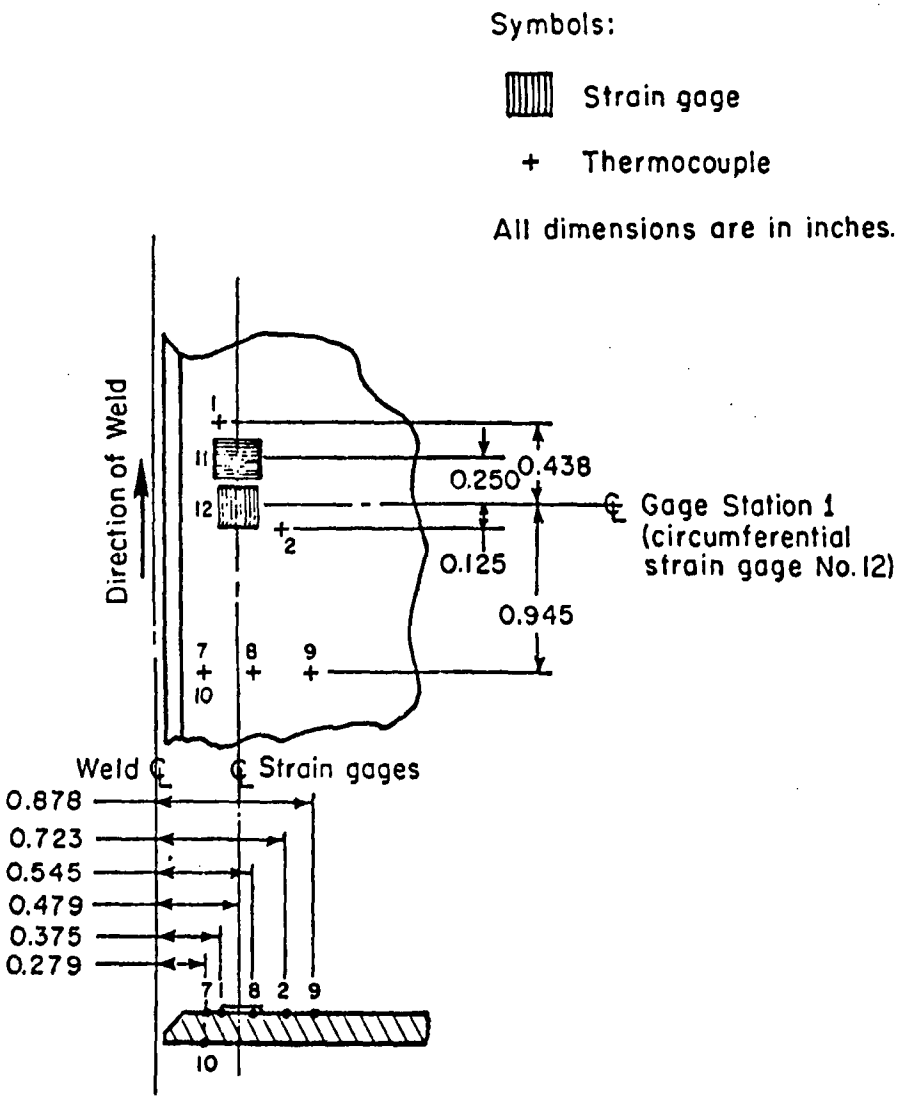

FIGURE 5. GAGE STATION 1 LAYOUT, BCL MODEL NO. 2

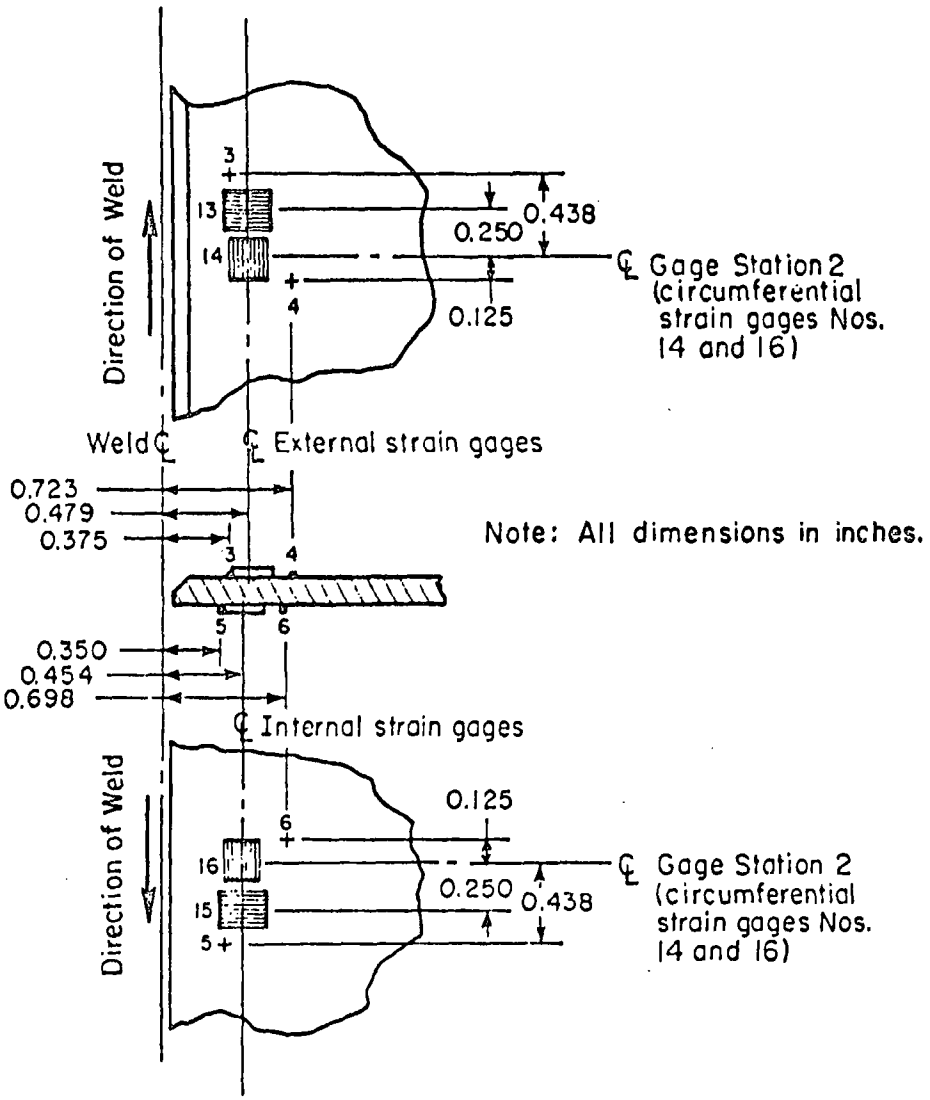

FIGURE 6. GAGE STATION 2 LAYOUT, BCL MODEL NO. 2

Strain Measurements During the Experiment

Three biaxial high-temperature electric-resistance strain gages were installed on BCL Model No. 2. The output of these gages and associated thermocouples were recorded on a multichannel oscillograph. Figures 5 and 6 show locations of the gages and thermocouples.

Figures 7 through 10 are plots of strain and temperature versus time as obtained for each weld pass. Rosette locations are 191 degrees and 286 degrees from the weld starting point. As expected, strains and temperatures increase rapidly as the weld torch passes the sensors and decay slowly thereafter.

Table 4 summarizes peak strains and associated temperatures, and peak temperatures and associated strains, for each weld pass. The strains have been corrected for temperature effects on the gage. Time zero represents the initiation of the first weld pass. Data are not shown for Gage No. 12 for the second weld pass since it failed during this time interval.

It is noted that the strains in Table 4 range in value from 10,785 με to 21,686 με. It is also noted that the strain levels for both passes are of the same general magnitude. Examination of the data shows no apparent trend between the time to reach peak strain and the time to reach peak temperature. In five instances, the maximum strain was reached after the peak temperature. In four instances, the maximum strain was reached shortly before reaching peak temperature, and in two instances, peak strains and temperatures were reached at the same time.

Upon reaching room temperature after the second weld pass, Gages 15 and 16 were found to be still operational. These gages were on the inside of the pipe and not subject to the intense radiant heat and thermal gradients seen by the outside gages. The final strains on these two gages were -2,869 με longitudinal and 685 με circumferential. It is noted that the strains obtained by the high-temperature gages are the result of the accumulated elastic and plastic deformations. The strains obtained by the chip removal technique reflect the locked-in residual stress state and are residual elastic strains. Hence, these values are not directly comparable.

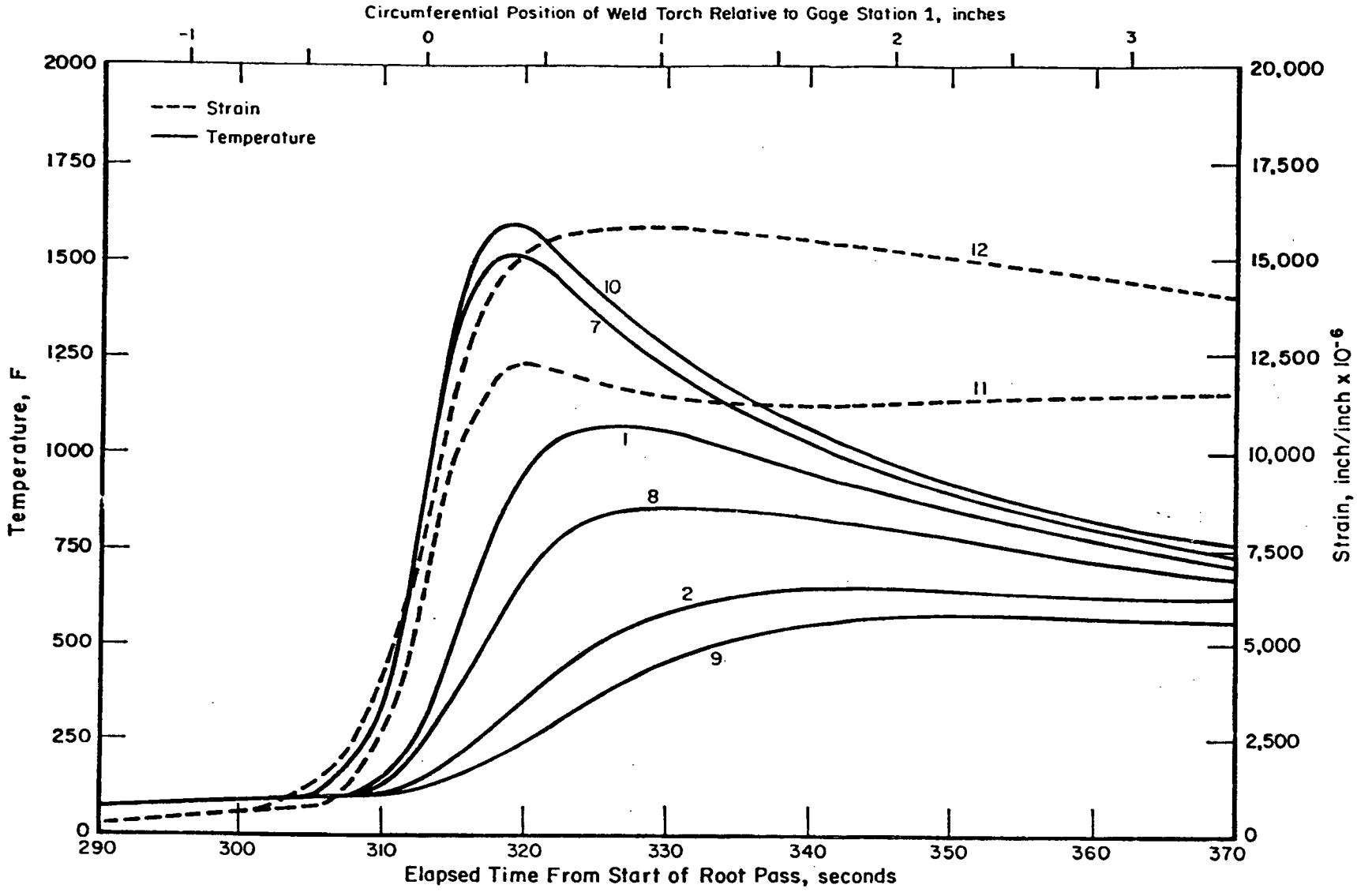

FIGURE 7. WELDING ROOT PASS GAGE STATION 1, BCL MODEL NO. 2

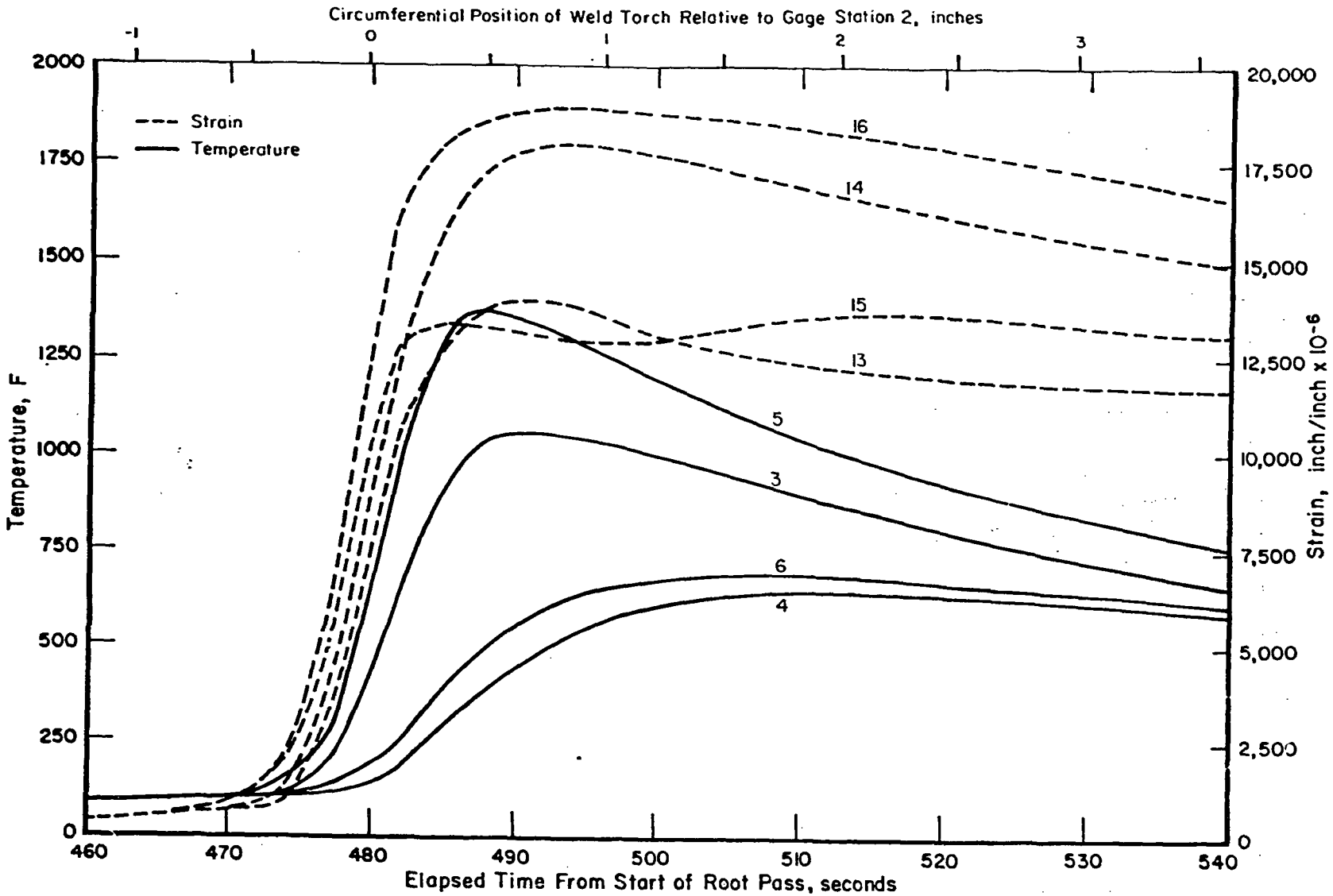

FIGURE 8. WELDING ROOT PASS GAGE STATION 2, BCL MODEL NO. 2

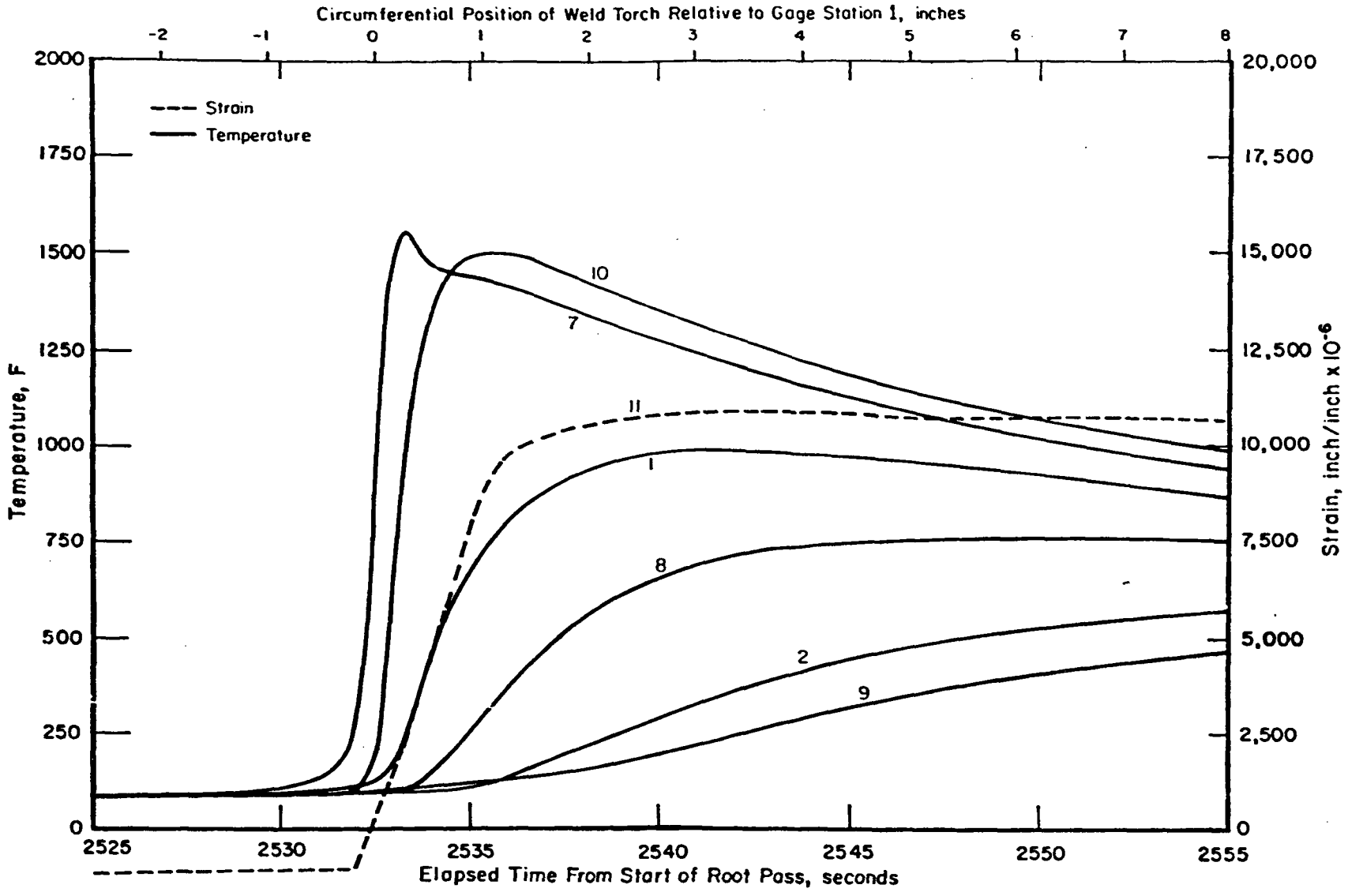

FIGURE 9. SECOND WELD PASS GAGE STATION 1, BCL MODEL NO. 2

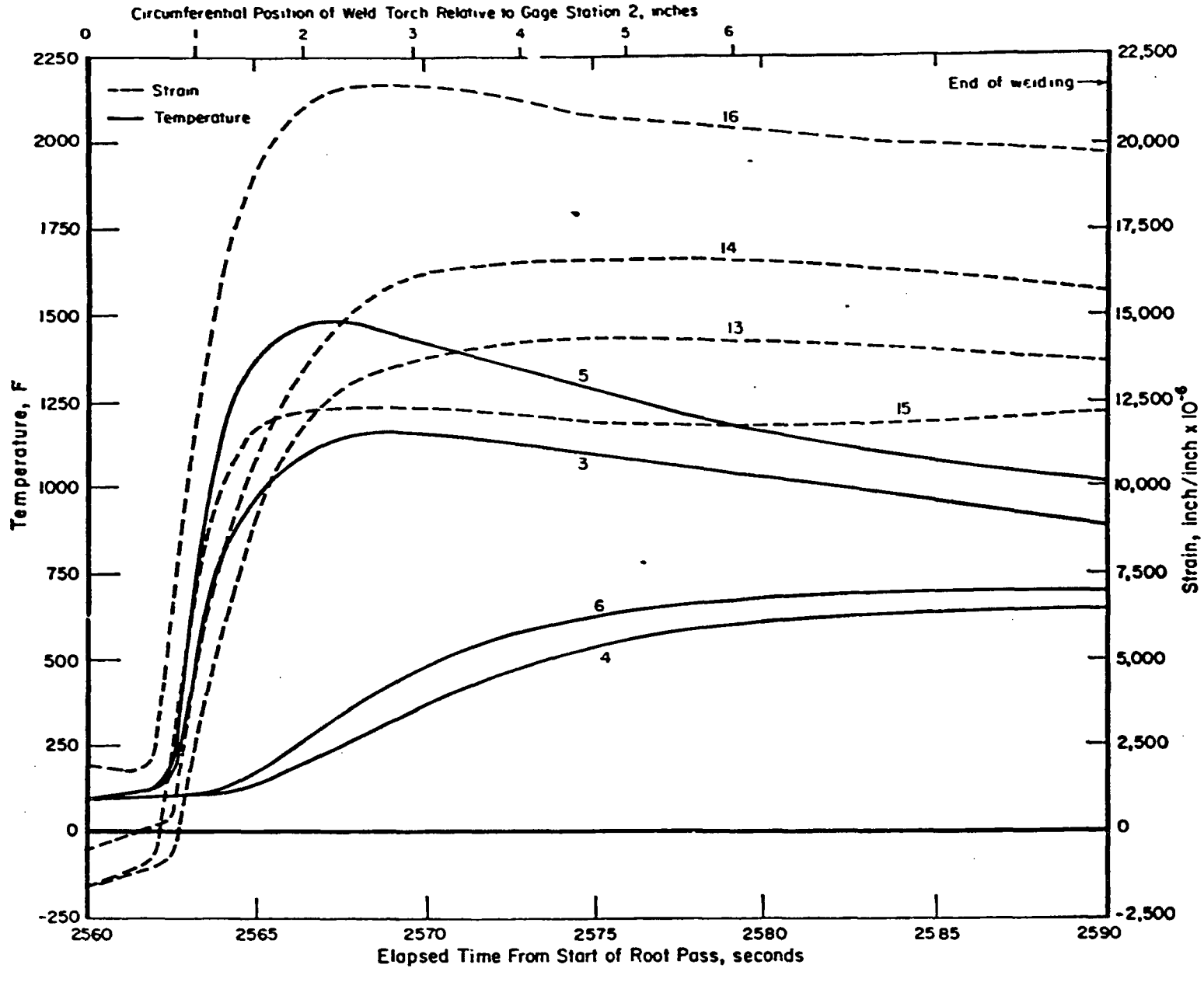

FIGURE 10. SECOND WELD PASS GAGE STATION 2

TABLE 4. SUMMARY OF PEAK STRAINS AND TEMPERATURES FOR BCL MODEL NO. 2

Event	Time, sec.	Gage No.	Max. Strain,	Temp, F	Max. Temp., F	Strain, με
First Weld Pass	318	11	11,971	650		
	327	11	--	--	945	11,590
	323	12	15,681	890		
	327	12	--	--	945	15,761
	438	13	13,360	835		
	495	13	--	--	900	13,294
	495	14	17,819	900		
	495	14	--	--	900	17,819
	520	15	13,550	855		
	490	15	--	--	1125	13,136
	515	16	18,214	895		
	490	16	--	--	1125	18,777
Second Weld Pass	2540	11	10,785	810		
	2542	11	--	--	945	10,804
	2580	13	14,303	900		
	2573	13	--	--	945	14,295
	2582	14	16,481	885		
	2573	14	--	--	945	16,492
	2590	15	12,217	925		
	2570	15	--	--	1150	12,378
	2570	16	21,686	1150		
	2570	16	--	--	1150	21,686

Residual Stress Measurements on BCL Model No. 2

A total of ten biaxial postweld strain gages were attached to BCL Model No. 2 girth-butt weld. Subsequently, the gages were trepanned out to obtain the change in strain gage readings. Residual stresses were then inferred from these measurements. The procedure is described as follows. Small biaxial strain gages are applied to the pipe at selected locations. A small surface chip of the pipe, containing the biaxial strain gages, is then removed using a dental burr trepanning technique as shown in Figures 11 and 12. Five strain gages were located on the outside of the pipe and five were on the inside. All gages were located close to Strain Gage Station 1 shown in Figure 5. The results of these measurements are shown in Figures 13 and 14. While these data appear to be consistent, their accuracy depends on the accuracy of the trepanning technique since no duplicate experiments or alternative measurements were conducted. However, recent trepanned strain gage work on high nickel-chrome steel indicates that, with good operator practice, the error due to technique will be between 0 and -6,000 psi.

Radial Deflections

Measurements were made on the radial dimensions of the completed weld assembly of BCL Model 2 to determine the radial distortions caused by the welding. Specifics of the measuring procedure are described in the section on the six-pass girth-butt weld. Relative deflections taken along four equally spaced longitudinal lines on BCL Model No. 2 are shown in Figure 15. As can be seen in the figure, welding causes an inward radial deflection at the edge of the weld of approximately 0.040 inch.

Experimental Details and Results for Six-Pass Girth-Butt Weld

The welded joint was made with the pipe machine-rotated in the horizontal position under a gas metal arc (GMA) welder.* Six weld passes were required. Each

* The initial (root) pass was a gas tungsten arc (GTA) weld with a handheld torch and filler wire added manually. The welded insert rings had not been received. This technique was used to simulate the heat input conditions as if an insert ring were used.

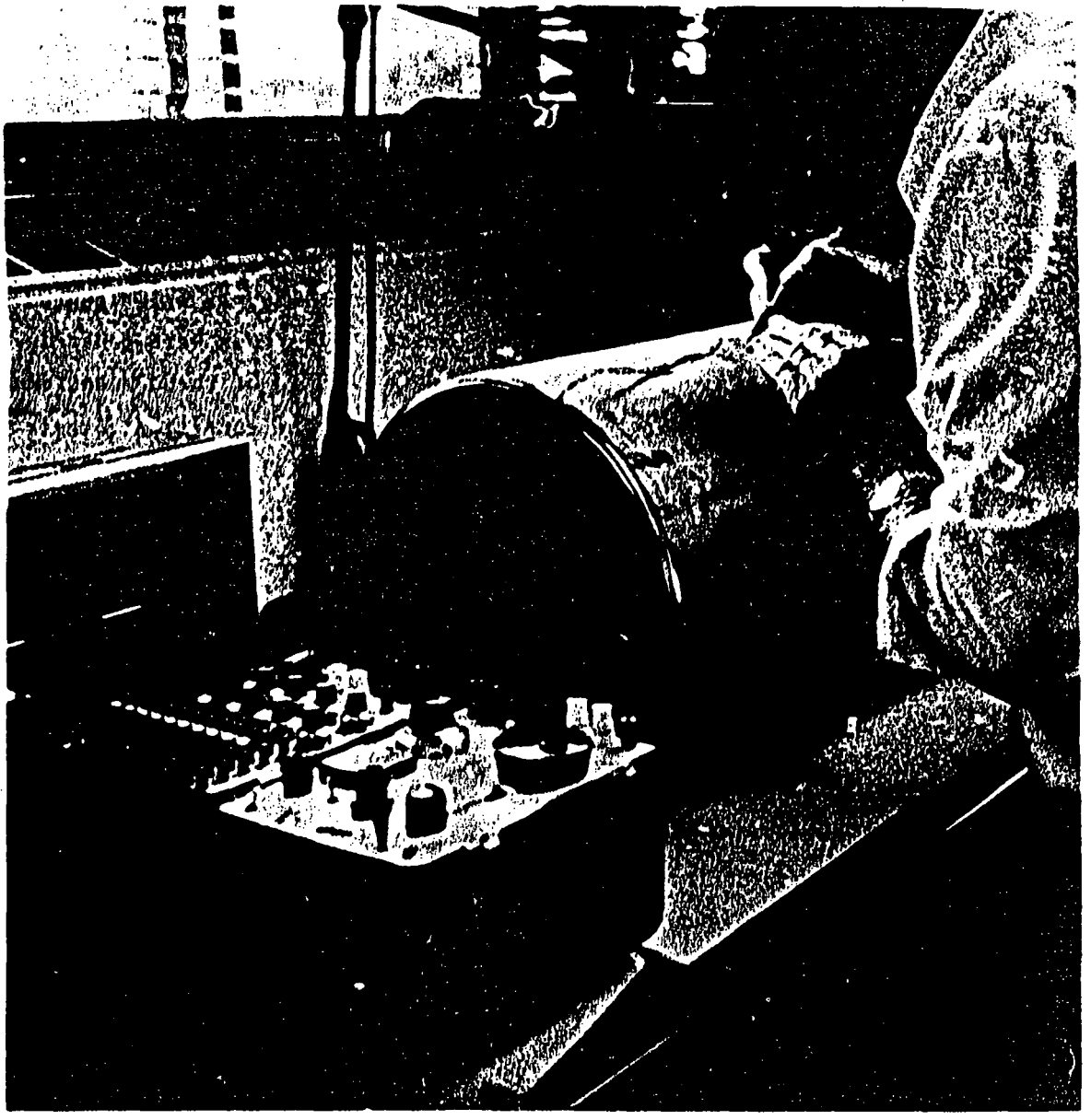

FIGURE 11. POSTWELD CHIP REMOVAL

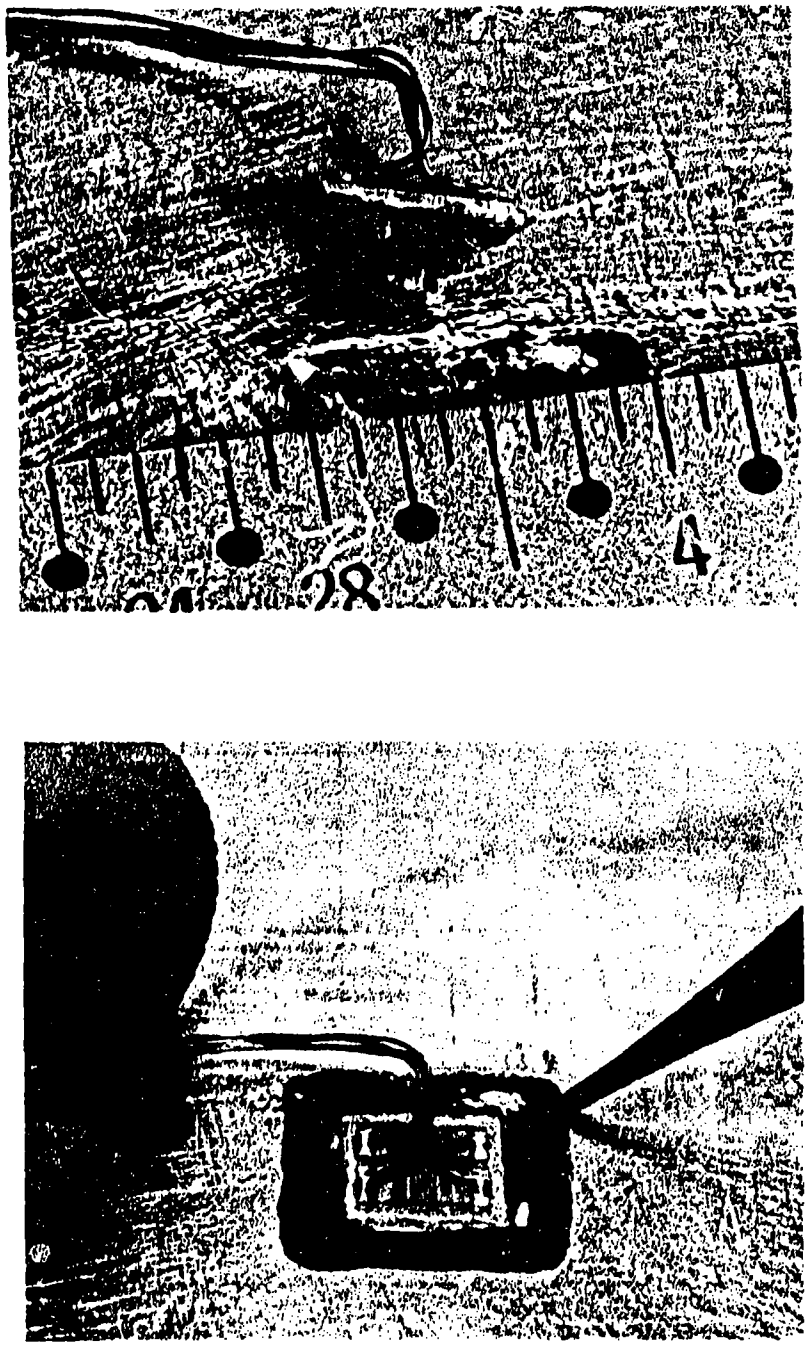

FIGURE 12. SURFACE CHIP WITH BIAXIAL STRAIN GAGE PATTERN

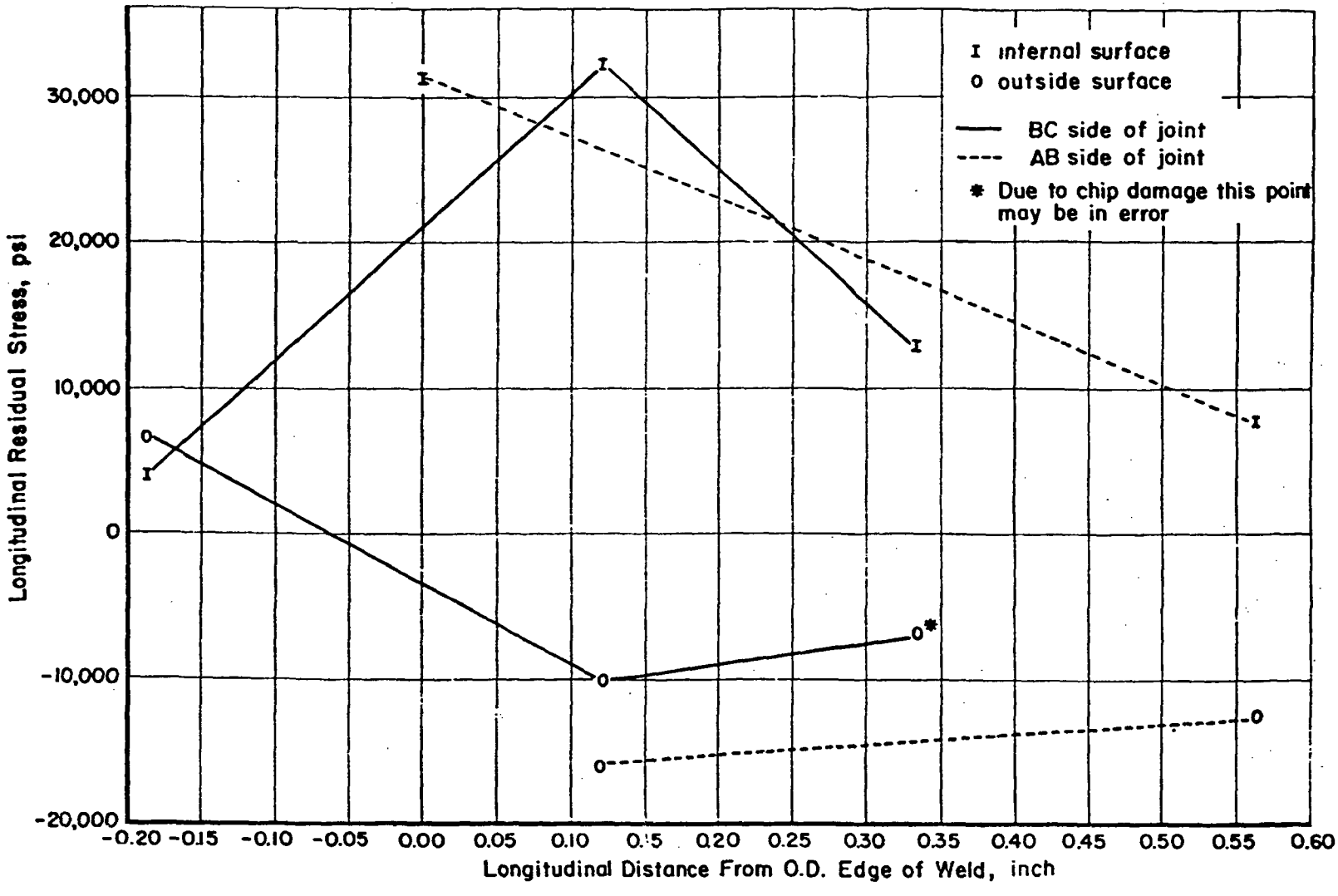

FIGURE 13. RESIDUAL STRESSES (TREPANNED STRAIN GAGE MEASUREMENT), BCL MODEL NO. 2

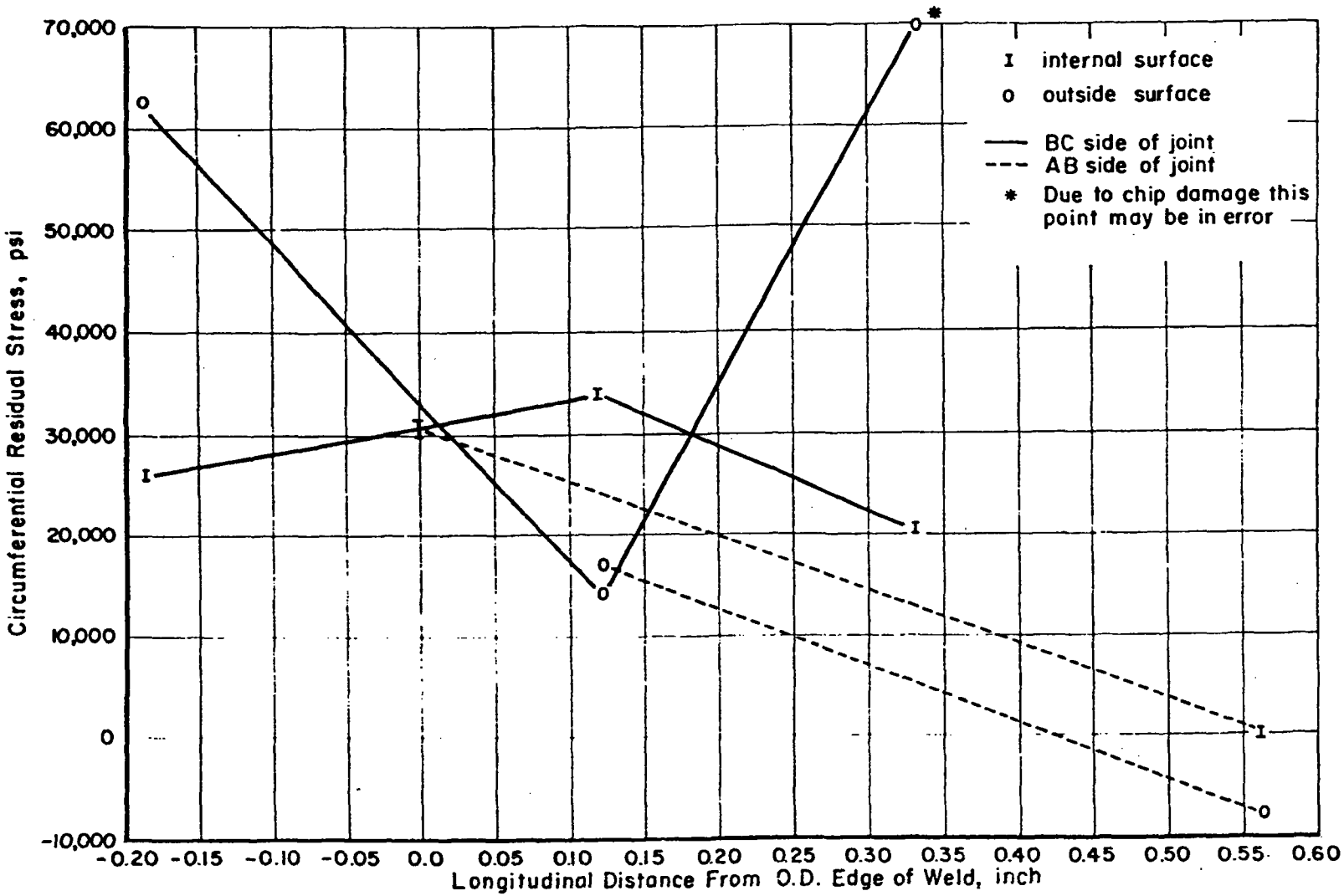

FIGURE 14. RESIDUAL STRESSES (TREPANNED STRAIN GAGE MEASUREMENT), BCL MODEL NO. 2

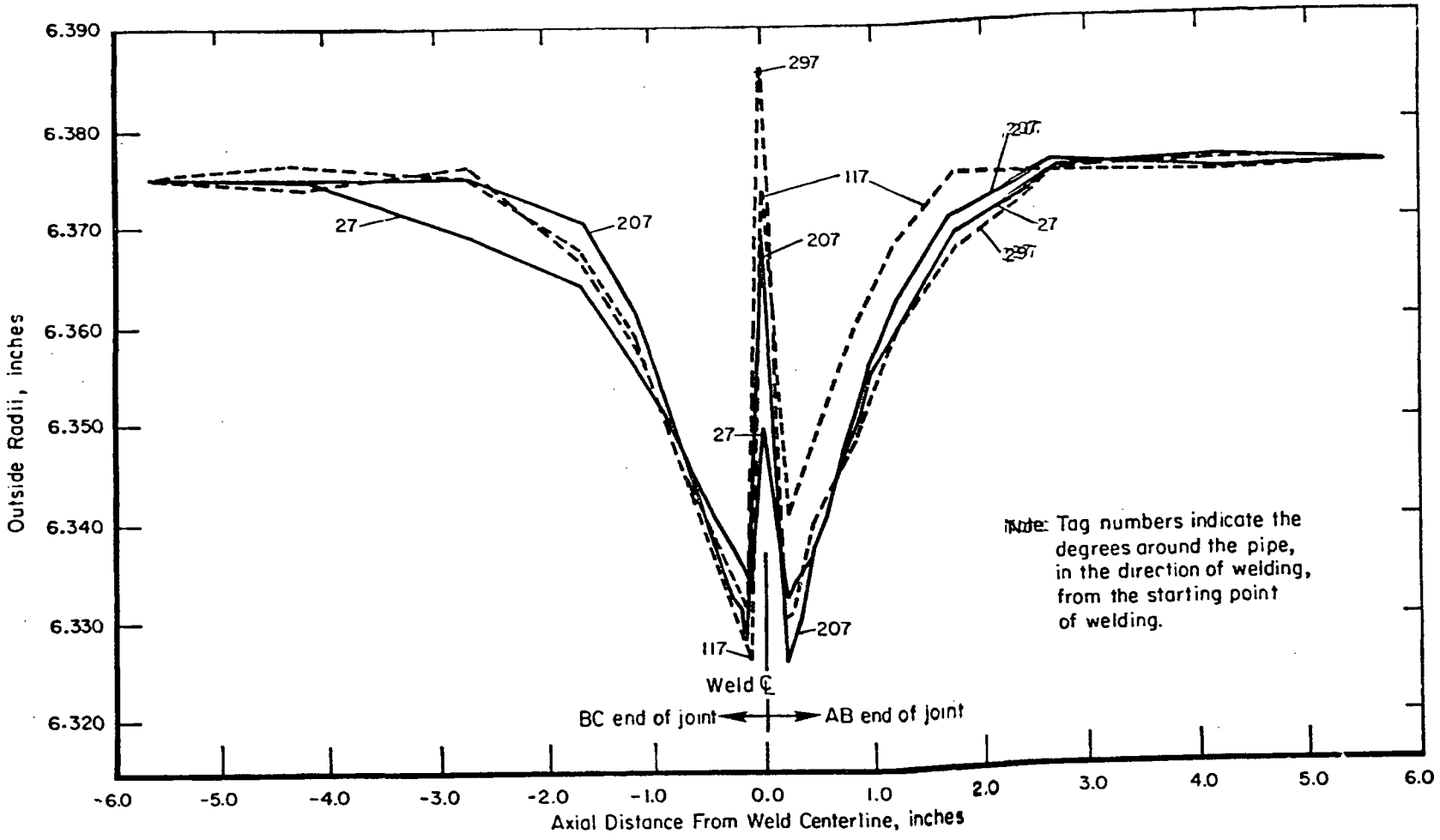

FIGURE 15. RADIAL DEFLECTIONS, BCL MODEL NO. 2

weld bead was started and terminated at the same point on the circumference. This point was selected to be the longitudinal weld seam.

Material

A 2-foot-long piece of 12-3/4 O.D. by 0.375-inch wall welded-seam 304 stainless steel pipe had its outer ends machined for a single U-groove weld preparation. The pipe was then sawed in half and the 1-foot lengths reversed to fit up the prepared outer ends for the weld joint. Excellent alignment was obtained. The Mill Test Report on the pipe material is contained in Table 5.

Welding

The single U-groove joint, shown in Figure 16, was aligned by hand, with a 1/16-inch gap, and tacked together at six equally spaced points with GTA welds each approximately 3/8-inch long. The pipe was then mounted on a specially constructed spider-type frame which adapts the assembly to the rotary drive machinery. The pipe was supported in the horizontal position and automatically rotated under the welding head at a preset rate. Since welding inserts were not received in time for the experiment, the root pass was made with the hand held GTA process at an average speed of 3.6 inches per minute (10.7 minutes of welding). There followed an 11.9-minute interval for setup of the instrumentation and the machine for the GMA process that was used for the remaining five filler passes. All passes started at the same point on the pipe, the longitudinal weld seam, and proceeded in the same direction. The five filler beads were applied at an average speed of 19.0 inches per minute (2.1 minutes per pass) with an average interval between passes of 5.2 minutes. The elapsed time from start to stop of the joining operation was 53.7 minutes. Additional welding parameters are summarized in Table 6.

The six-pass weld was done first. Some difficulty in obtaining smooth flow and wetting at the edges of the beads was experienced in this weld. As a result, there were locations along the edges of the cap beads where the weld metal did not flow and fuse properly to the adjacent bead. A defect of this type can be seen in Figure 17. However, the heat and metal input rates appear to have been uniform and consistent with the medium heat input rate desired. The effects of defects was eliminated by taking data at locations away from these defects.

TABLE 5. MILL TEST REPORT DATA FOR TYPE 304 PIPE USED IN BCL MODEL NO. 3

Size	Chemical Analysis									Yield Point Lbs. per sq. Inch	Tensile Strength Lbs. per sq. Inch	% Elong. in 2 Inches	Hardness
	C.	Mn.	P.	S.	Si.	Ni.	Cr.	Mo.	Co.				
12" Sch 40s	.046	1.67 Cu .11	.018	.014	.57	8.82	18.24	.33	.29	42600	87500	54.	BHN 151

Transverse Tension Test Satisfactory
Flattening Test Satisfactory
Hydrostatic tested at 883 P.S.I. minimum Satisfactory

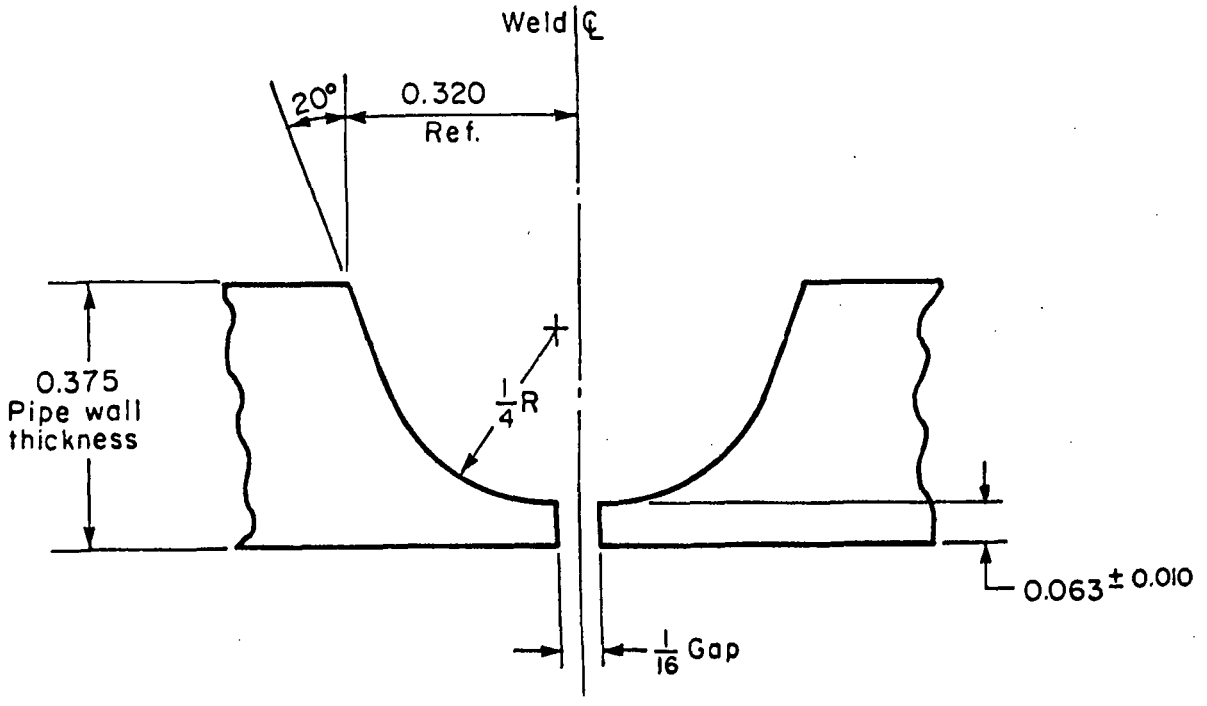

FIGURE 16. SINGLE U-GROOVE WELD PREPARATION

TABLE 6. WELDING PARAMETERS FOR BCL MODEL NO. 3

Pass No.	1	2	3	4	5	6
Welding Process	GTA	GMA	GMA	GMA	GMA	GMA
Wire Size, (inch)	0.0625	0.045	0.045	0.045	0.045	0.045
Current, (amps) (min)	116.	185.	216.	208.	208.	200.
(max)	152*	200.	232.	232.	224.	216.
Voltage, (volts)	13-14	26.5	26.	24.	24.	23.5
Polarity	Straight	Reverse	Reverse	Reverse	Reverse	Reverse
Travel Speed, (ipm)	3.6	19.0	19.0	19.0	19.0	19.0
Time for the Pass, (min)	10.7	2.1	2.2	2.1	2.1	2.0
Interval between Welds, (min)	11.9	5.4	4.8	5.4	5.3	
Contact Tube-to-Work Distance, (inch)	—	1/2	3/8	3/8	3/8	3/8

* For approximately the first minute, 160-175 amps.

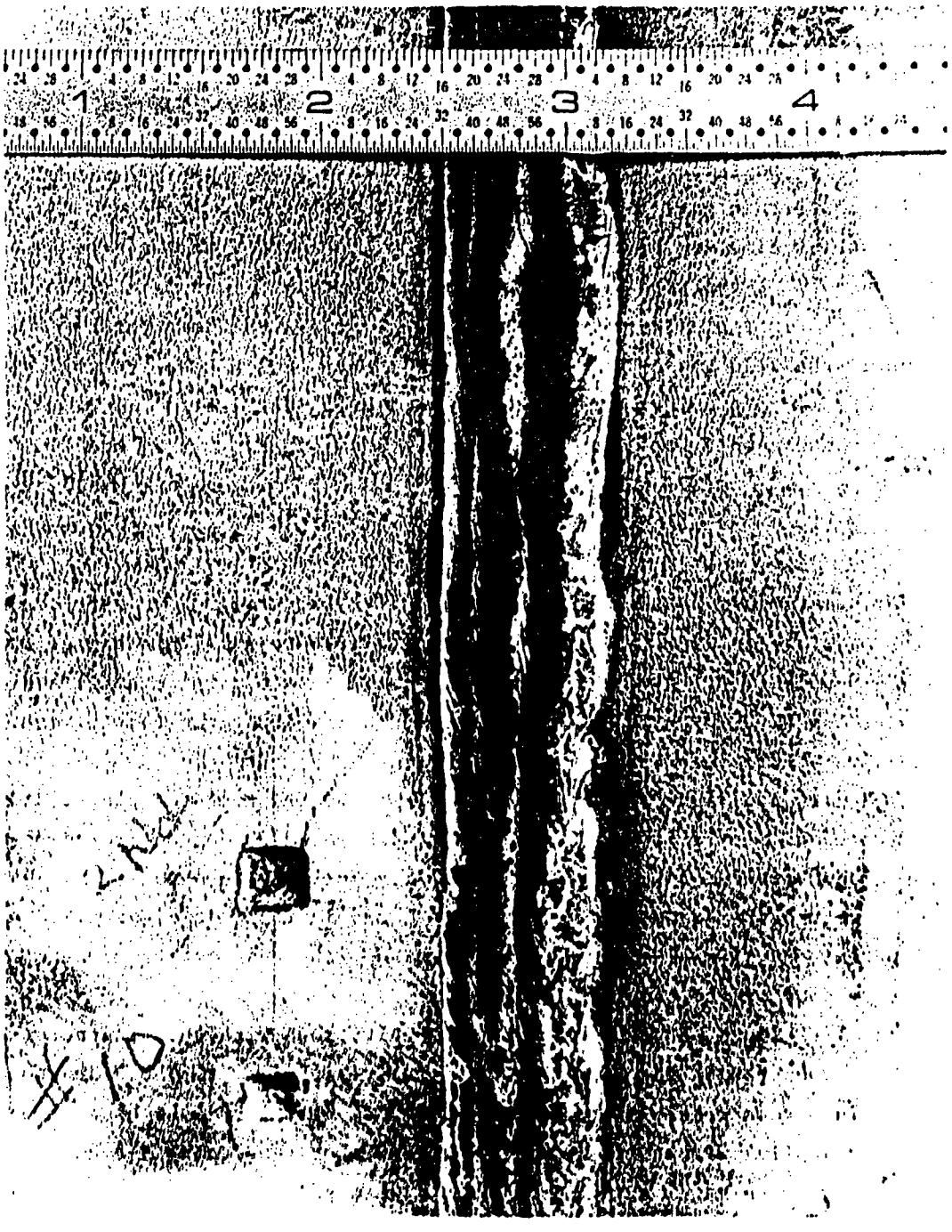

FIGURE 17. EXTERIOR APPEARANCE OF THE FIRST TEST WELD

Temperatures

Thirteen thermocouples were spot welded to the pipe in the array shown in Figure 18. The positions of the thermocouples were determined by and correlated with the strain gage locations. A portion of the dynamic record of temperature versus time for five thermocouples on the outside of the pipe is shown in Figure 19. Except for maximum temperature obtained, the data shown in Figure 19 are fairly typical of each weld pass. That is, the temperature is constant until the weld passes the thermocouple. Then peak values are followed by gradual cooling to a uniform interpass temperature. Maximum and minimum thermocouple measurements for each weld pass are shown in Figures 20 and 21.

Strains

Nineteen Micro-Measurements 350-ohm foil-type strain gages were applied to the pipe prior to welding. Sixteen of these gages were a 1/32-inch gage designated WK-09-031-CF-350. Two 1/16-inch gages were in a biaxial configuration and designated as WK-09-062-TT-350. One gage had a 1/4-inch gage length with the designation WK-09-250-BG-350.

The gage positions on the pipe correspond to the thermocouple positions shown in Figure 18. Six additional gages were located at 90 degree increments around the circumference on the inside and outside surfaces in a position, relative to the weld, that corresponds to Thermocouples 3 and 13 shown in Figure 18. All gages except the one biaxial element were oriented with their active element in the axial direction of the pipe.

The literature on these gages and consultations with the manufacturer indicated that the type WK gage would have normal reliability to 550 F and would produce useable strain readings under short-term temperatures as high as 750 F. The gages were applied with the recommended high-temperature epoxy M-Bond 610. The pipe sections with gages attached and wired were subjected to combined preconditioning/thermal calibration cycles in a furnace. One pipe section, with the majority of the gages attached, briefly saw a maximum temperature of 670 F. The other section with two gages saw a maximum of temperature of 570 F. While some temperature effects were apparent in observed permanent offset strains due to the preconditioning cycles, these appeared to be minor. However, in-depth studies

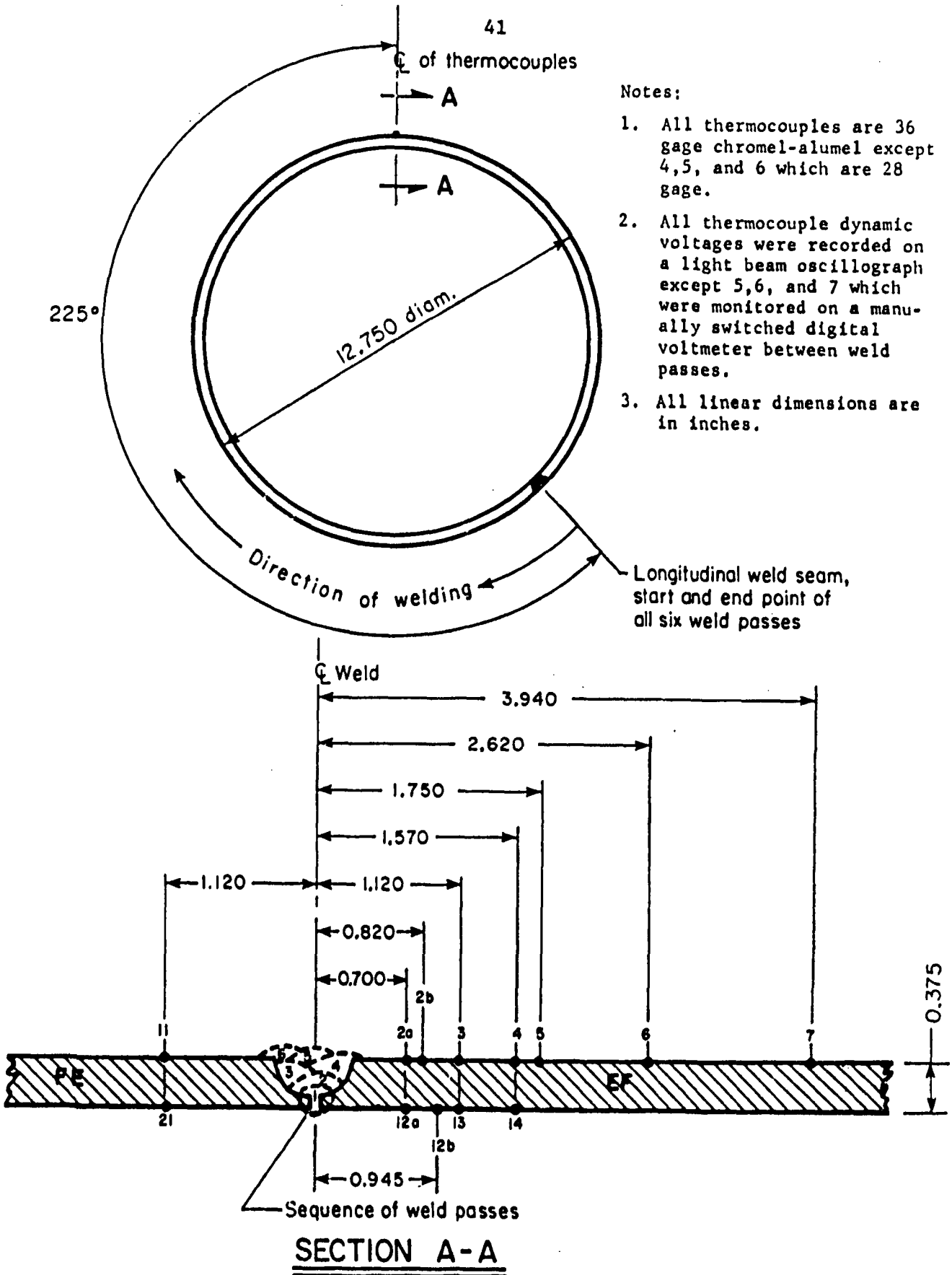

Notes:

1. All thermocouples are 36 gage chromel-alumel except 4,5, and 6 which are 28 gage.
2. All thermocouple dynamic voltages were recorded on a light beam oscillograph except 5,6, and 7 which were monitored on a manually switched digital voltmeter between weld passes.
3. All linear dimensions are in inches.

FIGURE 18. THERMOCOUPLE ARRAY FOR SIX-PASS WELD

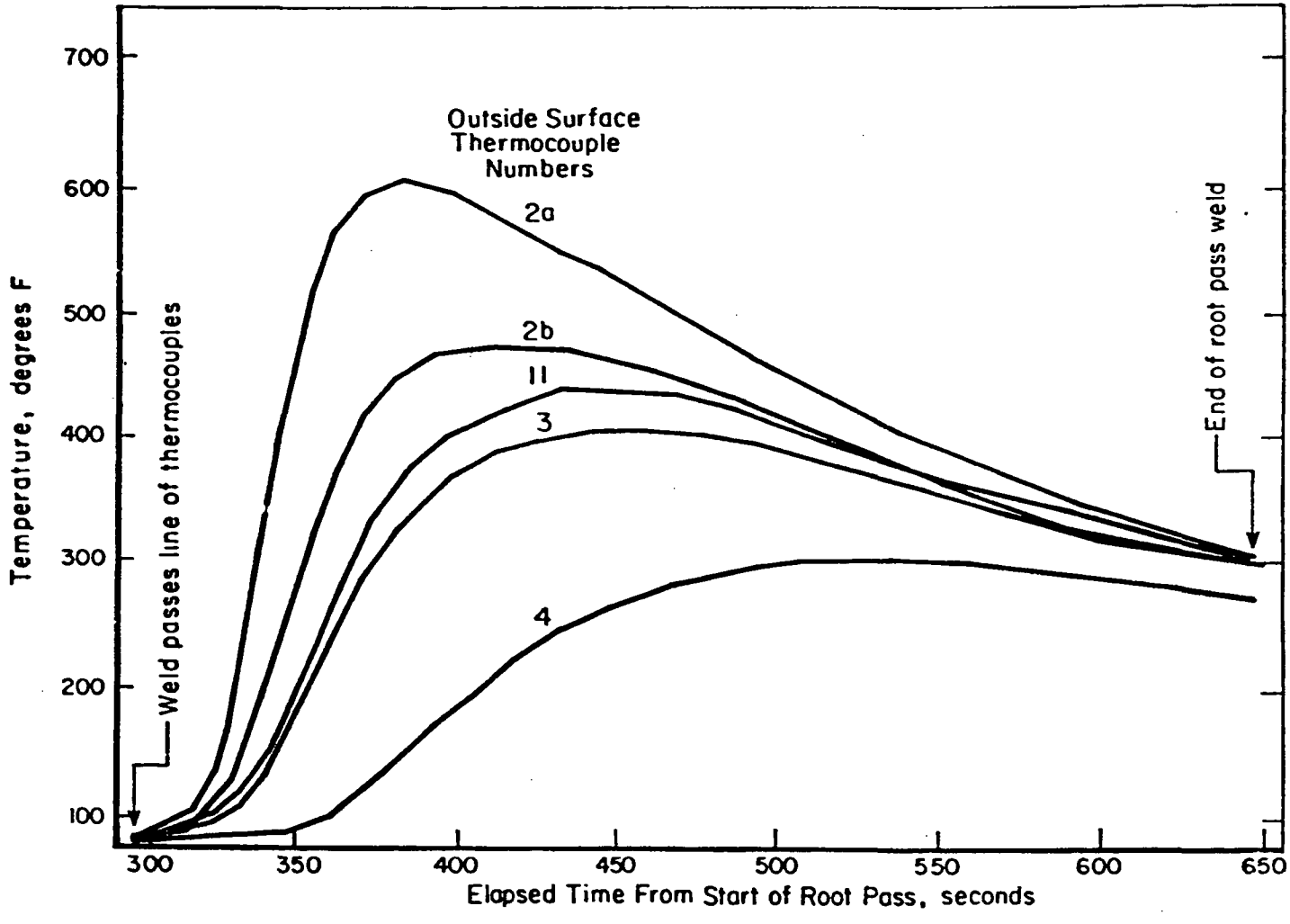

FIGURE 19. ROOT PASS TEMPERATURES ON OUTSIDE SURFACE

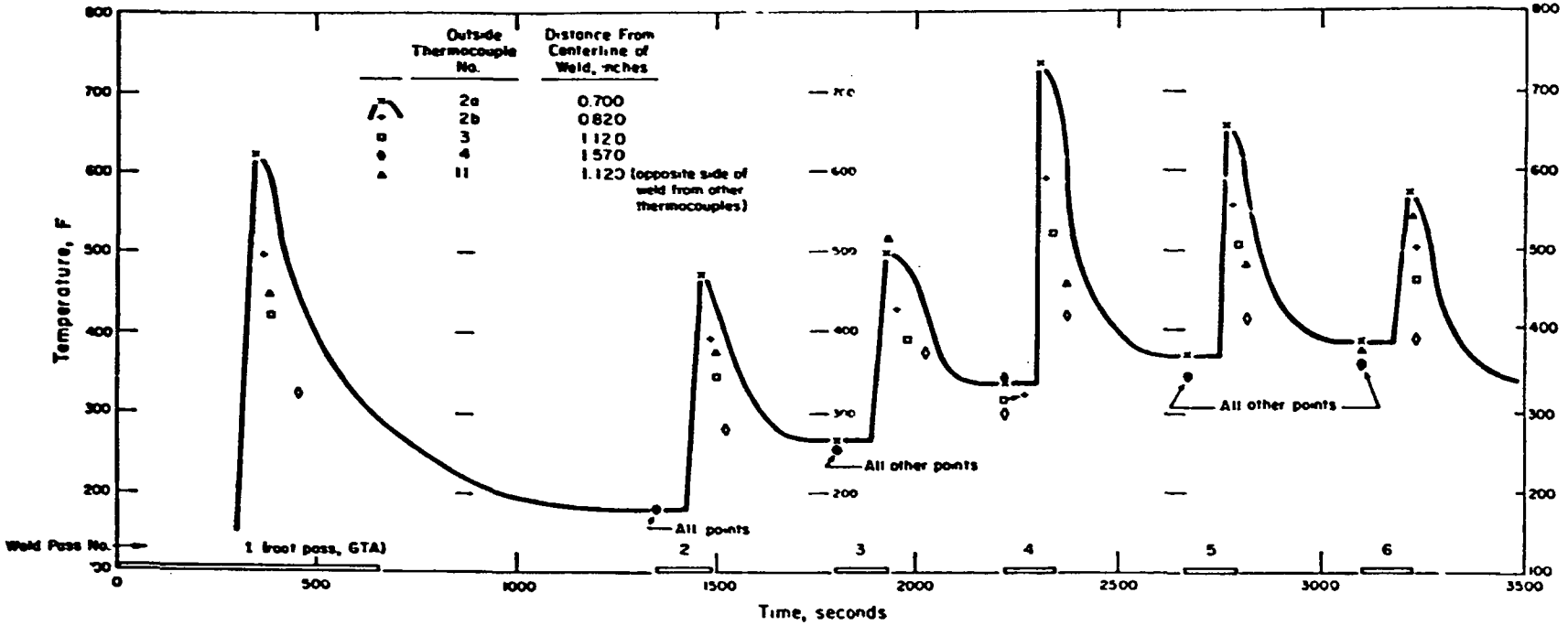

FIGURE 20. OUTSIDE MAXIMUM AND MINIMUM INTERPASS TEMPERATURES

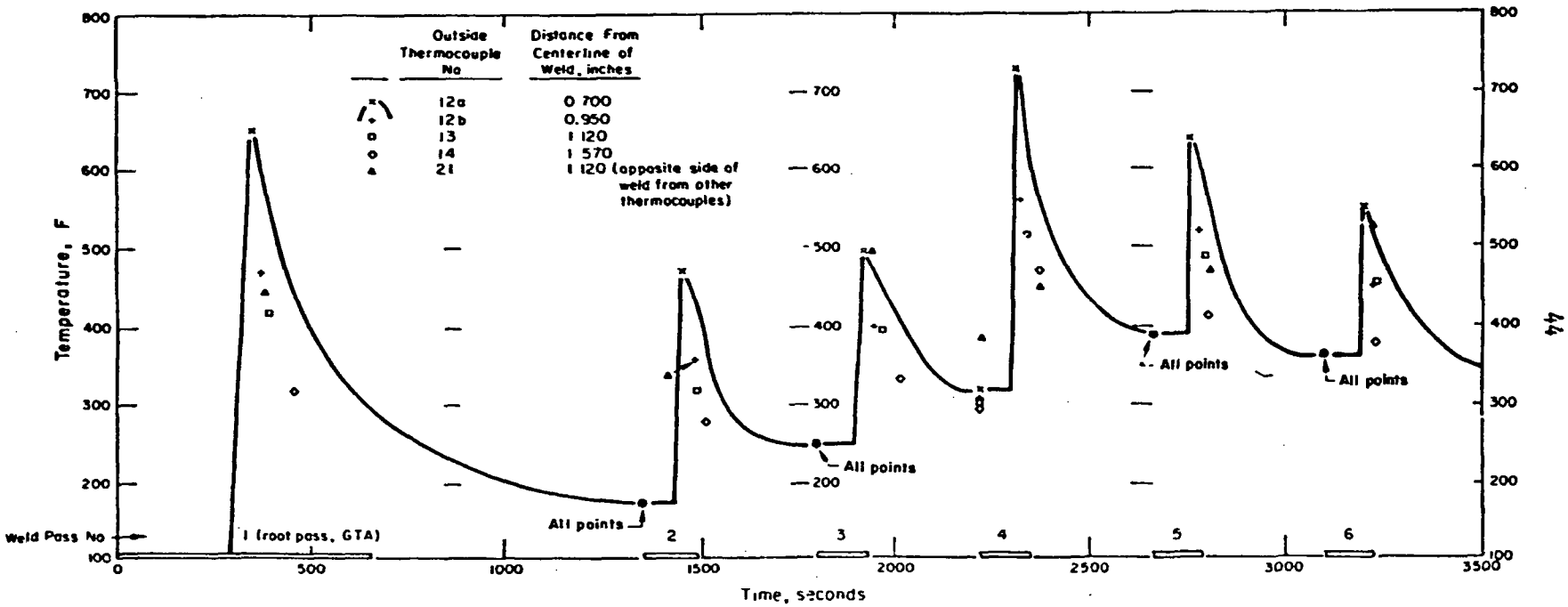

FIGURE 21. INSIDE MAXIMUM AND MINIMUM INTERPASS TEMPERATURES

of the gages and the bonds showed that the bonds had been damaged so that they could not be used for residual stress data.

A total of twenty-one biaxial postweld strain gages were attached to BCL Model No. 3. The gages were trepanned out to obtain the change in strain gage readings. Residual stresses were inferred from these readings. The procedure is described in the section on the two-pass weld. The results of these measurements are shown in Figures 22 and 23.

Measurements of Radial Deflections

A special pipe mounting frame was constructed and used to make the displacement measurements. This frame has a heavy 4-inch outside diameter center pipe extending beyond the ends of the pipe segments to be welded. The mounting is fitted with lugs that can be expanded to the internal diameter of the 12-3/4-diameter pipe sizes. This frame serves two purposes. First, it is an intermediate support member that interfaces with welding machine's rotary drive. Secondly, it has centers on each end that positively locate the pipe-frame assembly in a large lathe where radial deformation measurements can be taken.

Measurements were taken along four equally spaced longitudinal lines. The results are shown in Figure 24. The maximum radial deflection for this pipe is about .063 inch.

Cross Section of the Weld

A photomacrograph of the etched cross section of the six-pass girth-butt weld from BCL Model No. 3 is shown in Figure 25. The figure includes a schematic drawing of the section identifying various features of the weld. As in the two-pass weld, each pass after the root pass has a tear drop shape at the root of the pass. As discussed in the two-pass weld section, this is characteristic of welds made by the gas metal-arc process.

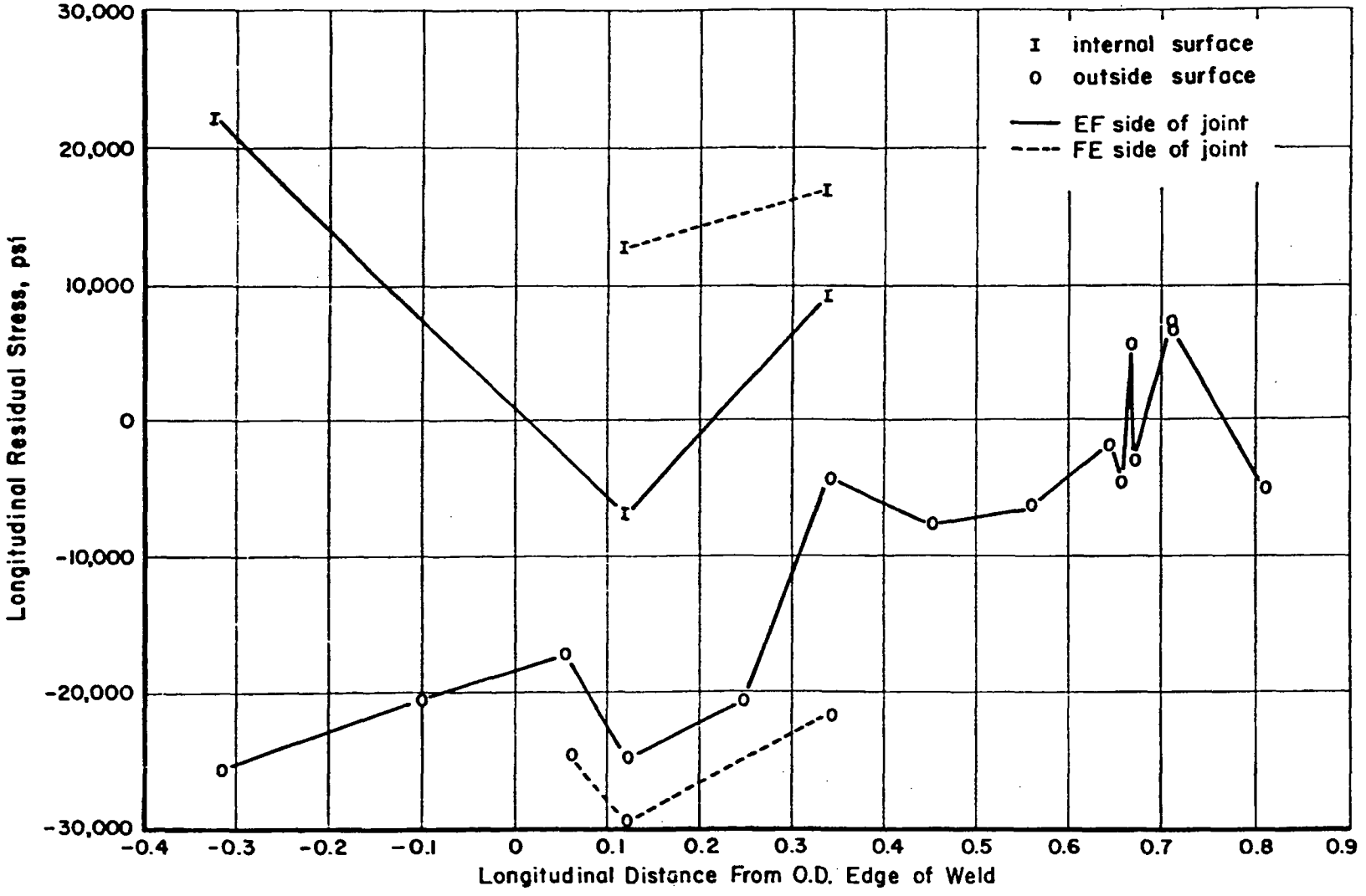

FIGURE 22. RESIDUAL STRESSES (TREPANNED STRAIN GAGE MEASUREMENTS), BCL MODEL NO. 3

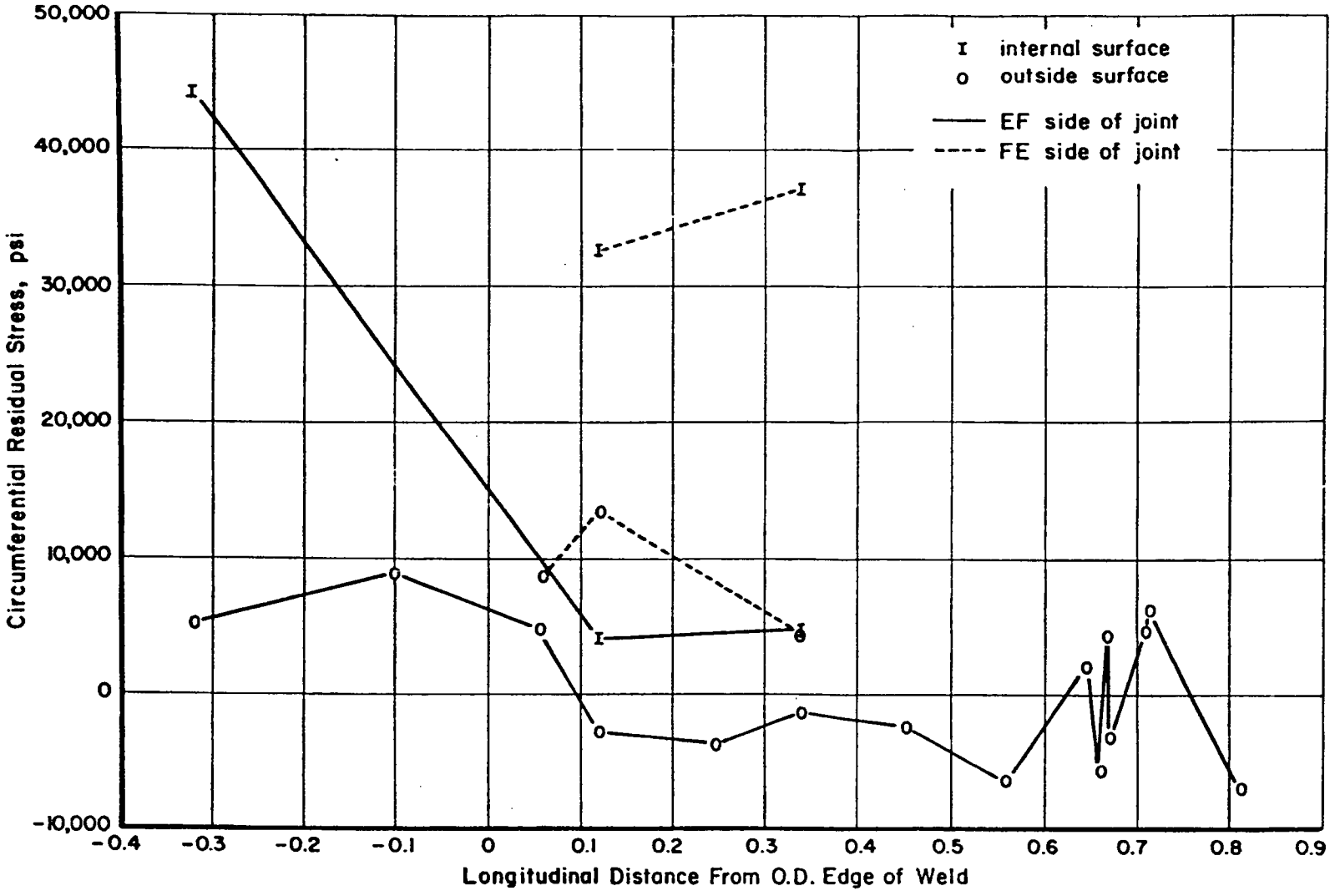

FIGURE 23. RESIDUAL STRESSES (TREPANNED STRAIN GAGE MEASUREMENTS), BCL MODEL NO. 3

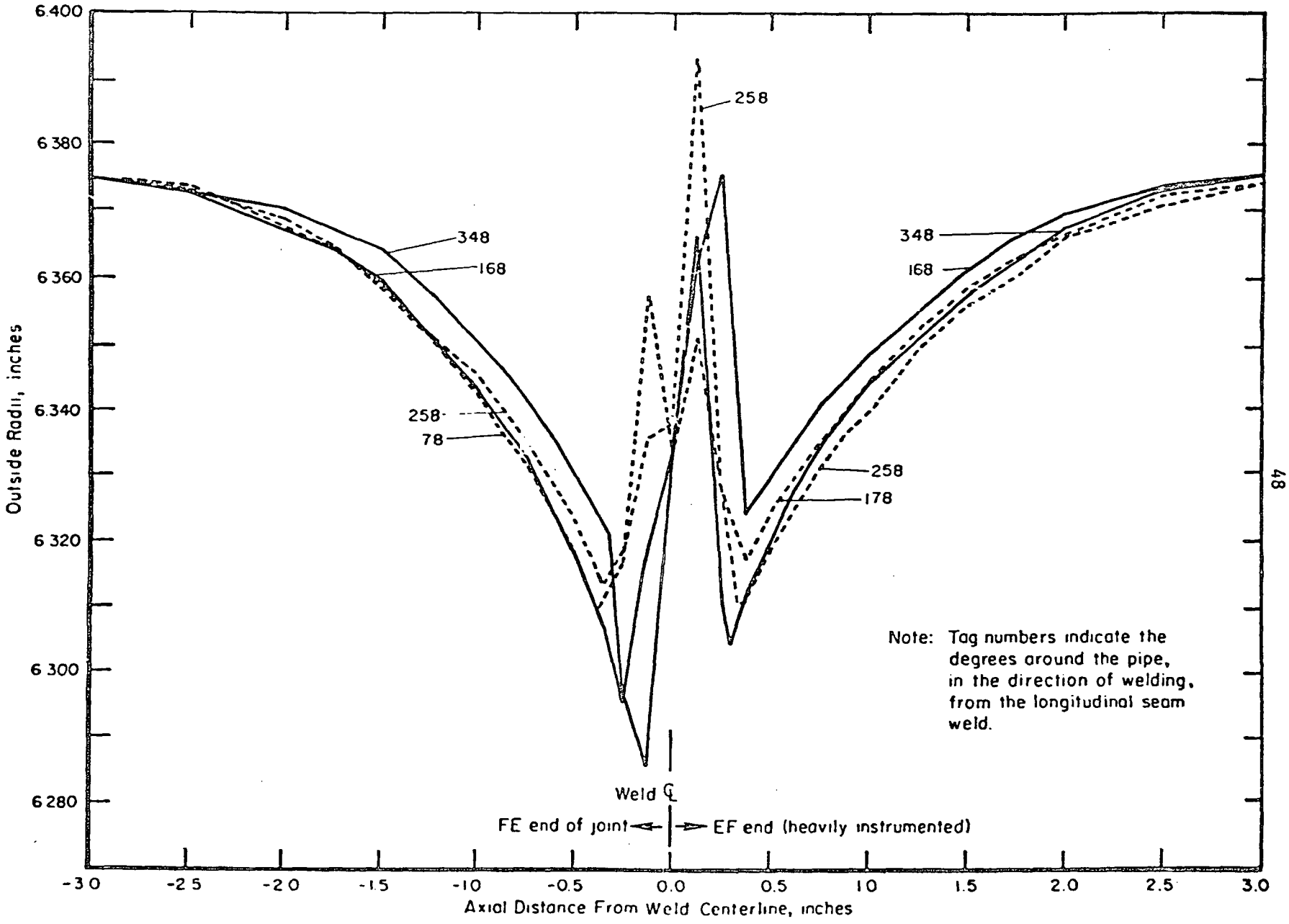

FIGURE 24. RADIAL DEFLECTIONS, BCL MODEL NO. 3

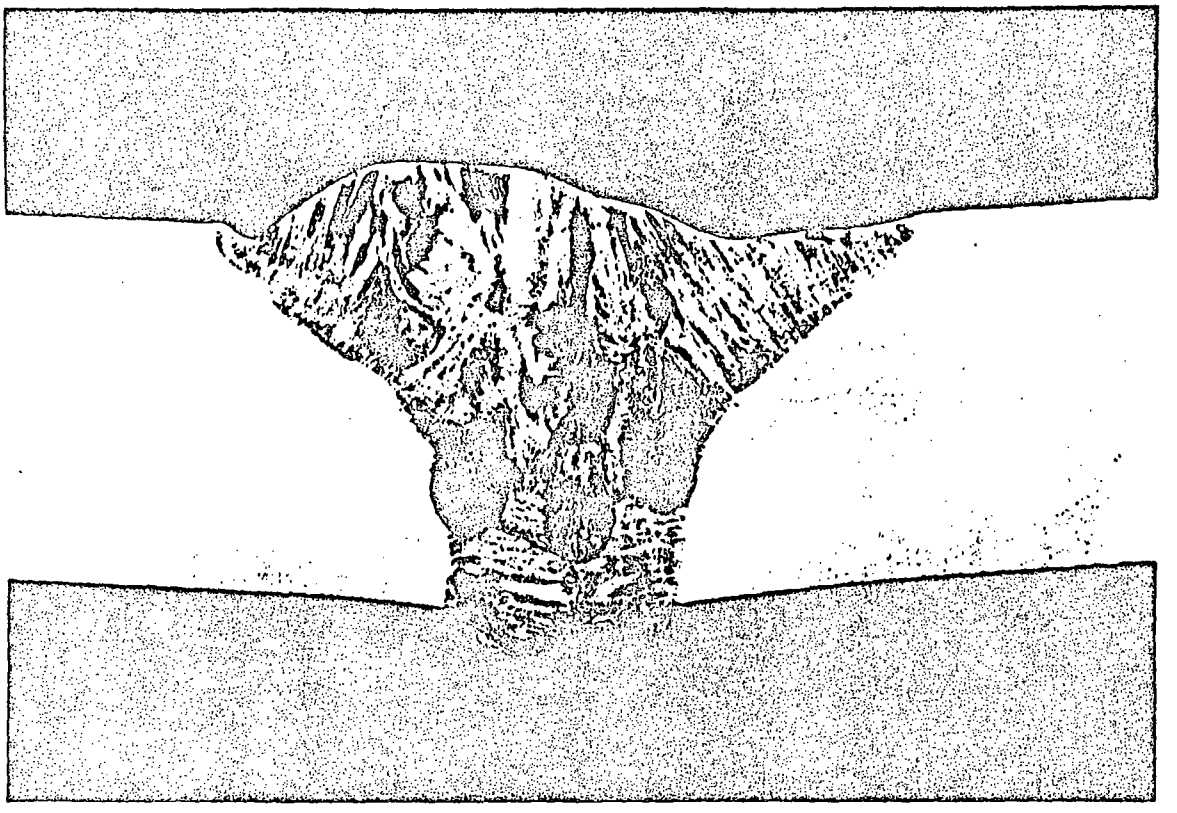

Photograph, Etchant 97 HCl-$3H_2O_2$ - $\frac{1}{2}$ gm $Cu\ Cl$ 0.1701

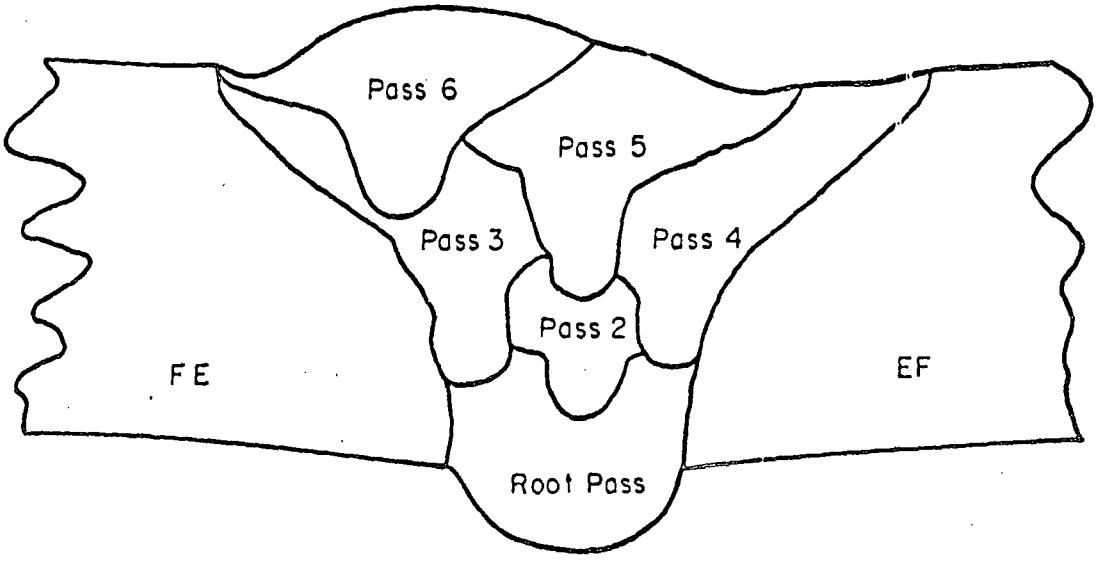

Schematic

FIGURE 25. WELD CROSS SECTION BCL MODEL NO. 3

IV. TEMPERATURE ANALYSIS MODEL AND RESULTS

The mathematical model for residual stresses due to welding consists of two parts. The first part is a heat flow model that gives the time dependent temperature distributions. The temperature model contains the influence of the weld parameters. The second part of the residual stress model is a stress analysis model. The coupling between these two is that the temperature model provides temperature distributions that are the input for the stress analysis model. The following sections describe each model and their applications.

Temperature Analysis Model for Welding

A numerical technique was developed for obtaining temperature distributions due to welding of cylindrical pipe. The following presents descriptions of the procedures for modeling the temperature distributions and numerical results for testing the model.

The technique is based on the distribution of temperatures around a moving point-heat source in an infinite solid. Figure 26 shows a point-heat source moving in the x direction with a velocity V. The temperature due to this moving heat source is given by

$$T(r,\xi) = T_o + \frac{q}{4\pi K} \frac{\exp\left(-\frac{V\xi}{2a}\right) \cdot \exp\left(-\frac{Vr}{2a}\right)}{r}, \qquad (1)$$

where

T = temperature (F)
T_o = ambient temperature (F)
q = heat input (btu/sec)
K = thermal conductivity (btu/in.-sec-F)
V = heat source velocity (in./sec)
ξ = X-distance from heat source (in.)
r = distance from heat source (in.)
c = heat capacity (btu/in.^{3} - F)
a = K/c (in.^{2}/sec).

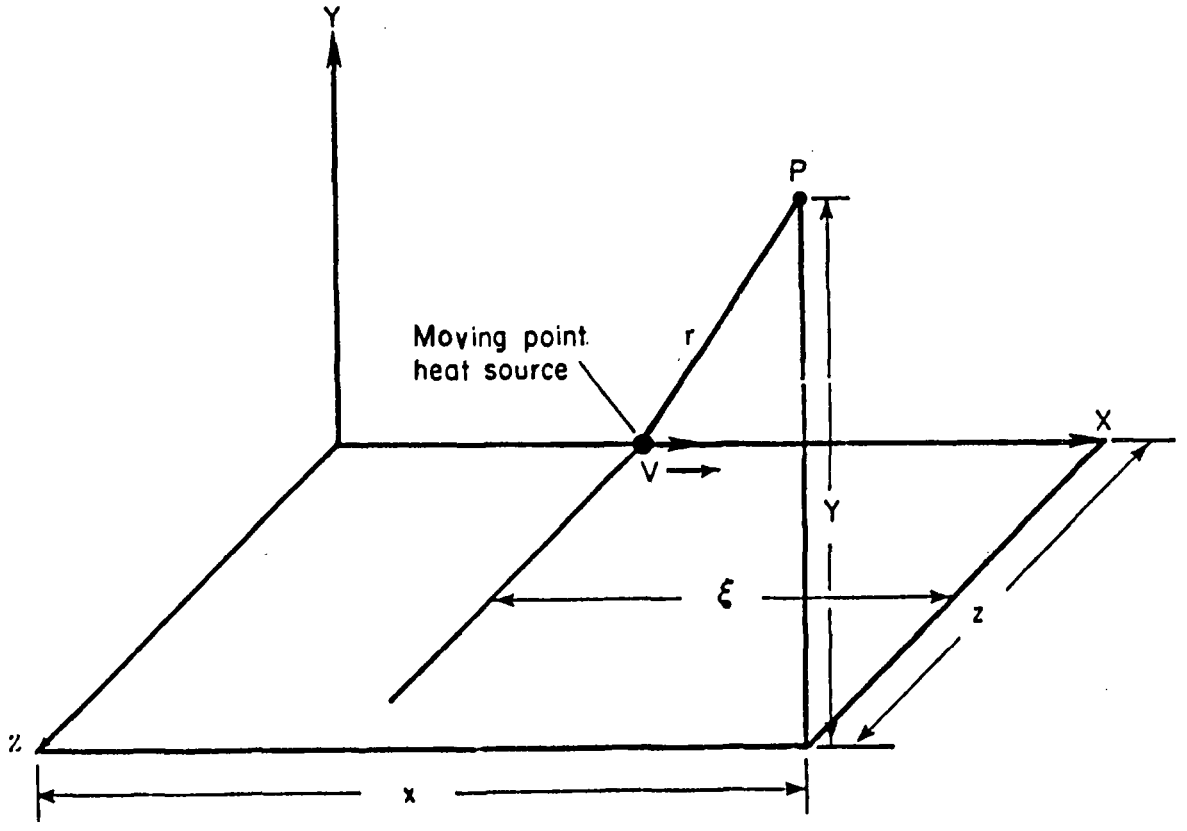

FIGURE 26. MOVING HEAT SOURCE IN AN INFINITE SOLID

Equation (1) is identical to that presented by Rosenthal[39]. Time does not explicitly appear as a variable in Equation (1) because, although the temperature distribution is a variable with respect to a stationary point in a solid, it is unchanging with respect to the heat source since steady-state cqnditions are assumed to be present. However, time does appear implicitly in Equation (1) since

$$\xi = X_o - Vt \quad , \tag{2}$$

where X_o is the distance between the stationary point and the heat source when $t = 0$.

The numerical technique approximates the temperature rise due to the moving source in a finite thickness plate by superposing a series of heat sources, as shown in Figure 27. In this figure, the welding heat source is WS. Heat source I_1, a mirror image of WS, is added to eliminate the source heat transfer through the inside pipe surface. Likewise, a mirror image, O_1, is added to eliminate the source heat transfer through the outside pipe surface. Heat source O_2 and I_2 are added to eliminate the heat transfer of I_1 through the outside surface and O_1 through the inside surface, respectively. The actual plate temperature is obtained by superposing at least 28 of these additional temperature sources.

The superposition of heat sources is used with Equation (1) to compute a time-temperature curve for the heat source moving along the circumference of a pipe at a specified thickness. These curves are generated by treating the pipe as a flate plate with the same length as the circumference of the pipe.

The solution for the point heat source given by Equation (1) assumes physical properties are independent of temperature. The solution is applied outside the fused zone of the weld.

The multipass welding of a pipe was modeled by the following procedure. Temperatures were calculated for the root pass by locating the heat source at the centroid of the fused zone. For the second pass, temperatures were calculated by locating the heat source at the center of the fused zone area corresponding to the second pass. The total temperature was obtained by adding the temperatures to an experimentally determined ambient temperature for the second pass. For subsequent passes, the temperature is determined in the same manner.

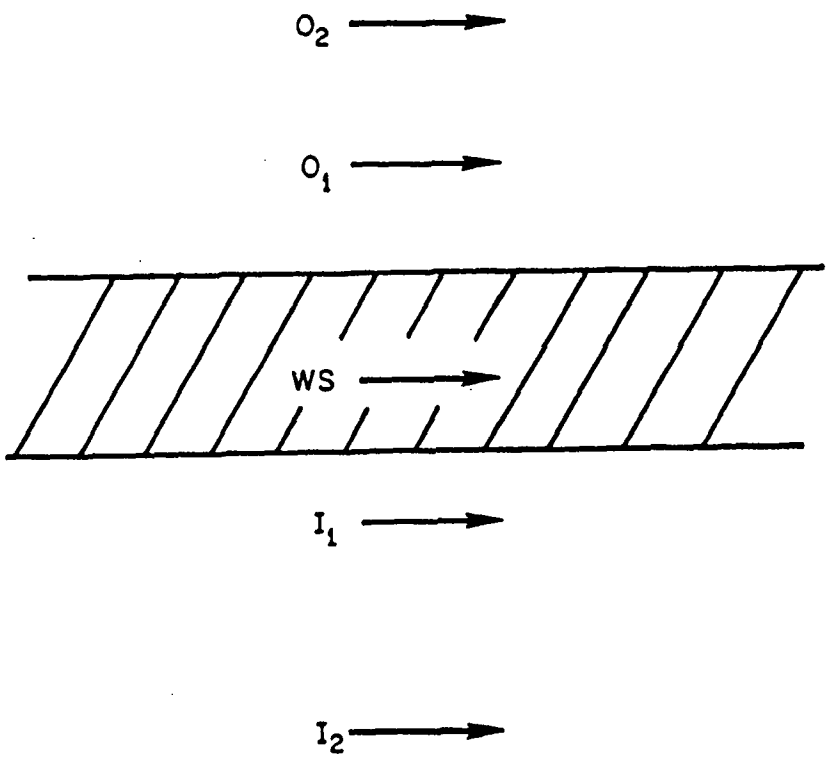

FIGURE 27. SUPERPOSITION OF HEAT SOURCES

The analytical model described above is similar to that developed by Vaidyanathan, Weiss, and Finnie[26] except that the peak temperature instead of average temperatures were calculated. Kamichika, Yada, and Okamoto[24] used the point heat source model to predict temperature distributions during weld-overlaying of stainless steel plates and obtained good agreement with experimental data. Paley, Lynch, and Adams[4] also used the point heat source model to study the peak temperatures at or near welds made in thick HY-80 and T-1 steel plates. Their results showed that peak temperatures could be calculated to within 5 percent of experimentally determined temperatures.

Numerical Results

A computer program was developed for determining welding temperatures based on the mathematical model described above. Table 7 lists the input data and output parameters for the computer program.

Numerical test cases were run to demonstrate that the thermal model could predict transient temperature profiles that occur during welding. Two stainless steel cylinders, denoted by BCL Model Numbers 2 and 3, were used in this study. As described in the section on experimental results, BCL Model Number 3 is a six-pass weld and BCL Model Number 2 is a two-pass weld. The first test case modeled the GTA root pass of a 3/8-inch thick, 304 stainless steel pipe with an outside diameter of 12.75 inches. This pipe is BCL Model Number 3. Figure 28 shows a comparison of the model results with thermocouple measurements taken during the root weld pass of the initial project experiment. Time t = 0 corresponds to the time at which a thermocouple (2a) located 0.07 inch from the weld centerline reached its maximum temperature. The agreement of the analytical results with the experimental data provides a check that the thermal model can accurately predict welding temperatures.

Five other check cases were run. These cases were based on three additional passes of BCL Model Number 3 and both passes of BCL Model Number 2. Figure 29 shows a comparison of the analytical results with thermocouple measurements taken during the second pass of BCL Model Number 3 experiment. The time t = 0 seconds corresponds to the time at which a thermocouple located 0.70 inches from the weld centerline reached its maximum temperature. Figures 30 and 31 show similar comparisons for the fourth and sixth passes of the same experiment.

TABLE 7. INPUT AND OUTPUT PARAMETERS FOR THE POINT HEAT SOURCE MODEL

Input Parameters

Name	Description	Units
F	Distance from next source to outside cylinder surface	in.
G	Distance from heat source to inside cylinder surface	in.
V	Heat source velocity	in./sec
TMAX	Period of one weld pass	sec.
K	Conductivity	Btu/in.-sec-F
Q	Heat input	Btu/sec
C	Heat capacity	$Btu/in.^3$-F
NPNC	Number of temperature output points	
NSMAX	Number of imaginary heat sources	
Y_i	Y coordinate of temperature point	in.
Z_i	Z coordinate of temperature point	in.
T_o	Ambient temperature	F
T	Time	sec.
X	X coordinate of temperature point	in.

Output Parameters

Temp	Temperature	F
$\overline{T}$	Average temperature	F
IERR	Integration error	F

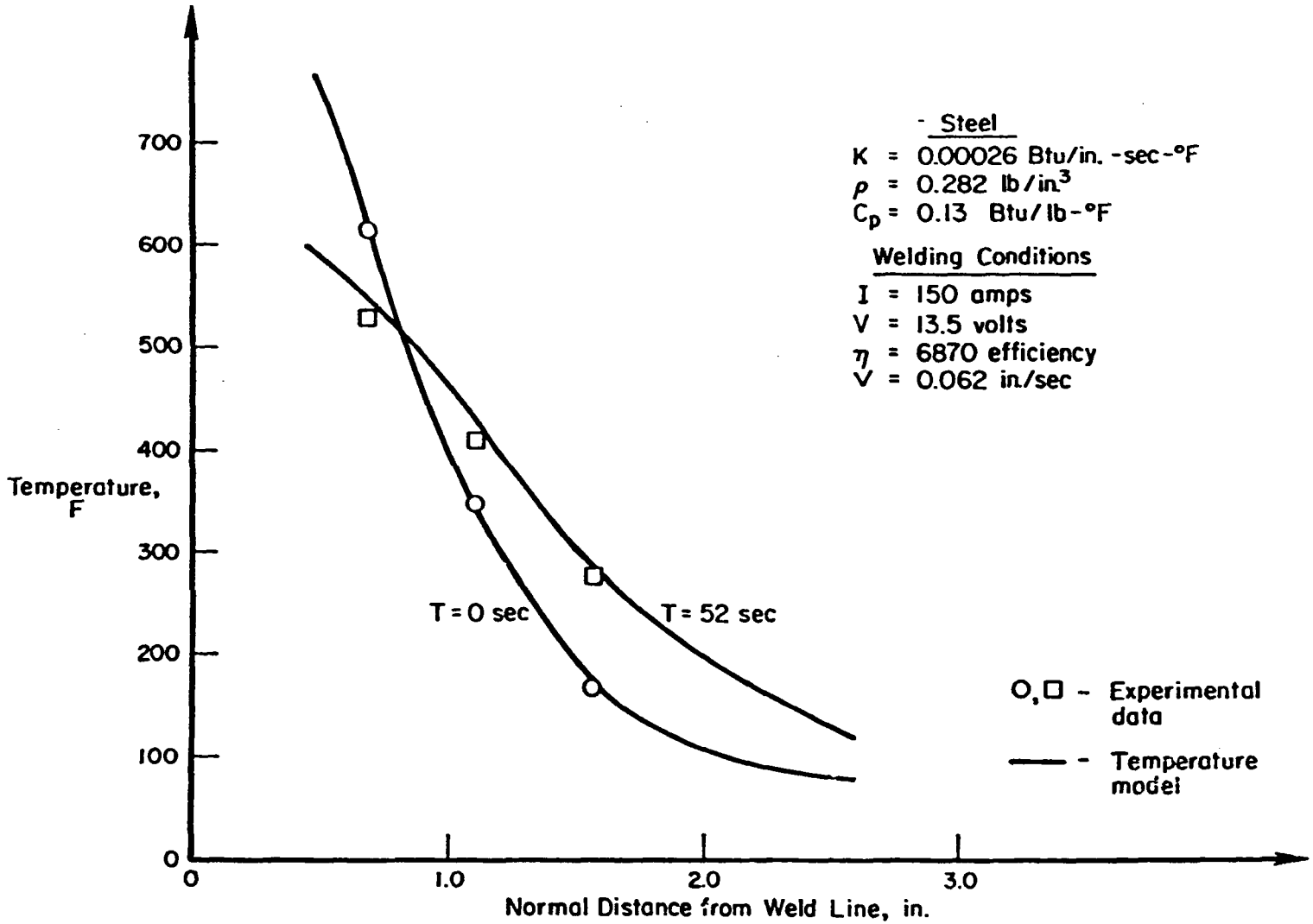

FIGURE 28. ANALYTICAL CURVE AND EXPERIMENTAL DATA POINTS FOR THE ROOT PASS OF BCL MODEL NO. 3

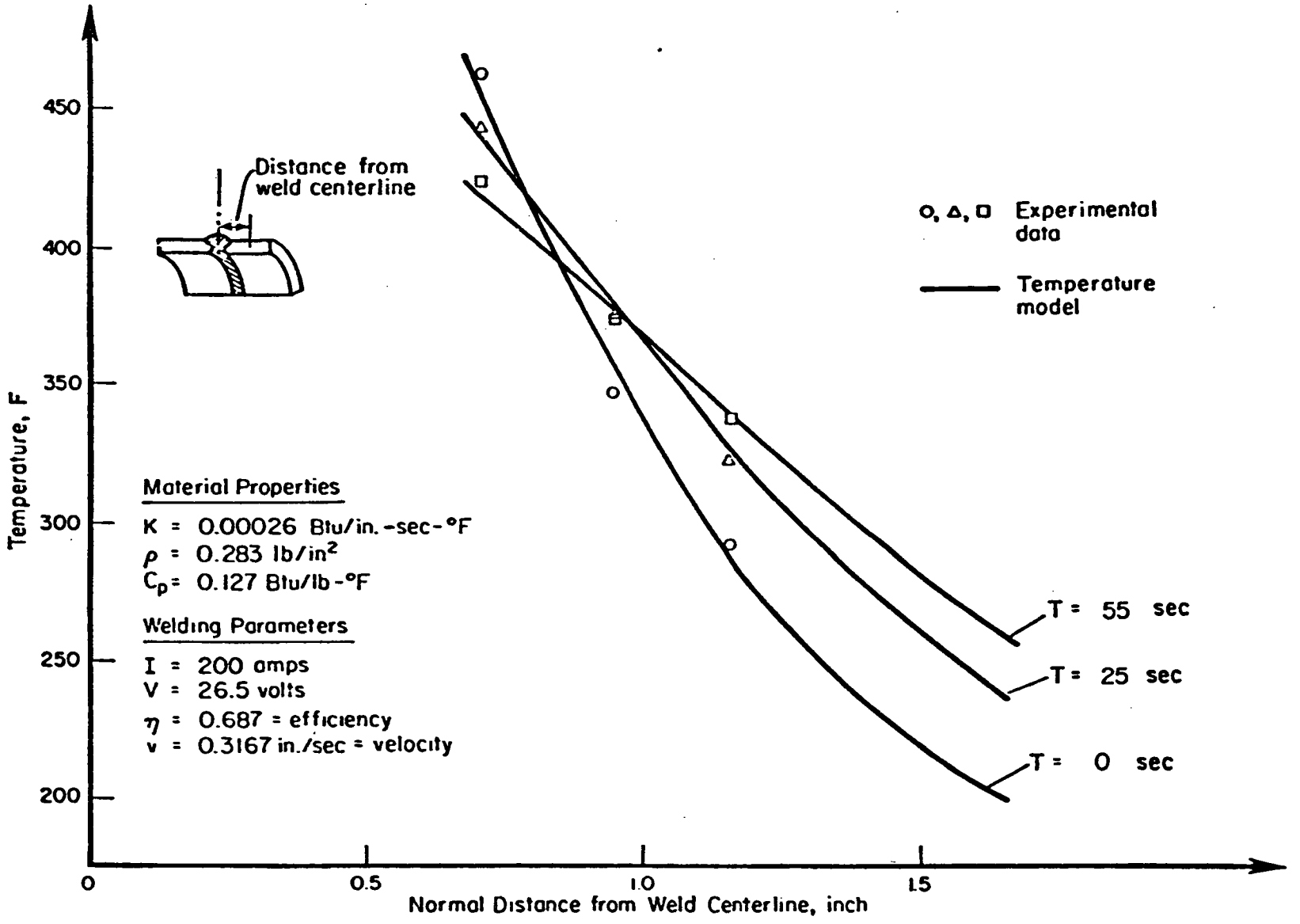

FIGURE 29. CALCULATED TEMPERATURE CURVES AND EXPERIMENTAL DATA POINTS FOR THE SECOND PASS OF BCL MODEL NO. 3

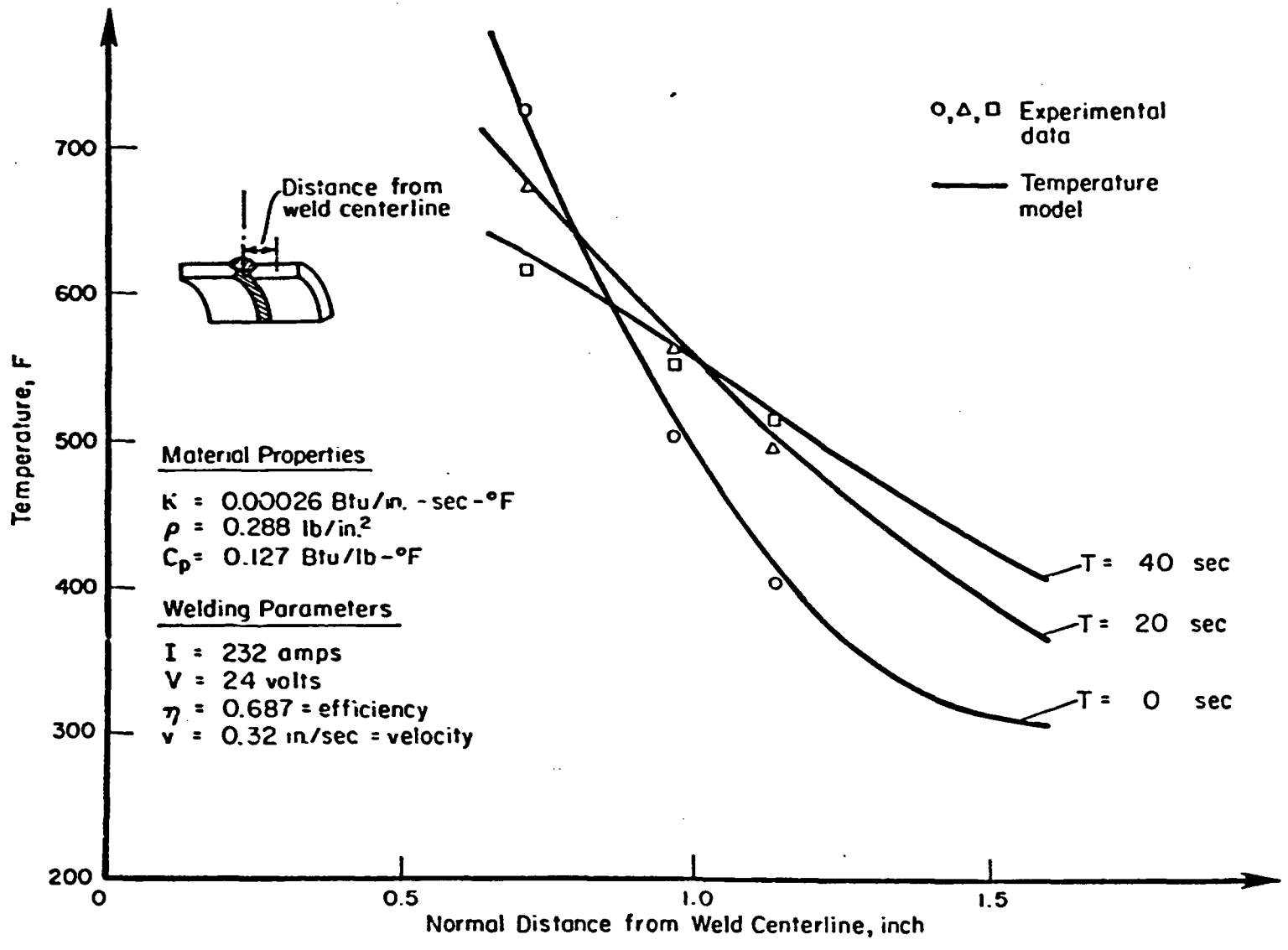

FIGURE 30. CALCULATED TEMPERATURE CURVES AND EXPERIMENTAL DATA POINTS FOR THE FOURTH PASS OF BCL MODEL NO. 3

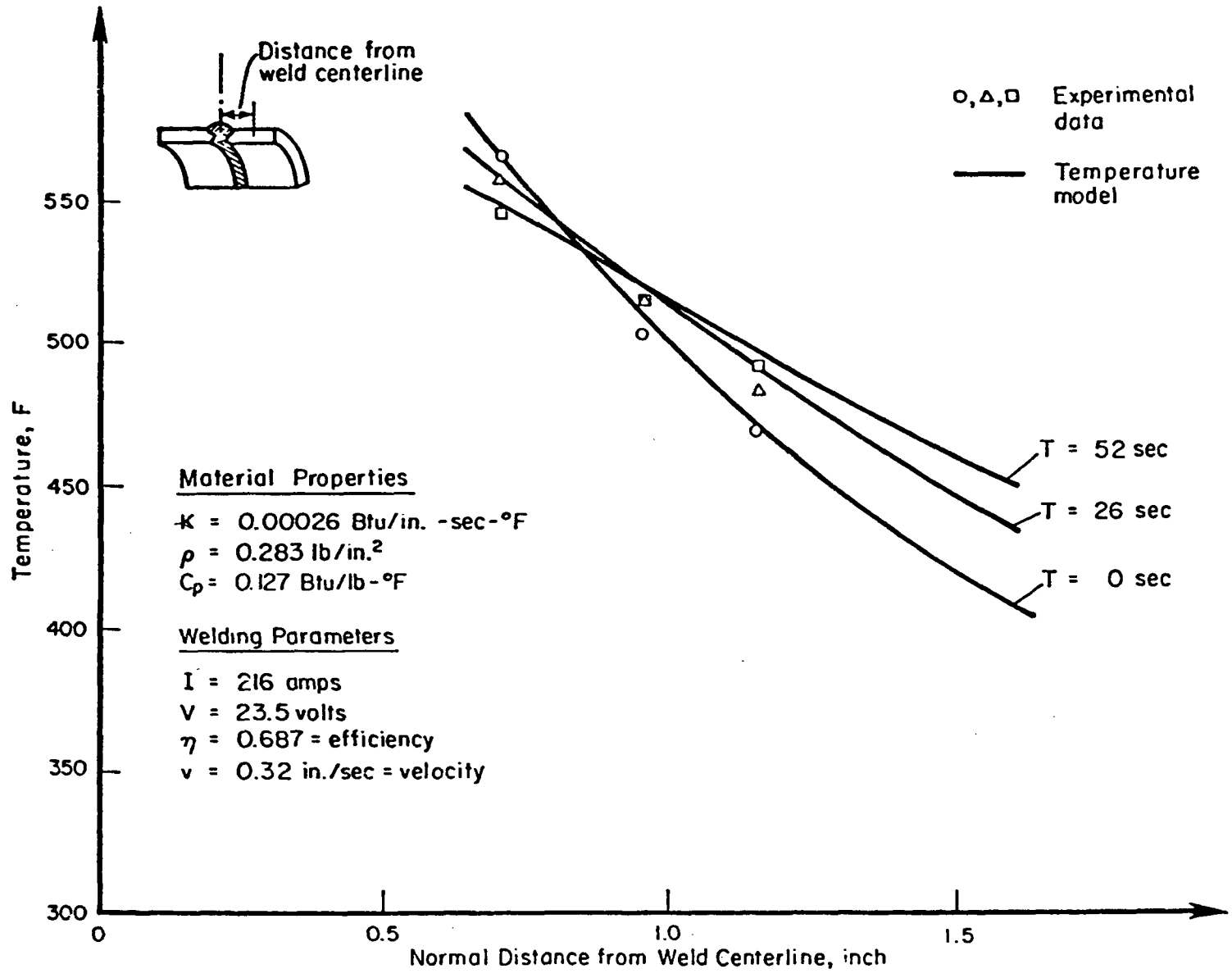

FIGURE 31. CALCULATED TEMPERATURE CURVES AND EXPERIMENTAL DATA POINTS FOR THE SIXTH PASS OF BCL MODEL NO. 3

For passes two and four, the temperature model deviated from the experimental data by no more than 7 percent. For pass six, the model data varied no more than 17 percent from the experimental data.

Comparisons between the temperature model and thermocouple data from BCL Model Number 2 are shown in Figures 32 and 33. Figure 32 displays comparisons for the gas tungsten arc root pass for the BCL Model Number 2 experiment while Figure 33 shows comparisons for the second and final gas metal arc pass. The smallest time value in each figure corresponds to the time at which the thermocouple nearest the weld centerline reached its maximum temperature. The deviation of the temperature model from the experimental data was no more than 9 percent for the first pass and no more than 17 percent for the second pass.

These six cases show good correlation between data and the temperature model. This, coupled with the fact that references cited in the related work section also found good comparisons between experimental data and a similar type of model, demonstrate that the model is a useful tool for obtaining time dependent temperature distributions due to welding.

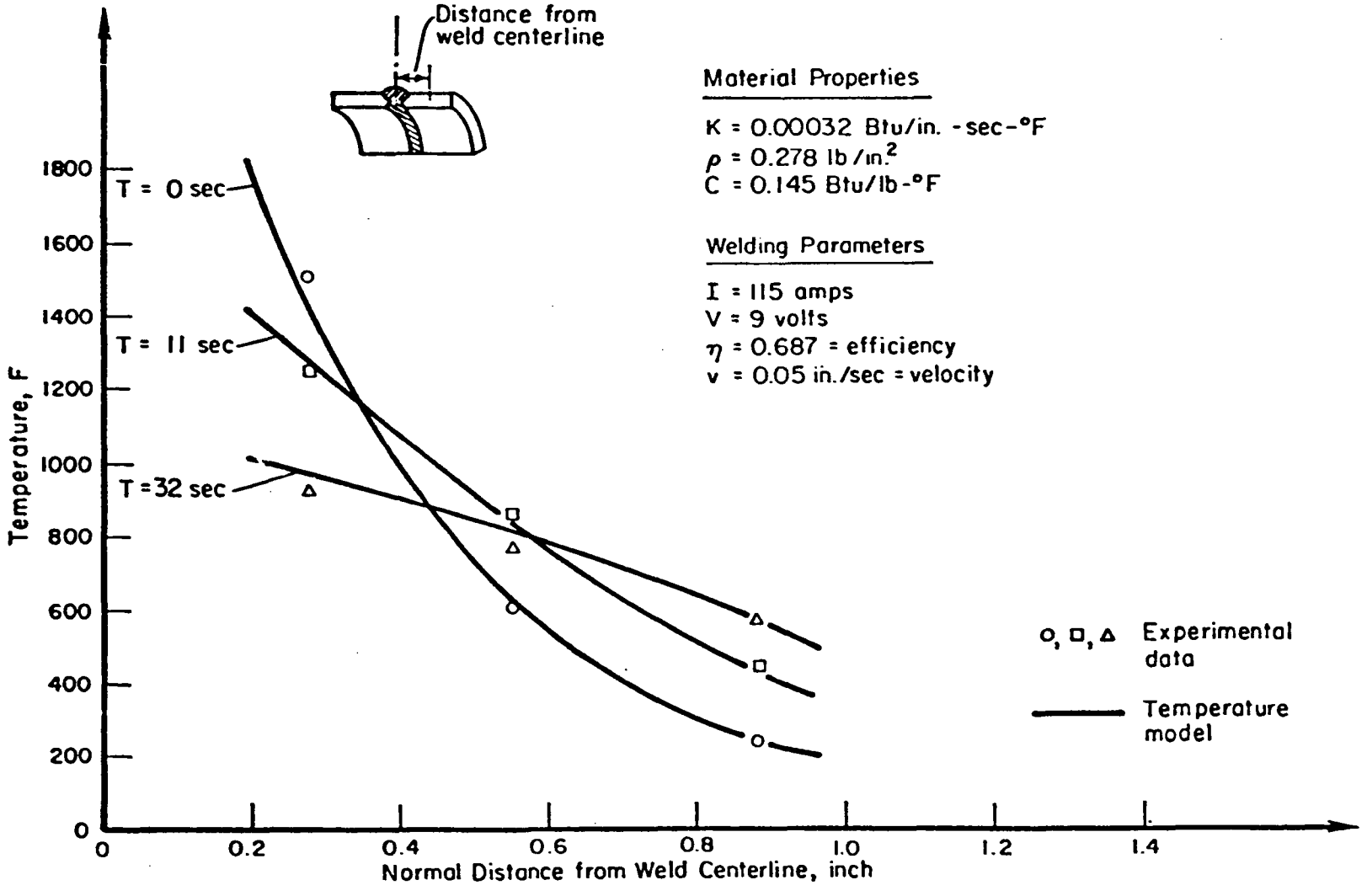

FIGURE 32. COMPARISON OF TEMPERATURE MODEL AND EXPERIMENTAL DATA FOR THE ROOT PASS OF BCL MODEL NO. 2

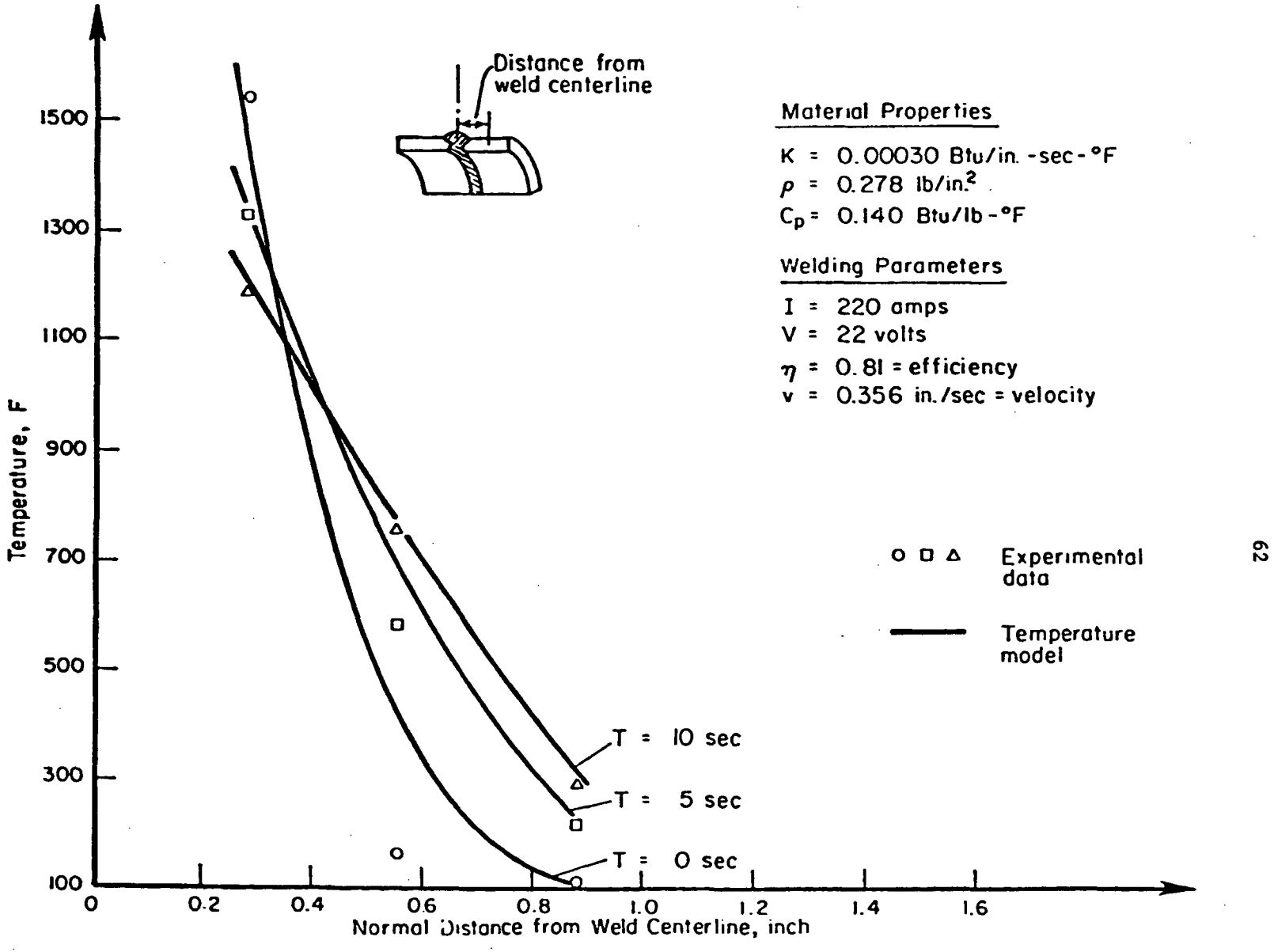

FIGURE 33. CALCULATED TEMPERATURE CURVES AND EXPERIMENTAL DATA POINTS FOR PASS 2 OF BCL MODEL NO. 2

V. STRESS ANALYSIS MODEL AND RESULTS

The purpose of the analysis phase of the program is to develop an analytical method or methods for the calculation of residual stresses at girth-butt welds. Before describing the stress analysis model, it is appropriate to examine some of the mechanics associated with the welding process. This will provide background for the description of the stress analysis model and the results. The following presents a discussion of mechanisms contributing to residual stresses at butt welds in plates. While the plate is different from the butt-welded pipe, the concept of stress producing mechanisms is the same.

Mechanisms Contributing to Residual Stresses at Butt Welds

Residual stresses at a welded joint result from the contraction of the weld bead and the plastic deformation produced in the base-metal region near the weld. The residual stresses are also influenced by external constraints.

A typical residual stress distribution at a butt weld is shown in Figure 34.[2] Figure 34b shows the distribution of residual stress σ_x along the direction normal to the weld direction. High tensile stresses occur near the weld region. These stresses decrease rapidly and become compressive at a normal distance several times the weld width.

The distribution of residual stress, σ_y, along a line parallel to the weldline will depend on the length of the weld, the welding parameters such as heat input, and velocity, and also the boundary conditions on the plate. For thin plates, this distribution will be constant through the thickness of the plate. For thicker plates, in which temperature gradients occur through the thickness of the plate, the residual stresses will also depend on the position in the thickness direction. If the edges of the plate are unconstrained, and the plate is thin, these σ_y stresses will generally be smaller than the σ_x stresses.

The distribution and magnitude of residual stresses at butt welds are determined primarily by the expansion and contraction properties of the weld and base metal and the yield strength versus temperature characteristics of the weld and base metal. The influence that these material properties have on the formation of residual stresses can be discussed in terms of the characteristics of stress distributions that occur during a butt weld.

...CALCULATED TEMPERATURE CURVES AND EXPERIMENTAL DATA
...POINTS FOR PASS 2 OF BCL MODEL NO. 2

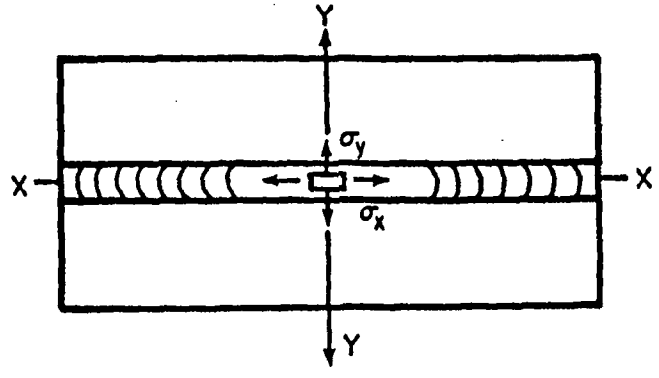

a. Butt Weld Stress

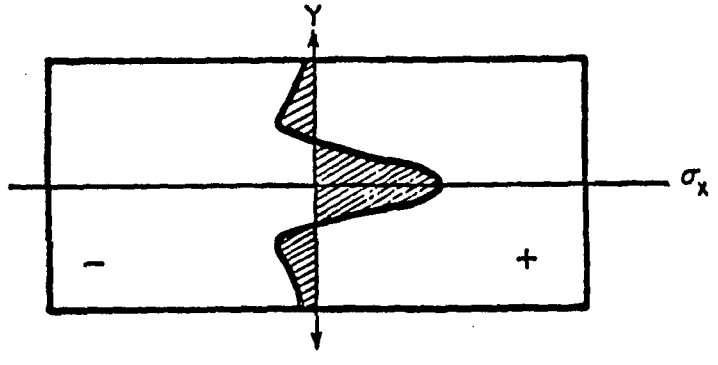

b. Distribution of Longitudinal Stress σ_x Along YY

FIGURE 34. TYPICAL RESIDUAL STRESS PROFILE AT A BUTT WELD (REFERENCE [2])

During initial weld heat up and prior to the time the torch passes section YY of Figure 34, severe temperature gradients about the weld line produce compressive yielding in the welding or longitudinal direction. As more heat is input by the arc, temperatures rise sharply and the yield strength of the molten base material approaches a negligible value. This small value of yield stress relieves the plastic deformations in the molten material. All the base material adjacent to the molten weld bead is in a state of plastic compressive stress. As the fusion zone metal solidifies, compressive yielding takes place because of the increase in yield stress. However, as further cooling takes place, the yield stress is increased to a level which causes elastic unloading from compression to tension. Thus, as cool-down continues, the portion of the weld metal in longitudinal tension increases until, at final cool-down, tensile longitudinal stresses can extend to several times the weld width, as shown in Figure 34b. Analytically predicted cooling and heating zones for BCL Model Number 2 are shown in Figure 35. Figure 35a depicts the zone boundary 5 seconds after weld solidification, while Figure 35b shows the boundary 34 seconds after solidification. Both of these figures illustrate that part of the plate is heating while simultaneously, another part is cooling.

The formation of hoop stresses in a girth welded pipe is similar to the σ_x stresses in the plate. However, there is a significant difference between the formations of axial stresses in the pipe and the σ_y stresses in the plate. The axisymmetric pipe geometry introduces bending deformations and stresses in the pipe. The deformations are visible as a diametal shrinkage in the weld region.

Description of the Stress Analysis Model

The process of joining two sections of pipe with multiple girth weld passes involves complex thermo-elastic-plastic material behavior in a three-dimensional geometry. Large deformations and plastic strains are prevalent throughout a large portion of the pipe material. Because the loading is due to transient thermal gradients, the loading is continually changing as the bead is put down and as the pipe again approaches thermal equilibrium.

As previously discussed, portions of the pipe are experiencing increasing temperature while at the same time other portions are experiencing decreasing temperatures. This complex thermal loading is particularly difficult to model

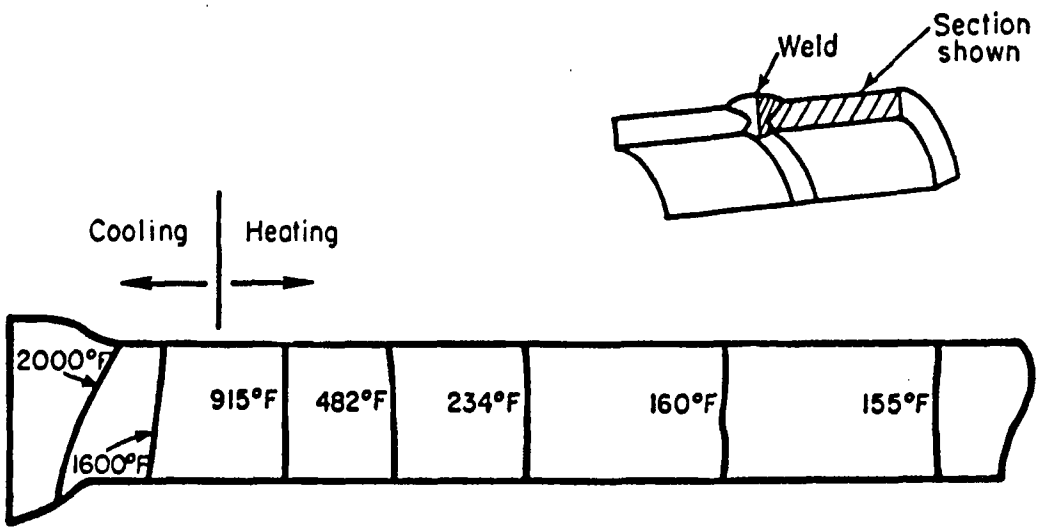

a. Heating and Cooling Zones at 5 Seconds after Solidification

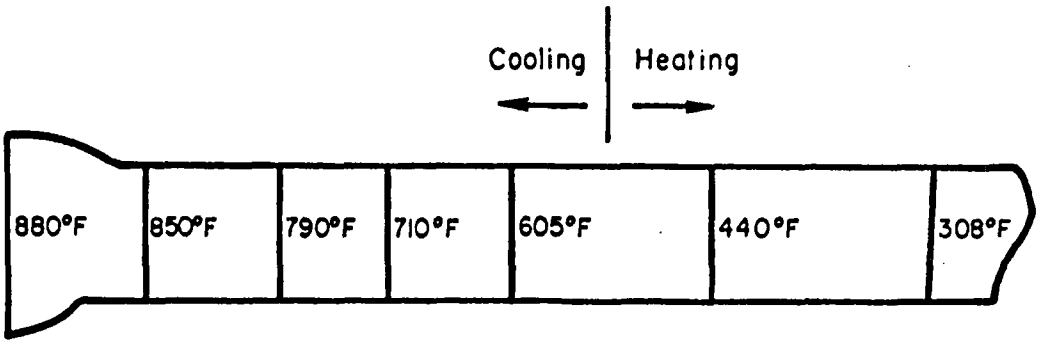

b. Heating and Cooling Zones at 34 Seconds after Solidification

FIGURE 35. CALCULATED HEATING AND COOLING ZONES FOR ROOT PASS OF BCL MODEL NUMBER 2

analytically because of the constantly changing principal stress directions at each point in the pipe. For an initial attempt at analytically modeling the girth welding procedure, the approach has been to make certain simplifying assumptions with the effect of emphasizing the more basic aspects contributing to the girth weld residual stress problem. Secondary aspects can be more efficiently studied after a basic understanding of the manner in which these stresses are induced is obtained.

One assumption which was made throughout this analysis was that the most important aspects of the girth weld procedure could be examined with an axisymmetric model. Other simplifications were made during the course of the study to reduce the computational costs. However, these were shown to have minimal effects on the results.

The finite element method was used to calculate residual stresses and displacements for given thermal loadings. A general axisymmetric finite element code was used. However, several modifications were required because of the unique nature of the girth-butt weld problem.

Finite Element Code and Modifications

General Description of the Finite Element Code

The analysis tool used in this study was a general purpose, two-dimensional thermo-elastic-plastic finite element computer program. The program uses constant strain triangles and quadrilaterals, which are an assemblage of four triangles, for the element stiffness formulation. The code allows temperature dependent material properties and a bilinear representation of the material stress-strain behavior. Because of the numerous unique aspects of modeling multiple pass girth-butt welds, several modifications were made to the finite element code.

Modifications to the Finite Element Code

Changes in the axisymmetric finite element computer program were made to include the capability to model elastic unloading from an elastic-plastic state of stress, as shown in Figure 36. The need to include unloading of the

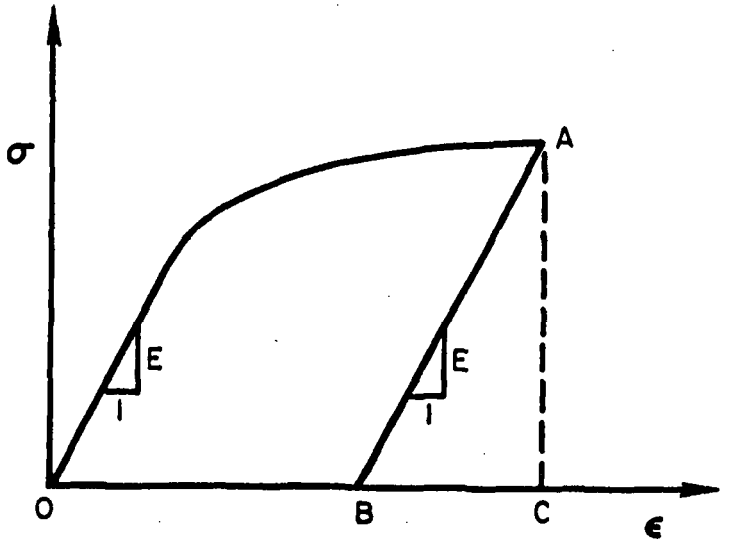

FIGURE 36. STRESS-STRAIN MODEL FOR ELASTIC UNLOADING FROM AN ELASTIC-PLASTIC STATE OF STRESS

type shown in Figure 36 arises because the stresses that occur near the weld early in the temperature cycle are reduced as the weld and base metal cool. Thus, finite elements in the heat-affected zone must permit a reduction in stress while maintaining a residual plastic strain. In the computer program, an unloading criterion is automatically checked at each element. The criterion is a reduction of equivalent stress between two consecutive load increments. If an element meets this criterion, then during the next load increment that element is assigned a stiffness based on the elastic material properties.

A numerical test case for unloading was conducted to demonstrate that the stress-strain behavior of the elements could follow the input stress-strain curve. A stainless steel with a yield stress of 32 ksi, a thermal expansion coefficient of 9.8×10^{-6}, a modulus of 27×10^{6} psi, and a modulus of 3×10^{6} above the yield stress was selected for the test case. A thermal load of 150 F was applied to a 1 x 3-inch steel plate of unit thickness in four load increments, and reduced to 92 F in four increments. All sides of the plate were rigidly clamped. The stress-strain behavior of a typical element during this loading history is shown in Figure 37, along with the theoretical curve for the stress-strain behavior. The agreement provides a check that the unloading capability is working.

The possibility of reloading after elastic unloading is also evident because of the use of multiple girth weld passes and, therefore, this capacity was also included. In making these modifications, no allowance was made for Bauschinger effects. The material was made to follow the virgin material stress-strain behavior regardless of the past loading and unloading history. The Von Mises equivalent stress and the equivalent plastic strain were used to relate the biaxial stresses and strains to the uniaxial stress-strain curve.

Another unique aspect of the girth-butt weld problem which required modifications to the finite element code, involves the method in which thermal loading is applied. Because molten material is applied to relatively cool base pipe, the stress-free temperature for the weld material is not the same as for the pipe material. The stress-free temperature for the weld material is that temperature at which the cooling weld material first gains strength and for the pipe material is the uniform ambient temperature existing before welding began. To allow this behavior to be modeled by the finite element code, required modifications so that different reference or stress-free temperatures could be given to different portions of the finite element model.

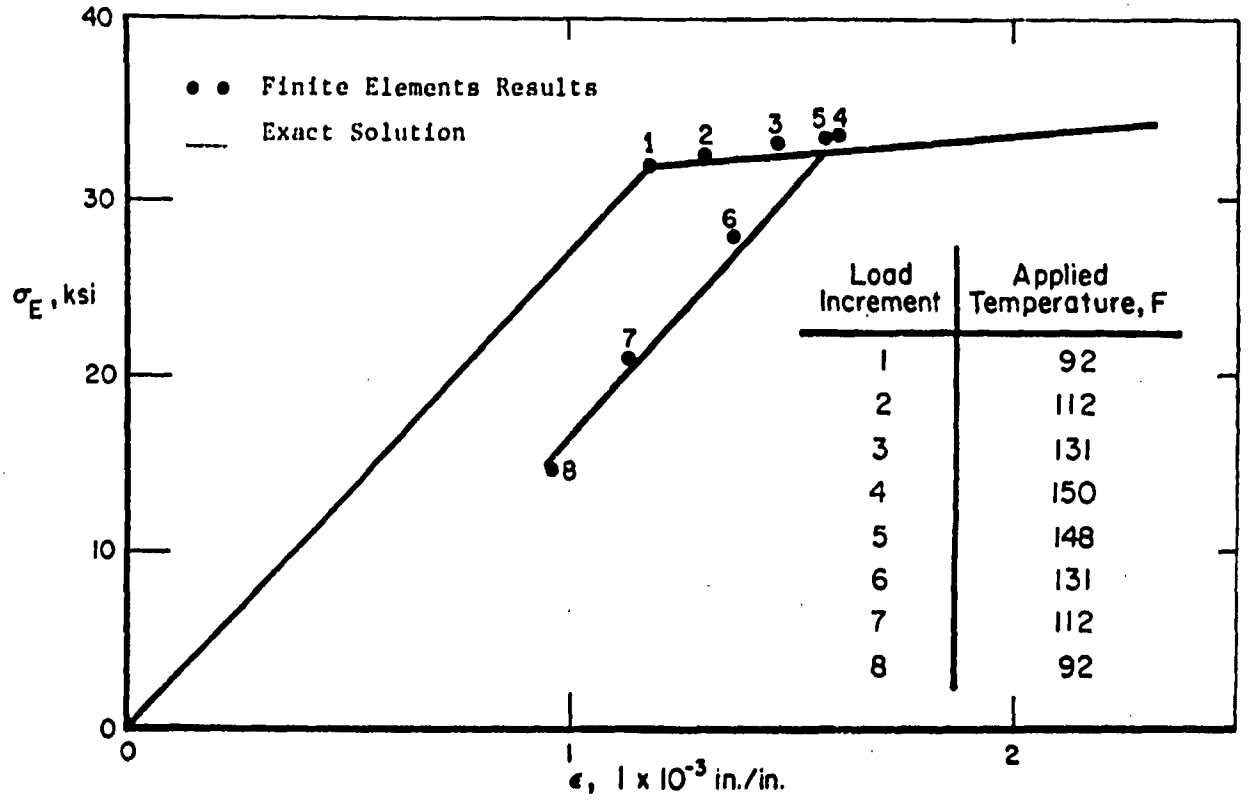

FIGURE 37. STRESS-STRAIN RESPONSE OF TYPICAL ELEMENT IN THE PLASTIC ZONE FOR LOAIDNG AND UNLOADING

As mentioned earlier, one major difficulty with modeling the girth weld process is that in actual welded pipe, the thermal loading is constantly changing. This transient nonproportional loading causes the principal stress directions at each material point to continually change with time as well as to periodically undergo loading, unloading, and reloading. To rigorously simulate this type of constantly changing load, requires many small incremental steps in the finite element solution so that the changes in temperature distribution and principal stress direction are small between increments. Experience shows that the change in the equivalent plastic strain for each solution should be only a few percent of the yield strain. It was determined early in this study that the number of analysis increments required to satisfy this condition is prohibitive. To simulate the temperature loading, while at the same time keeping the number of incremental solutions, and therefore the cost, at a reasonable level, it is necessary to approximate continually changing load temperature distributions by a piecewise linear representation. This type of approach is indicated in Figure 38. To be consistent with decreasing the number of piecewise linear segments, changes in logic of the finite element code were made to predict the stress change for the resulting large increments.

In simpler problems than the girth weld problem, the stress change predictor linearly extrapolates the results of the last load increment to predict when each e is going to reach yield. If the loading is proportional, and small amo.. f plasticity are occurring, this prediction can be made in terms of the changes in equilvalent stress without regard to the changes in the stress components. If, however, the loading is nonproportional or large portions of the model are deforming plastically, the principal stress directions will not remain constant from one load increment to the next, and the prediction for when yielding will occur, must be made based on all the stress components rather than just the equivalent stress. In the case of girth welds, both nonproportional loading and large plastic regions occur. In fact, the entire pipe cross section can become plastic with the plastic zone reaching to more than one pipe thickness in the axial direction.

As mentioned above, it was determined that piecewise linear approximations to the thermal loading was the way to approach the nonproportional loading problem because of the large decrease in the number of solutions and the resultant

Temperature Time History for an Arbitrary Point During the Application of One Pass

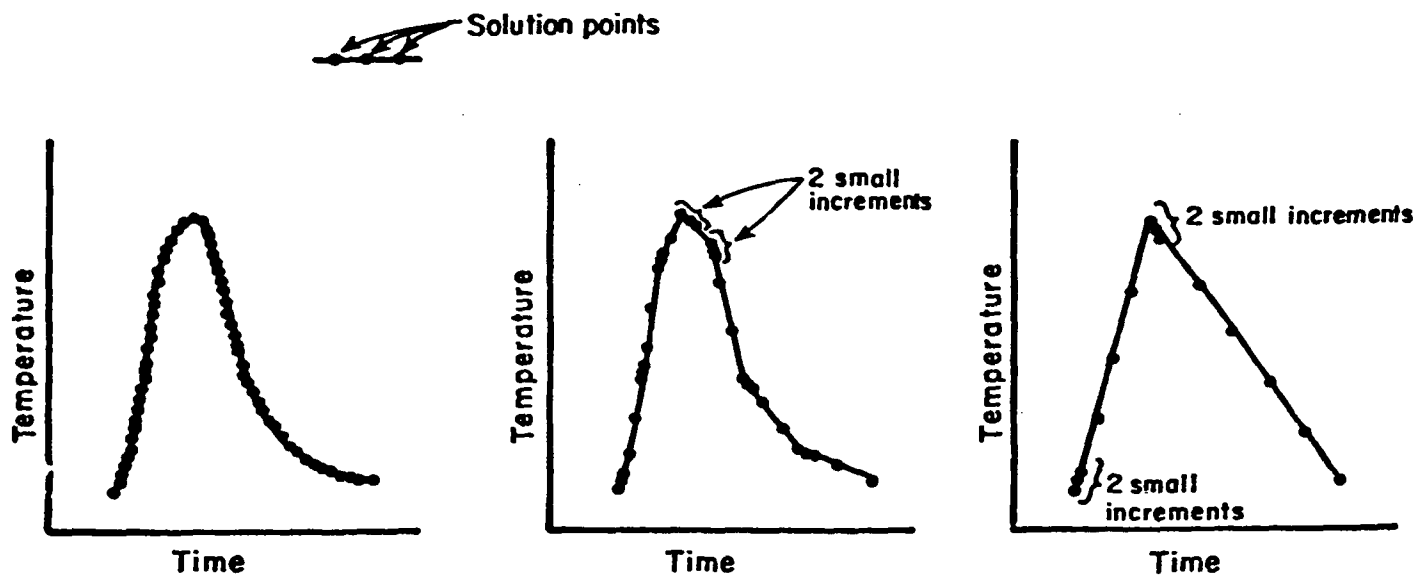

Rigorously follow the load history for each solution

Approximate the history with several piecewise linear segments

Approximate the history with two piecewise linear segments

FIGURE 38. COMPARISON OF THREE APPROACHES TO REPRESENTING NONPROPORTIONAL THERMAL LOADING

reduction in computational cost. As a result of this approach, because of the number of solutions, there had to be a corresponding increase in the size of the solution steps. With this increase in step size, the nonproportional loading, and the large amounts of plasticity, it was necessary to make the stress prediction portion of the finite element code more sophisticated.

The purpose of the stress prediction portion of the finite element code is to determine for each element what portion of the next load increment will cause loading, what portion will cause unloading, and for the loading portion, if any, what part of this loading will cause plasticity. Essentially, the method involves the determination of a path in four-dimensional stress space (axisymmetric assumption) which the element is expected to follow. This path is based on the change in stress components from the previous load step. The distance along this path that the stress state is expected to move is based on the assumption that a similar change in load, as applied in the previous load increment, will cause a similar change in stress state. Based on this predicted path, it can be determined what portions of the next step will be loading and what portion will be unloading and furthermore what portion of the loading will be plastic. This information is then used in the element stiffness formulation.

A simplified two-dimensional example in which the three principal stress directions remain constant and the third principal stress magnitude remains constant is shown in Figure 39. If the stress state at a point in the body is expected to move from C to B, then the material at this point will unload while going from C to A and load while going from A to B. Furthermore, the loading from A to D will be elastic while the loading from D to B will be plastic. If the stress state is expected to move from C to E, then there will be both unloading and loading but no part of the loading would be plastic. It should be noted that the equivalent stress did not reach zero before starting to reload.

The method of predicting the change in stress state based on piecewise linear changes in the thermal loading, requires that upon the change from one linear segment to the next, that two very small increments be taken. These are shown schematically in the second and third curves of Figure 38. The purpose of the first increment is to determine for each element of the model, whether the new linear segment of loading is going to cause loading or unloading. The second step is required in order to determine the direction of the stress path

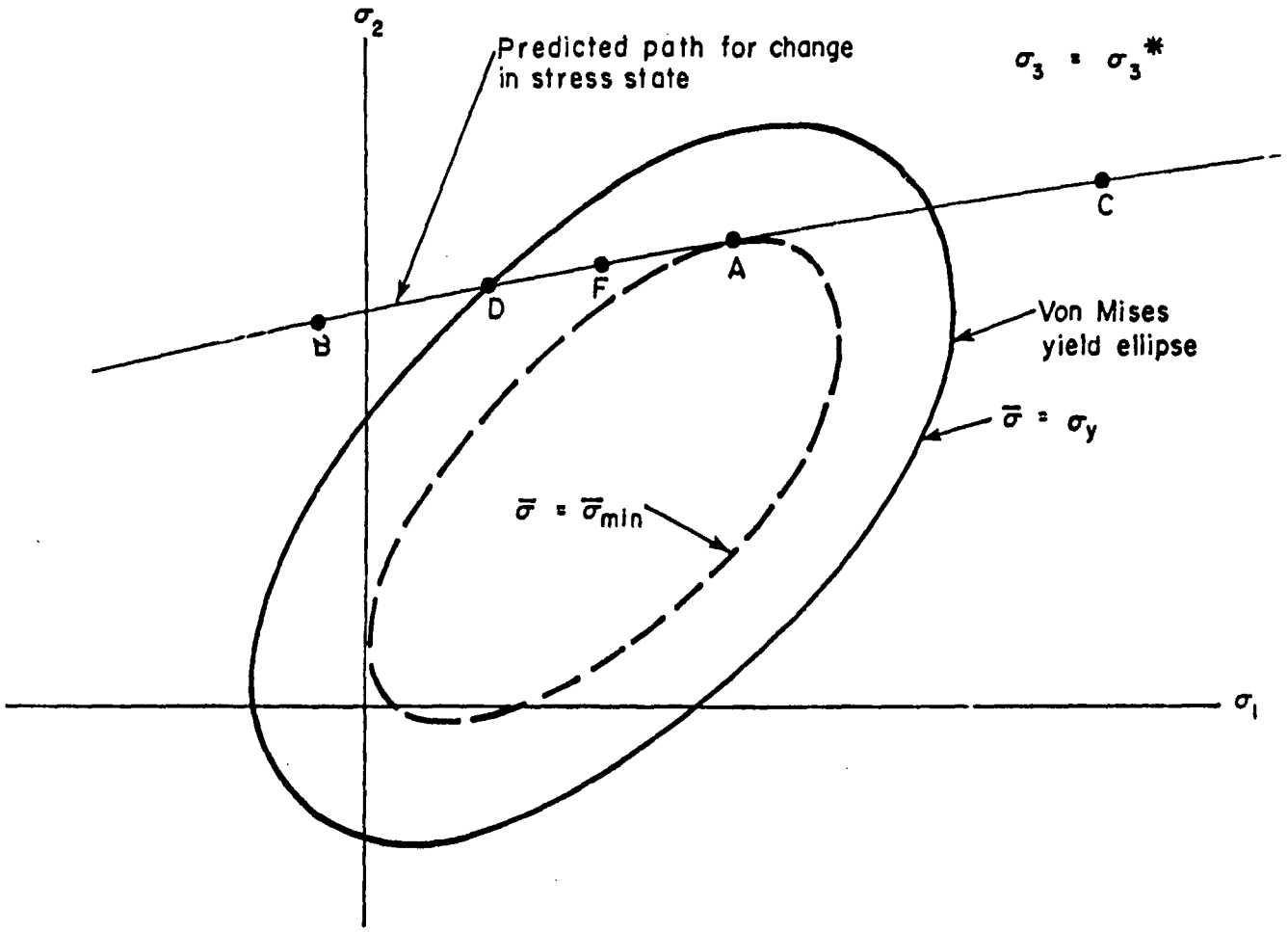

FIGURE 39. EXAMPLE OF MODIFIED STRESS PREDICTOR LOGIC FOR NONPROPORTIONAL LOADING

for each element. The size of these increments must be such that the calculated incremental stress, strain and displacements be negligible compared of the sum of these quantities for the previous increments.

Another important aspect of the computer program which is affected by the size of load increment is the incremental plasticity formulation. The size of load increments here is measured in terms of the change in stress or plastic strain during that increment. The material's elastic-plastic constitutive relations and thus the stiffness are dependent on the stress state. Experience shows that the conventional incremental plasticity formulation requires that the change in plastic strain between increments be less than a few percent of the yield strain. If large incements are taken, the resulting calculated stress/strain state will be in error with the evidence of this being that the stress and strain states do not correspond to a point on the material's stress/strain curve. Because the strains which are experienced over a large portion of the girth weld region are as high as three and four percent, the number of increments required to allow these small increments to be taken would be prohibitive. For example, based on a ten percent criterion, this would require approximately 200 increments per pass. Therefore, the standard plastic stiffness formulation was modified to reduce the number of increments per pass.

Basically, the change in the stiffness formulation was done for economic reasons and involved generating the stiffness independent of the stress state in a similar manner as for elastic material behavior. While it is understood that this formulation is not valid, it was shown that the errors in applying this formulation numerically are much smaller than those that are obtained by using the usual plastic formulation with increments which result in incremental plastic strains as large as twice the yield strain. Another factor, which further justifies the use of this modified plasticity formulation, is the inherent difficulty in using the standard incremental plasticity approach for nonproportional loading.

Approach to Modeling Girth-Butt Welds with Finite Elements

Simplifying Considerations

In addition to the axisymmetric simplification of the girth-butt weld program, several additional simplifications were examined. One which was included primarily because of the reduction in computer costs, was treating the girth-butt weld procedure as being symmetric about the plane which is perpendicular to the axis of the pipe and passes through the center of the weld bead. This resulted in a computer cost savings of approximately 50 percent. Closely related to this simplification and in part resulting from it, was the modeling of a sequence of weld passes as a layer rather than as individual weld passes. The savings resulting from this simplification is dependent on the pipe size and number of passes, with the savings being greater for pipes with more passes. The method of modeling a general multipass girth-butt weld under these two assumptions is shown in Figure 40.

Boundary Conditions

Since the cost of analyzing a girth-butt weld is dependent on the size of the finite element model which is used, it is desirable to model a minimal length of pipe in the axial direction. On the other hand, the stresses and displacements in the weld region will be effected if too little of the pipe in the axial direction is modeled. It was found that significant stress and displacements were still present as far as four thicknesses from the centerline of the weld in the axial direction. Therefore, to ensure that the boundary conditions at the remote end of the finite element model had little effect on stresses and displacements near the weld region, the finite element models were made to extend to approximately eight times the pipe's wall thickness. This rule of thumb, however, becomes more conservative as the pipe thickness increases. This is because the heat input for applying girth weld passes is not increased proportionately with the pipe wall thickness. To approximate the effect of the remainder of the pipe at this artificial boundary, all the axial displacements at this cut off end were constrained to the same value. This value of displacement was calculated as part of the finite element solution so that it produced a zero net axial force condition.

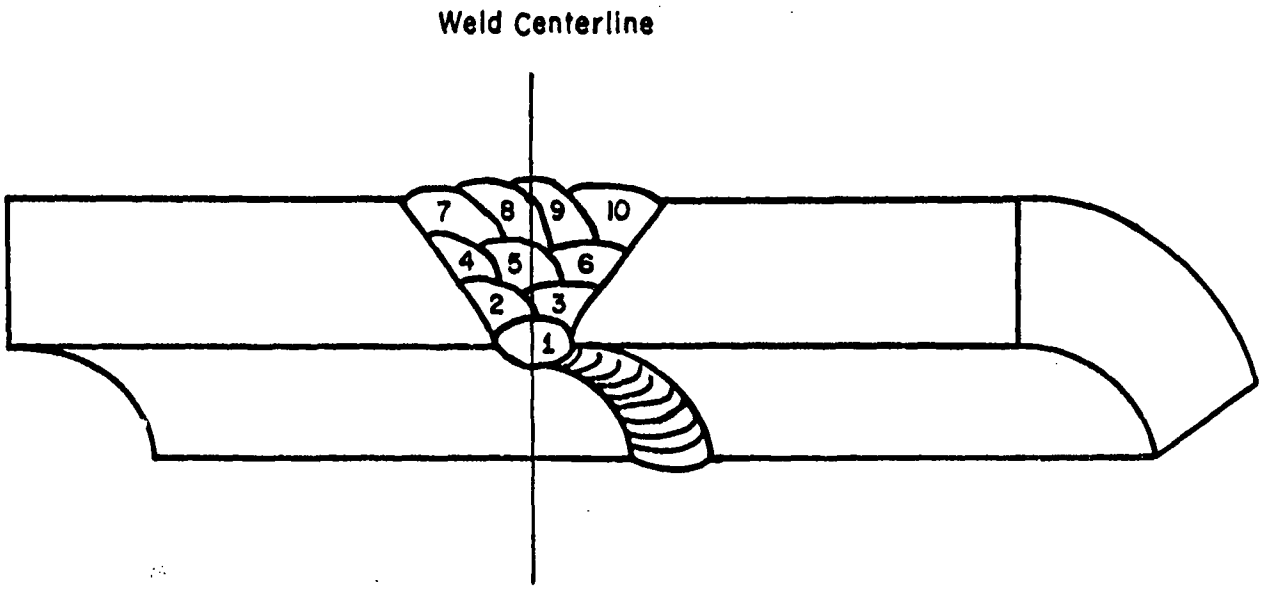

a. Weld Cross Section Geometry with Ten Passes

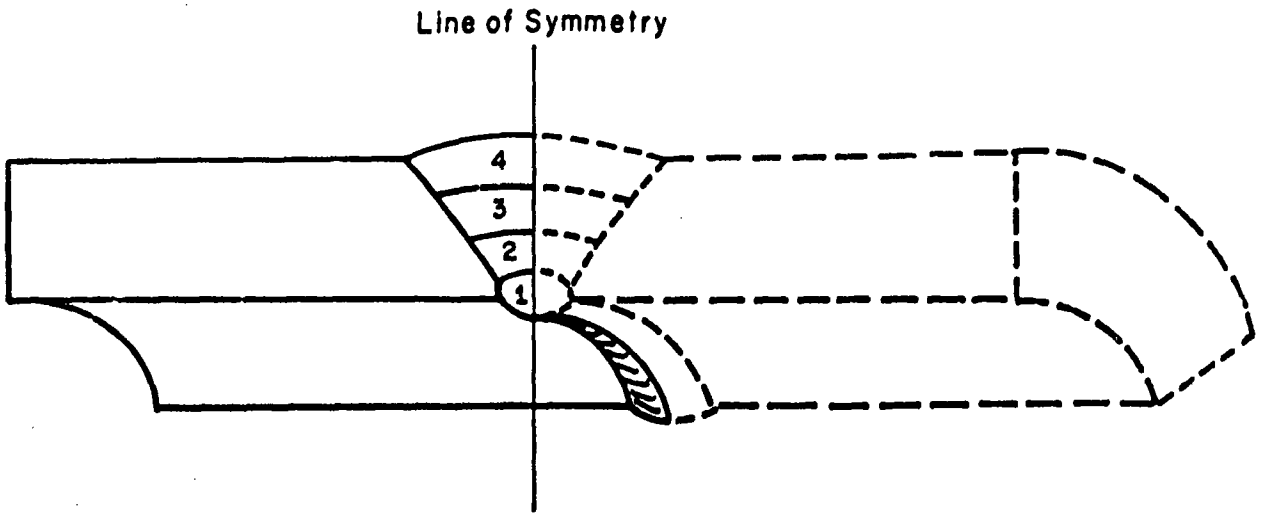

b. Model of Weld Cross Section Geometry Using Four Layers

FIGURE 40. COMPARISON OF ACTUAL AND MODEL WELD CROSS SECTIONS

Using the simplification of weld centerline symmetry, requires special boundary conditions at the centerline boundary of the model. This type of symmetry requires that the only nonzero component of displacement at this boundary be the radial component.

Temperature Dependence of Material Properties

All of the girth welds modeled in this study were fabricated from 304 stainless steel. Since the material temperatures during the girth weld procedure can vary anywhere between room temperature and the melting point, the temperature dependence of 304 stainless steel material properties was an input for the analysis. Figure 41 shows the temperature dependence of the material properties as they were used in the finite element analyses.

Analysis Procedures

Modeling of Thermal Loads

As mentioned previously, the problem of transient thermal loading was simplified by approximating the change in temperature distribution by several piecewise linear changes. Associated with this technique of approximating the changes in temperature distribution is the problem of deciding how many linear changes can be used and how they can be placed in time so as to most closely approximate the actual temperature changes. The criterion by which the placement of the piecewise linear changes was evaluated was based on the resulting calculated residual stresses.

A sensitivity study was conducted for the two-pass BCL Model Number 2 pipe to determine the effect of the placement and number of linear changes. The number of linear segments was varied from one per pass to nine per pass. It was found that the calculated stresses are most sensitive to changes in the temperature distributions corresponding to the first fifteen seconds after the bead is put down. This corresponds to fifteen seconds after the heat source passes. It was also found that greatly reducing the number of linear changes after the first fifteen seconds had relatively little effect on the final calculated residual stresses. In fact, it was later found that the results from

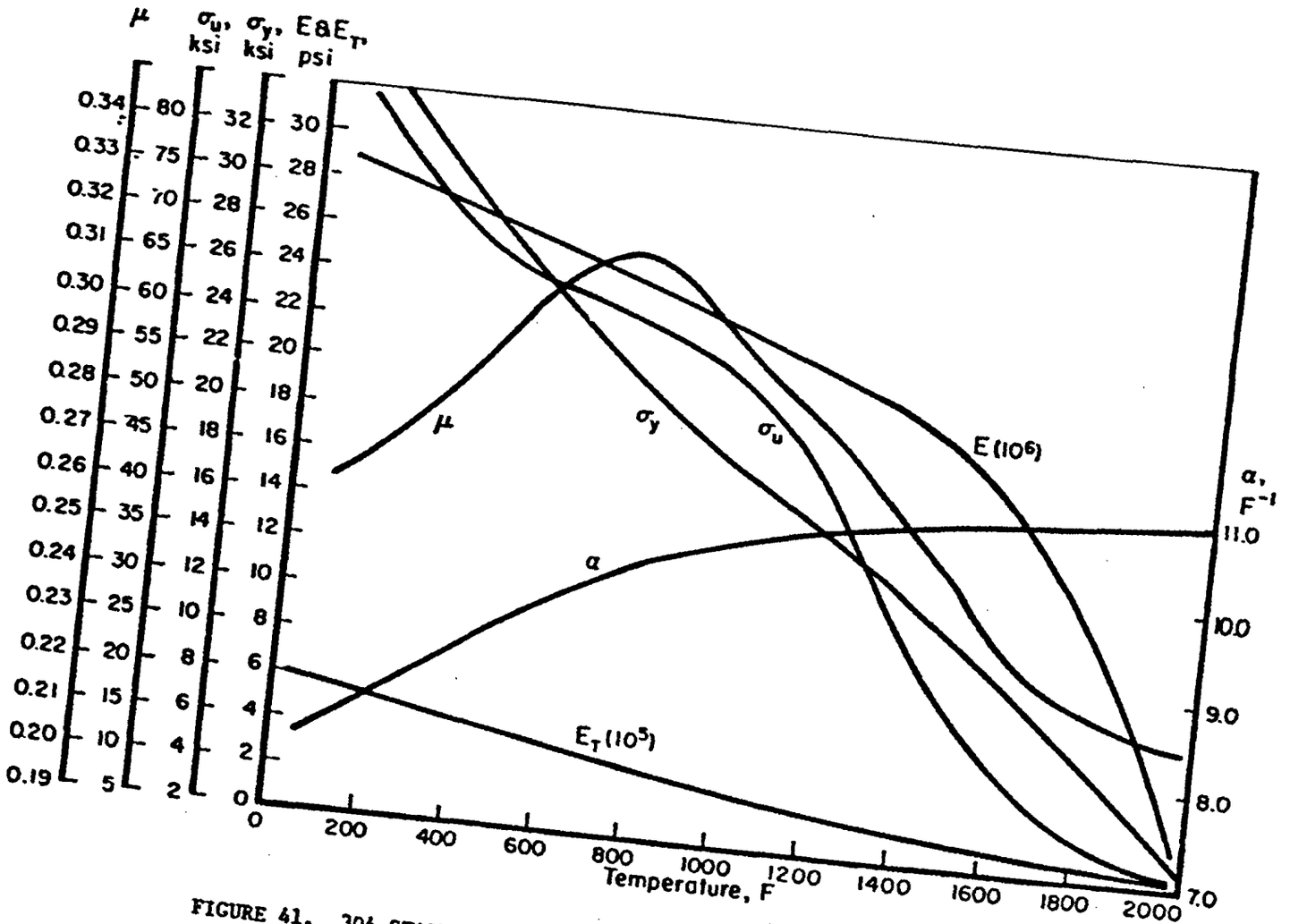

FIGURE 41. 304 STAINLESS STEEL TEMPERATURE DEPENDENT PROPERTIES USED FOR FINITE ELEMENT STRESS ANALYSIS

using one linear change in temperature to represent the heating phase and one to represent the cooling phase of each pass application were in good agreement with experimental measurements.

Based on the basic discovery that good residual stress calculations could be made using only a heating phase and a cooling phase to represent the thermal loading, two fundamentally different approaches were considered. One approach essentially assumed that at some time during the transient thermal loading, a "most severe" distribution occurs which is the prime factor determining the final residual stress state. The second approach differed in that the effect of temperature distributions throughout the time of thermal transients would be included. Two possible variations on this second appproach are (1) to take the time average of the change in temperature at each material point and (2) to take the maximum temperature change at each material point. During this study, both the first approach and the second variation of the second approach were evaluated. Figure 42 shows a comparison of temperature prifiles for these two cases. For the first approach, temperature distributions corresponding to specific times were chosen from the time temperature history of the pass being laid down. To determine the sensitivity of the residual stresses to the selected time, stresses were calculated for the distributon corresponding to temperatures between 1500 F and 2100 F. It was found that the calculated stresses for these various times and corresponding weld bead temperatures did not differ greatly. It was, therefore, decided that the distribution corresponding to 2100 F would be used because this temperature corresponds to the point at which the cooling weld material starts to gain significant stiffness.

The thermal loads were specified for the finite element code in terms of element centroid temperatures, the element's stress-free temperature and the temperature dependent coefficient of thermal expansion. The finite element program then determined the change in temperature for each element at each incremental solution, obtained the coefficient of expansion corresponding to the element temperature by interpolating in the material property table, and combined the two quantities to formulate the thermal loads.

Modeling the Deposition of Weld Metal

Because of the addition of material during the girth-butt weld process, the finite element model must in some way account for the resulting change in weld region geometry. In order to accommodate the automation of the analysis,

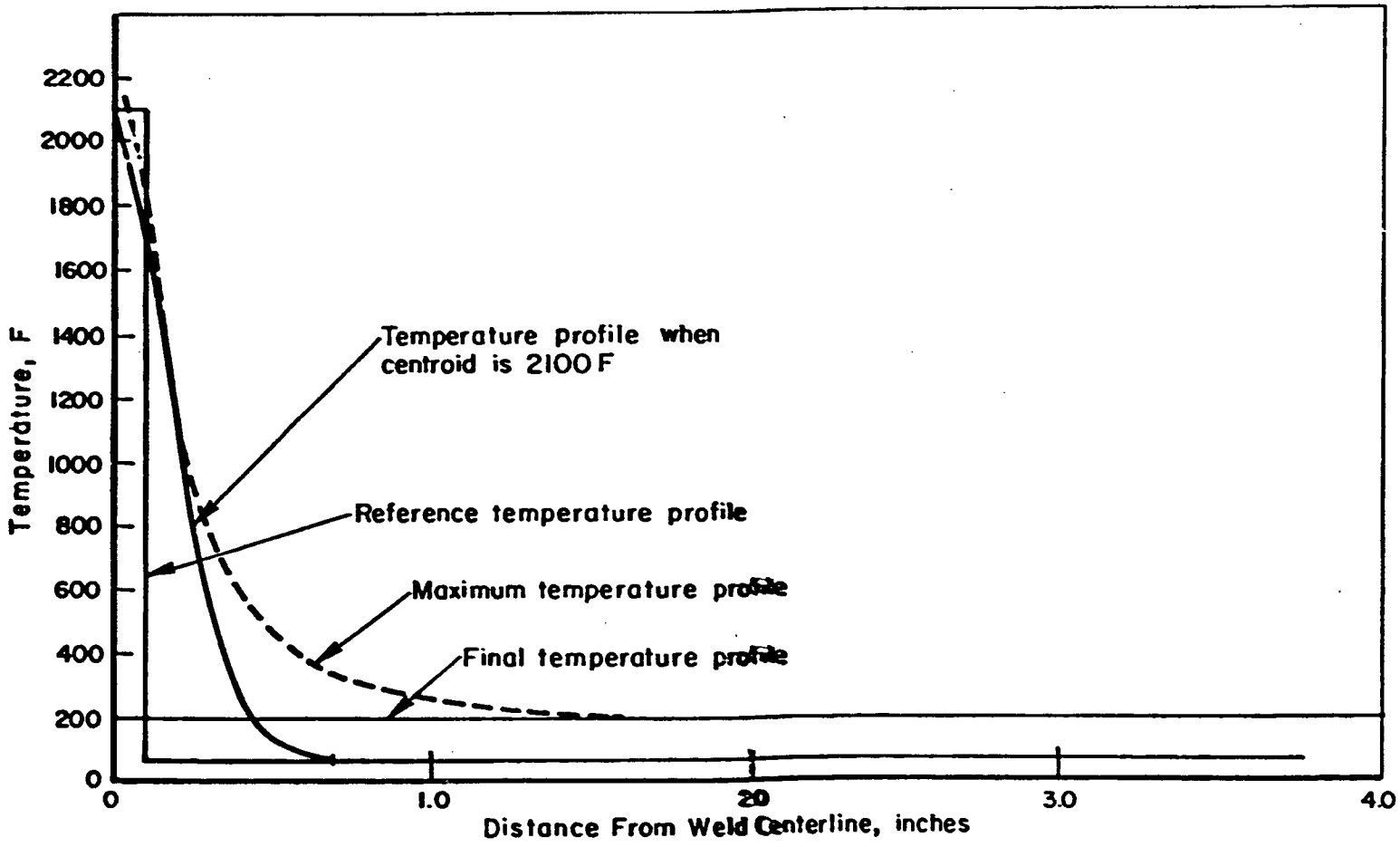

FIGURE 47. COMPARISON OF MAXIMUM TEMPERATURE PROFILE AND TEMPERATURE PROFILE AT TIME CORRESPOND TO 2100 F AT THE PASS CENTROID

it is desirable to have the elements representing all the weld passes in the model for all pass applications regardless of whether or not the material which they represent has been deposited. To do this, advantage was taken of the fact that the loading is thermally induced, that the element stresses are proportional to the element stiffness, and that the stiffness becomes very small for elevated temperatures. The scheme by which these were used is shown in Figure 43. Basically, this scheme causes the effect of passes which have not been laid down to be negligible in terms of their affect on stresses in other portions of the pipe. Since the stresses in the elements representing passes which have not been deposited are very small (because of the small stiffness), the error in the final residual stresses due to these passes will also be small. Though the method described resulted in negligible errors in terms of stress, the effect on calculated strains in these passes was not small. However, since strains in this region were of no interest and since these errors did not affect the stresses elsewhere, this error was tolerable. If strains were of interest, then the strain components for each pass, except the first, could be zeroed before that pass was laid down in the modeling procedure. This would require a slight modification to the finite element code.

Modeling of Weld Pass Layers

It was mentioned previously that because of economic considerations, the simplification of using weld center line symmetry for the analysis made the modeling of weld layers rather than individual weld passes attractive. This simplification allows the application of several passes at one time and, therefore, results in a computer cost savings. The more passes that are contained in one layer, the larger the saving becomes. However, it is possible that the accuracy of using these assumptions is largely dependent on the thickness of the pipe which is being welded.

Generally speaking, for thin-walled pipes, only a few passes are required. For such pipes, the weld centerline and weld layer simplification can model the actual weld pass geometry. Figure 44a is a representation of a girth-butt weld for a thin-walled pipe. For this case, the geometry and temperature distributions will be symmetrical about the centerline throughout the weld process. The layer simplification is trivial in this case since each layer contains only one pass.

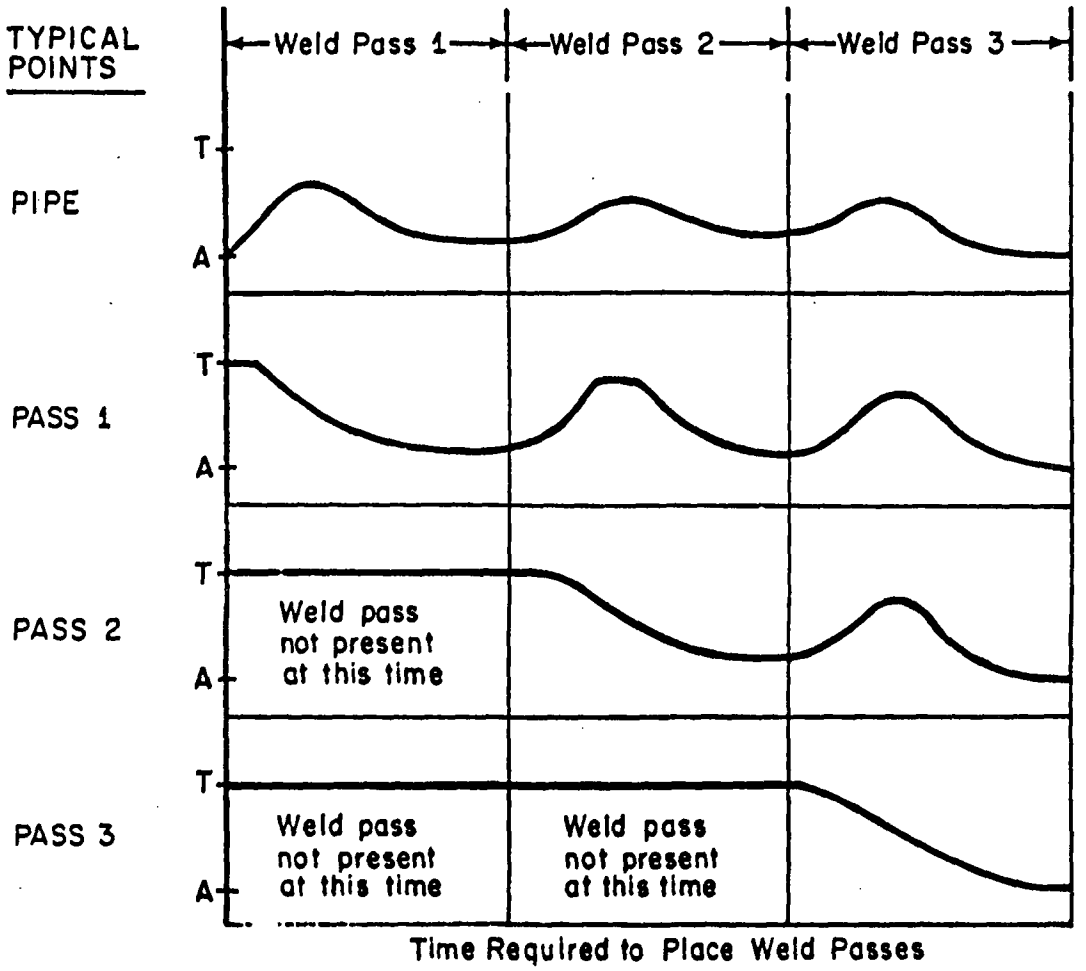

T - Temperature at which stiffness of 304 stainless steel becomes negligible

A - Ambient temperature

FIGURE 43. METHOD OF MODELING WELD PASS PLACEMENT BY THE FINITE ELEMENT MODEL

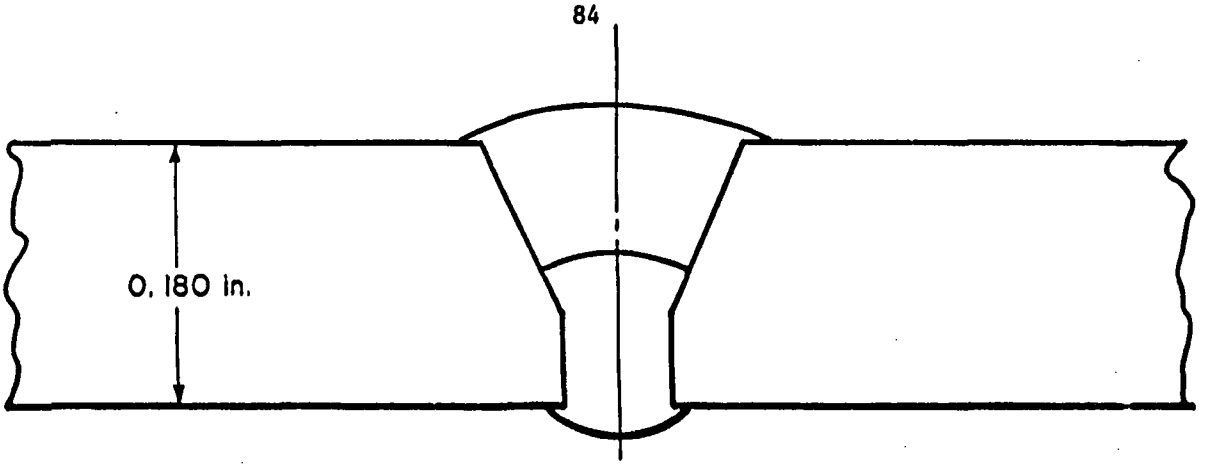

a. Two-Pass Weld: One Pass Per Layer

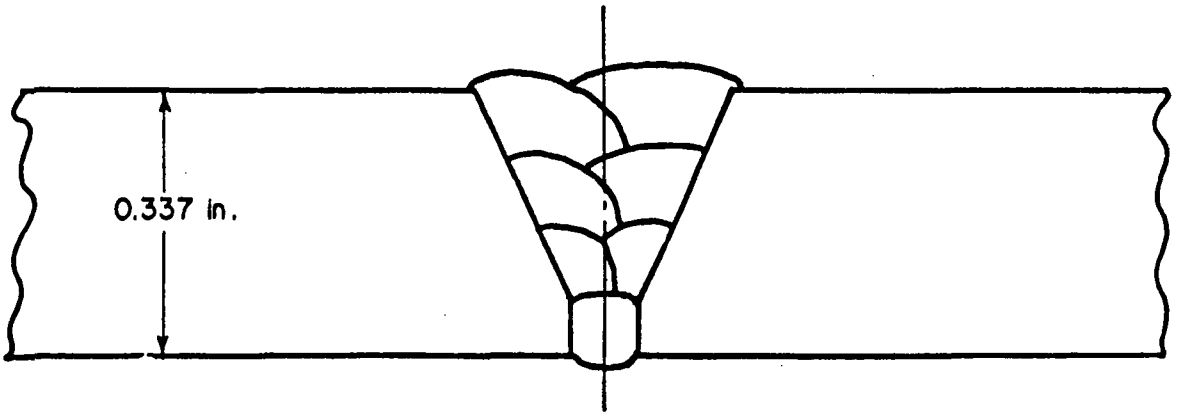

b. Seven-Pass Weld: One or Two Passes Per Layer

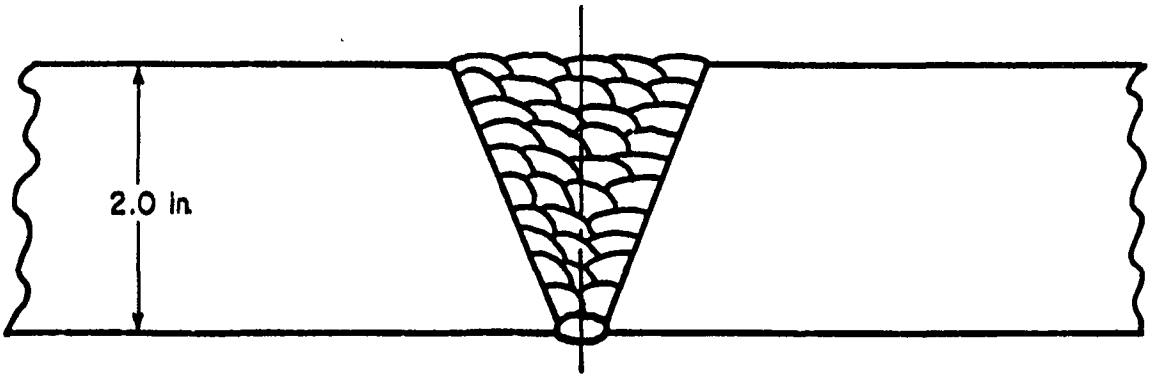

c. Thirty Eight-Pass Weld: One to Five Passes Per Layer

FIGURE 44. EFFECT OF PIPE SIZE ON GIRTH WELD GEOMETRY AND MODELING SIMPLIFICATIONS

For medium thickness and thick pipes, the number of weld passes increases so that more than one pass is required to make one layer. Figures 44b and 44c give examples of these pipes. For this size of pipe, the centerline symmetry and layer simplifications are not real. However, as long as the temperature distribution in the model is nearly the same for each pass of the layer, the layer assumption is good. Figure 45 illustrates how the temperature distributions for thin and medium walled pipes make the layer simplification feasible.

For heavy-walled pipe, in which there are typically more than three passes in each layer, the temperature distribution resulting from the left most pass of a layer can differ substantially from that of the right most pass. This type of behavior is shown graphically in Figure 45c. In this case, the layer assumption does not give as good an approximation to the temperature distribution as for the seven-pass weld of Figure 45b.

The reason for this is primarily the relative size of the weld passes and the pipe thickness. As the pipe size increases, the weld pass size cannot increase proportionately; therefore, the relative distance between the pass centroid and the weld centerline increases. Another result of the relative decrease in pass size and associated heat input, is that the temperature gradient in the axial direction becomes greater for the thicker pipe. This is because the heat can dissipate radially in addition to axially. Based on this, it might be contended that the usefulness of the layer simplification may decrease as the pipe size and number of passes increase. However, this may not be the case because for a large number of passes, the amount of material per layer will be small compared to the amount that has been layed down. Thus, the concept of a layered model may still be very useful.

Additional Modeling Considerations

Modification of Thermal Loading for Multipass Layers

Due to the simplification of modeling layers of passes, some questions arise on how well the actual thermal loading should be represented. In the simpler cases such as shown in Figure 45a and 45b, the largest possible discrepancy in using the temperature distribution resulting from the pass being at the centerline is the difference between the solid and broken lines. For larger pipes, however, the discrepancy tends to increase.

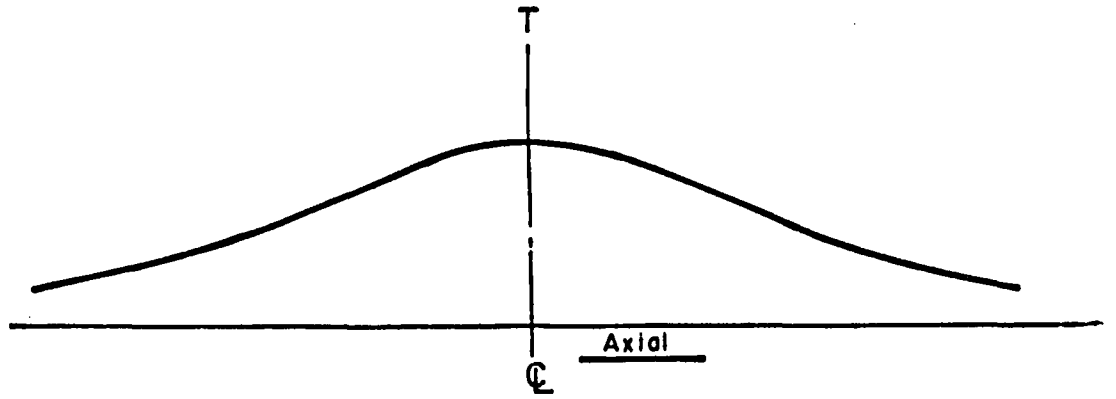

a. Two-Pass Weld: One Pass Per Layer

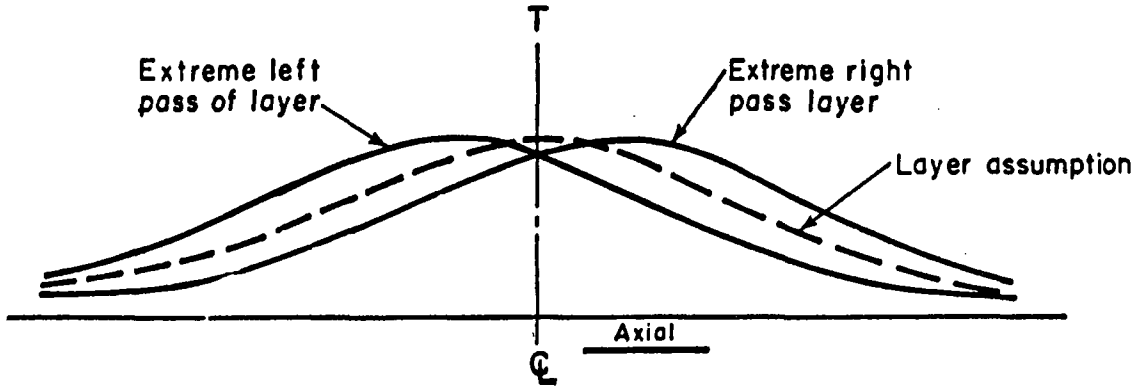

b. Seven-Pass Weld: One or Two Passes Per Layer

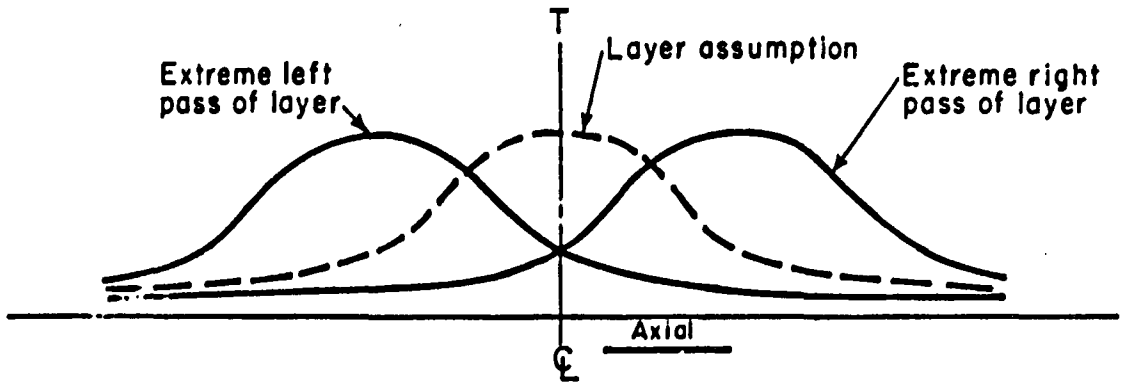

c. Thirty-Eight Pass Weld: One to Five Passes Per Layer

FIGURE 45. THE EFFECT OF PIPE SIZE ON TEMPERATURE DISTRIBUTION AND MODELING SIMPLIFICATIONS

To help rectify these discrepancies, two methods have been identified. The first method consists of placing several heat sources throughout the layer which is being modeled. The total heat input is close to that which was actually used for one pass, but instead of being concentrated at the centerline, the heat is applied over the entire layer. This tends to widen the bell of the bell shaped temperature distribution. A possible alternative to this approach would involve generating a family of distributions (one on each pass) such as in Figure 8c and then use the envelope of these curves for the temperature distributions. This, unlike the previous method, would essentially involve more energy than is put into any one of the passes of the layer. It would, however, involve much less than the sum of the energies for each of the passes. This representation was used for the thirty-pass weld analysis to be described later.

Method for Including Large Displacements

The analysis of girth-butt welds involves large deformations. To incorporate the effect of large deformations into the girth-butt weld model, the geometry of the model was updated after each incremental solution. Specifically, this was done by adding to each nodal point coordinate its corresponding incremental displacement. Using this technique enabled good correlations to be made with experimentally determined residual displacement patterns while each incremental solution could be obtained under the assumptions of small strain theory.

Modeling BCL Experiments, Two-Pass Weld

The experimental girth welded 304 stainless steel pipes were fabricated and residual stresses at the inner and outer surfaces determined. These experiments and the measurements taken are described in the weld experiment section. One experimental pipe was a 12.75-inch O.D. by 0.180-inch wall with a two-pass weld including the root pass. The other pipe was a 12.75-inch O.D. by 0.375-inch with a six-pass weld, including the root pass. Both of these experimental pipes were modeled analytically.

In this section, the modeling of the two-pass pipe is discussed. This pipe was used for most of the sensitivity studies rather than the six-pass pipe because of the fewer number of passes.

The finite element grid which has been generated for the two-pass pipe (BCL Model Number 2) is shown in Figure 46. The finite element model has 212 elements and 243 nodes. Calculations for the model included elastic-plastic material behavior with strain hardening and all the material properties were included as functions of temperature as shown in Figure 41.

Temperature Calculations

The temperatures which were used in the stress anlaysis model, were the only means of loading. The centroids of the elements for the finite element model were inputs for the temperature analysis model along with the welding parameters for the pass and the time at which the temperature distribution was selected. The welding parameters used for this model are shown in Table 8.

Residual Stress Calculations

In order to assess the sensitivity of the calculated stresses to the manner in which the thermal loading was applied, several different techniques were used. These are based on different reference temperatures and different ways of representing the intermediate temperature.

The Effect of Reference Temperature. One aspect of the analysis which was considered, was the effect of using two reference temperatures to depict that the new weld bead is cooling from another state while the rest of the material is being heated from the ambient temperature. The reason for needing two reference temperatures is clear from the description of the physical problem. However, the problem of applying this approach to a weld which cannot be sectioned for study is not known. Since knowledge of the size and location of the weld puddle is necessary to apply the two reference temperature technique, a study to determine the sensitivity of the stresses to neglecting this aspect of the problem was conducted.

One analysis was made in which only one reference temperature was used. This one reference temperature corresponded to the actual reference temperature of the pipe material. The other analysis assumed that the weld material had a reference temperature of 2100 F. For these anslyses, one temperature distribution corresponding to the time at which the weld material had cooled to

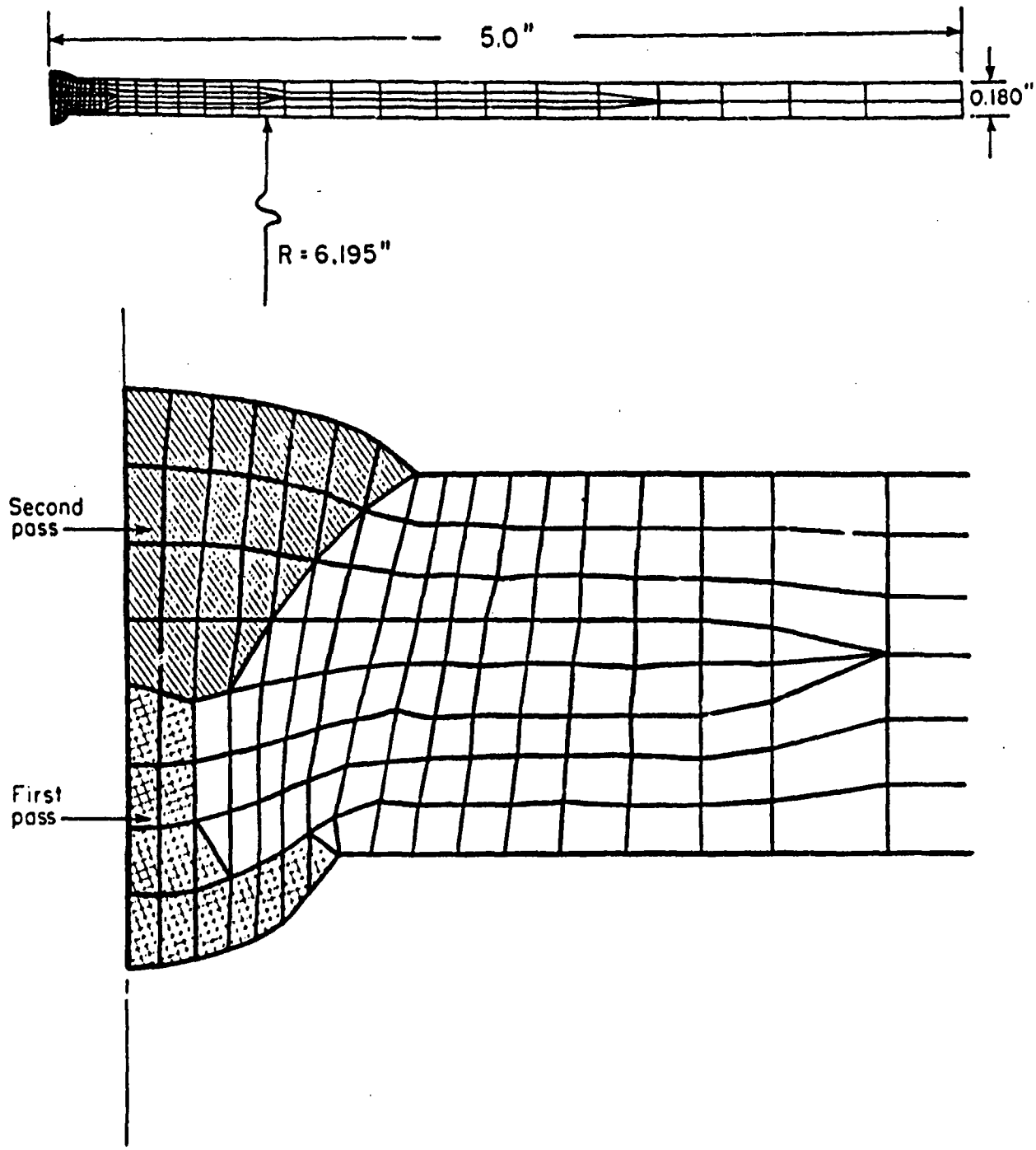

FIGURE 46. TWO-PASS FINITE ELEMENT MODEL FOR BCL MODEL NO. 2

TABLE 8. WELDING PARAMETERS AND GEOMETRY FOR GIRTH-BUTT WELD MODELS

Model	Layer	ID (inches)	OD (inches)	Velocity (in./sec)	Conductivity (Btu/in.-sec-F)	Heat Input (Btu/sec)	Heat Capacity (Btu/in.-F)	Initial Temperature (F)
Two Pass	Root	12.39	12.75	0.050	0.00032	0.63	0.0403	77.
	Second Pass			0.333	0.00032	3.23	0.0403	154.
Six Pass	One	12.00	12.75	0.062	0.00026	1.32	0.0360	77.
	Two			0.320	0.00026	3.46	0.0360	220.
	Three			0.320	0.00026	3.46	0.0360	355.
Seven Pass	One	3.826	4.500	0.0533	0.00037	1.58	0.0438	70.
	Two			0.0433	0.00032	1.21	0.0395	220.
	Three			0.1183	0.00030	1.45	0.0389	350.
	Four			0.1183	0.00030	1.00	0.0389	350.
Thirty Pass	Root	25.40	28.00	0.0267	0.00035	2.275	0.0413	70.
	Two-Five			0.0933	0.00030	2.079	0.0389	550.
	Six-Nine			0.1017	0.00030	2.506	0.0389	350.

2100 F was used as the intermediate distribution between the reference temperature and the final uniform temperature. The comparisons of results from these two techniques are shown in Figures 47 and 48. Also included in these figures are the experimental data. Though it is believed that the solution obtained with two reference temperatures is a better representation of the physical manner in which the residual stresses are created, this solution did not differ significantly from the solution using one reference temperature. Therefore, the results for this case show that the knowledge of the exact weld puddle size is not a prerequisit to making meaningful residual stress calculations. The effect of using one or two reference temperatures on residual displacements is shown in Figure 48. The fact that the use of one reference temperature had little affect on the results makes the possibility of developing a simplified (nonfinite element) girth weld model seem more probable.

The Effect of Increasing the Number of Intermediate Temperature Distributions. To further verify that temperature distributions occurring shortly after the bead is put down have the greatest effect on the final residual stress state, an analysis was made using one intermediate temperature distribution and an analysis was made using two intermediate distributions. Intermediate distributions here refer to those between the reference temperature distribution and the final uniform temperature distribution. For the case of one distribution, it corresponded to the time at which the weld material had cooled to 2100 F. For the case of two intermediate temperature distributions, the first was specified at 2100 F and the second one corresponded to the time at which the weld material had cooled to 1500 F. For both cases, the calculations were made with using only one reference temperature.

The results of these two analyses are shown in Figure 49 along with the experimental data. Although the solution involving the two intermediate distributions more closely approximated the actual changes in temperatures, it did not yield significantly different results. This reinforces earlier results, which indicate that the temperature distributions shortly after the application of the bead as being the most important in terms of final residual stresses.

Some indication of why this is true can be gained by studying the temperature information for a typical girth-butt weld pass in Figure 42. This figure shows a temperature distribution corresponding to the time at which the

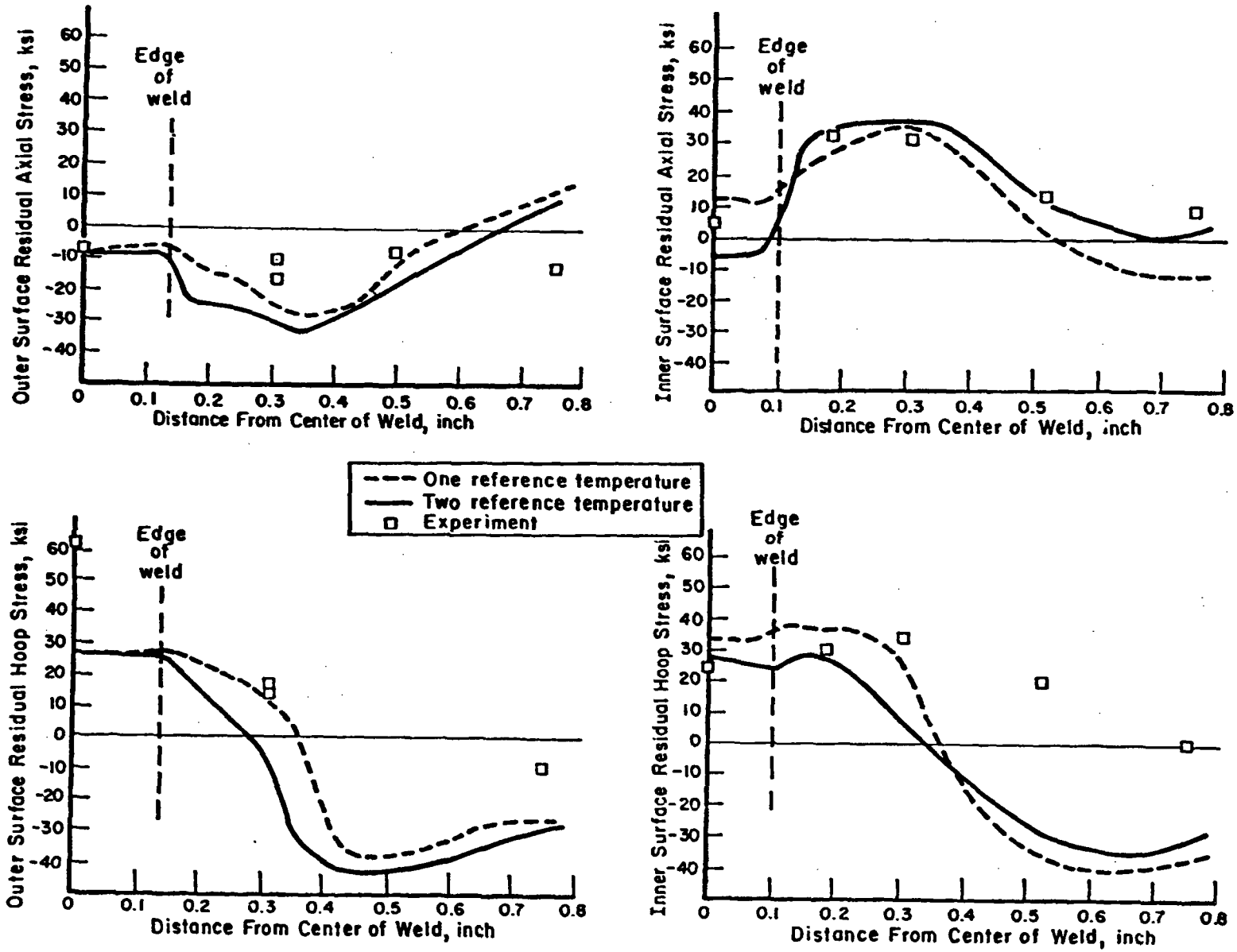

FIGURE 47. COMPARISON OF RESULTS FOR TWO-PASS PIPE USING ONE REFERENCE TEMPERATURE AND TWO REFERENCE TEMPERATURES

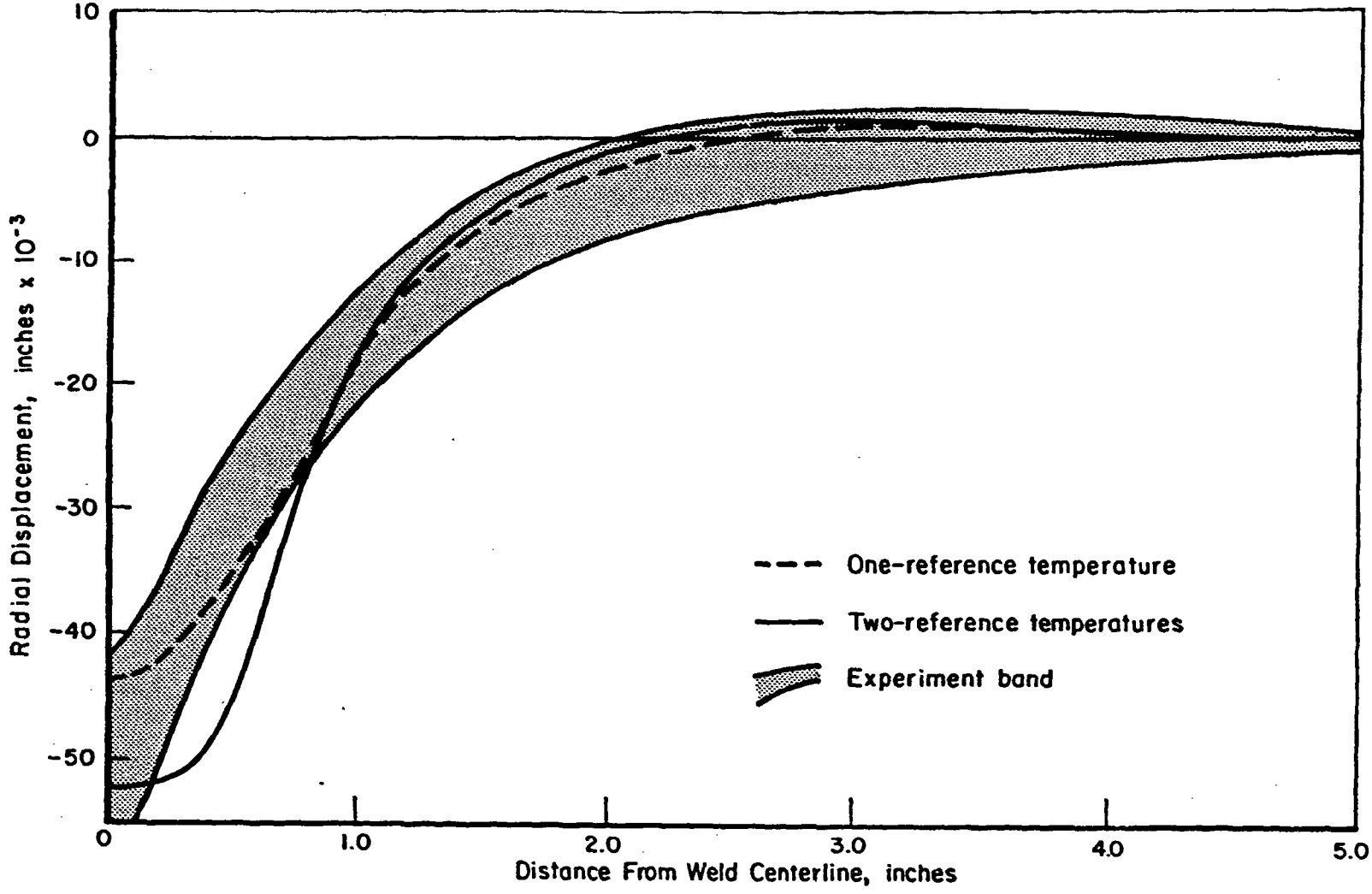

FIGURE 48. COMPARISON OF RESIDUAL DISPLACEMENT FOR TWO-PASS PIPE USING ONE REFERENCE TEMPERATURE AND TWO REFERENCE TEMPERATURES

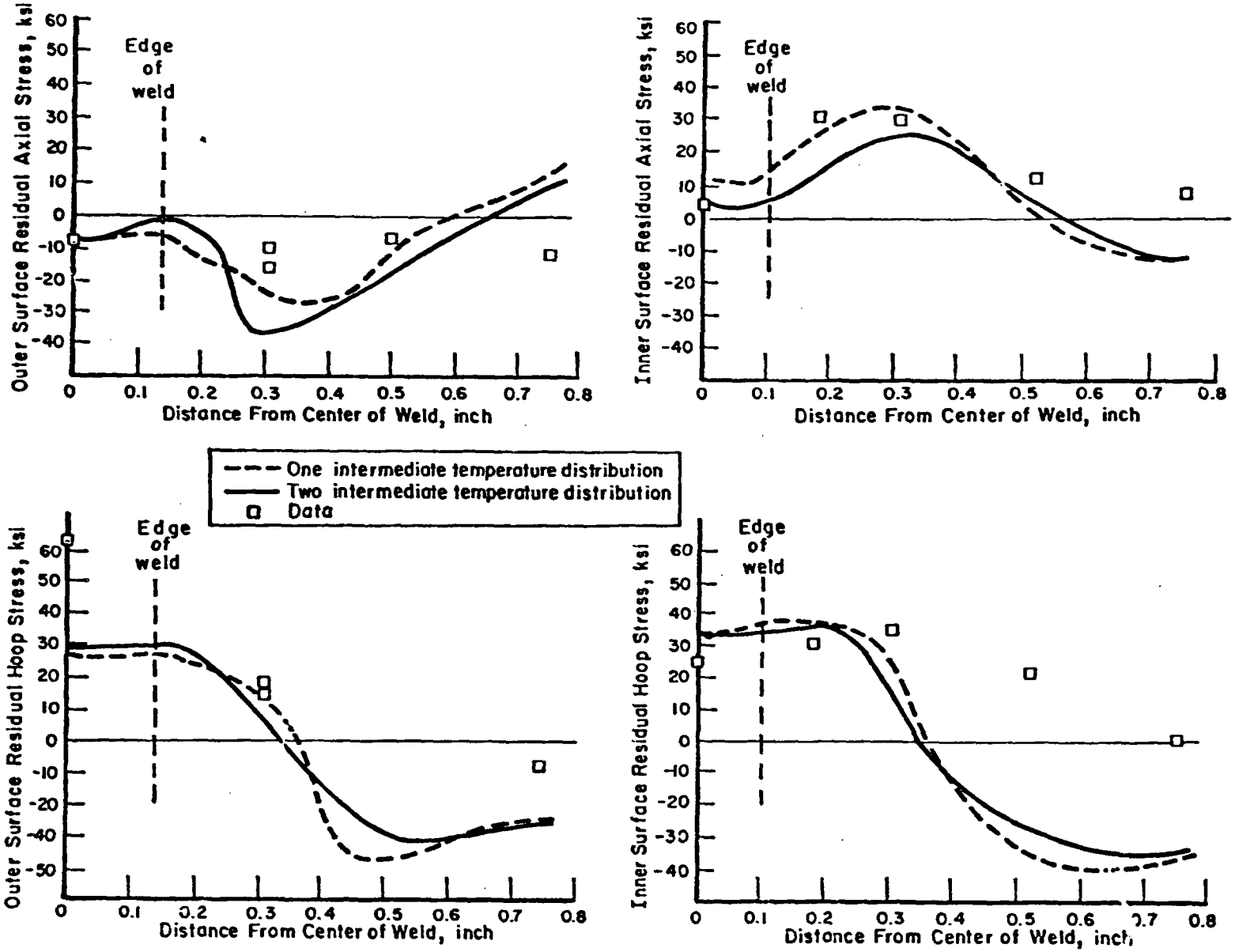

FIGURE 49. COMPARISON OF RESULTS FOR TWO-PASS PIPE USING ONE AND TWO INTERMEDIATE TEMPERATURE DISTRIBUTIONS

weld material begins to gain stiffness (2100 F) and a distribution based on the maximum temperature that the points experience. The maximum temperature distribution is in fact, the envelope within which all the temperature distributions must fall during the application of the pass. As can be seen from Figure 42, the gradients of th .e two curves are not significantly different. This indicates that a sizable por .on of the maximum temperature distribution is defined by the temperature distributions that are close in time to the one corresponding to 2100 F in the weld bead. Also, since the weld centerline temperature decreases, the gradients will have to become smaller at later times and may in fact cause portions of the pipe to undergo unloading.

In summary, it appears that most of the plasticity which occurs close to the welds, occurs early in time while the weld bead is still relatively compliant. As the weld bead temperatures continues to decrease, unloading occurs in the material adjacent to the weld while loading continues at locations further from the weld. Since it is the continued loading at these remote locations that is not modeled when only one intermediate temperature distribution is used, it appears that it is relatively insignificant in determining the residual stresses in and near the weld zone.

Additional Considerations. Two additional methods of modeling the BCL two-pass experiment were considered. One method considers the possibility of using the maximum temperature distribution as the one intermediate profile instead of the distribution occurring when the weld cools to 2100 F. The other considers the possibility of modeling the two-pass pipe as having only one pass and at the same time considering only the cooling portion of the thermal cycle. For this analysis, the welding parameters for the second pass were used to generate the temperature distribution.

The use of the maximum temperature distribution instead of the distribution at any one time was selected because it seemed likely that the widened bell shape of this curve relative to the 2100 F curve could possibly result in widening the bell shape of the calculated stress distributions. As Figures 47 and 49 indicate, this would generally result in better agreement with the experimental data.

The study treating both passes as though they were put down together and modeling only the cooling phase, was conducted in order to determine the sensitivity of the model to this procedure since this represents the most economical manner in which the analysis can be run. For example, this analysis

took four incremental solutions, while the analysis for two individual passes considering both the heating and cooling passes, took twenty-two incremental solutions.

The results of both of these alternative methods of calculations are included in Figures 50 and 51. As the figures show, the differences between these three different approaches are not significantly different. This also tends to indicate that for thin pipes, that a simpler approach to modeling girth welds may be possible.

The results for the maximum temperature distribution analysis did not tend to widen the bell shape of the stress distributions as had been expected. The displacements from this analysis also tended to be smaller than for the other analyses. Both of these results are believed to have resulted because the difference in temperature between the weld and the portion of the pipe remote to the weld was smaller for this distribution than for the 2100 F distribution. This difference can be seen in Figure 42.

The analysis in which both passes were modeled as being applied at the same time is believed to have given similar results to the other analyses parimarily because of the thin-walled pipe geometry. Because of the thinness of the pipe, the isotherms are very nearly radial at all points in time. This indicates that most of the heat is forced to flow axially and also indicates that during the application of the second pass, the first pass became hot enough that its stiffness dropped significantly. It is pointed out that for pipes in which the isotherms are not radial, this method is analysis would most likely give results that are not representative of the measured residual stress. Models for the case where the isotherms are not radial are described in the six, seven, and thirty-pass welds.

Modeling BCL Experiments, Six-Pass Weld

The finite element grid which has been generated for the six-pass pipe (BCL Model Number 3) is shown in Figure 52. The model has 212 elements and 248 nodes. The material is 304 stainless steel with the assumed temperature dependent mechanical properties shown in Figure 41.

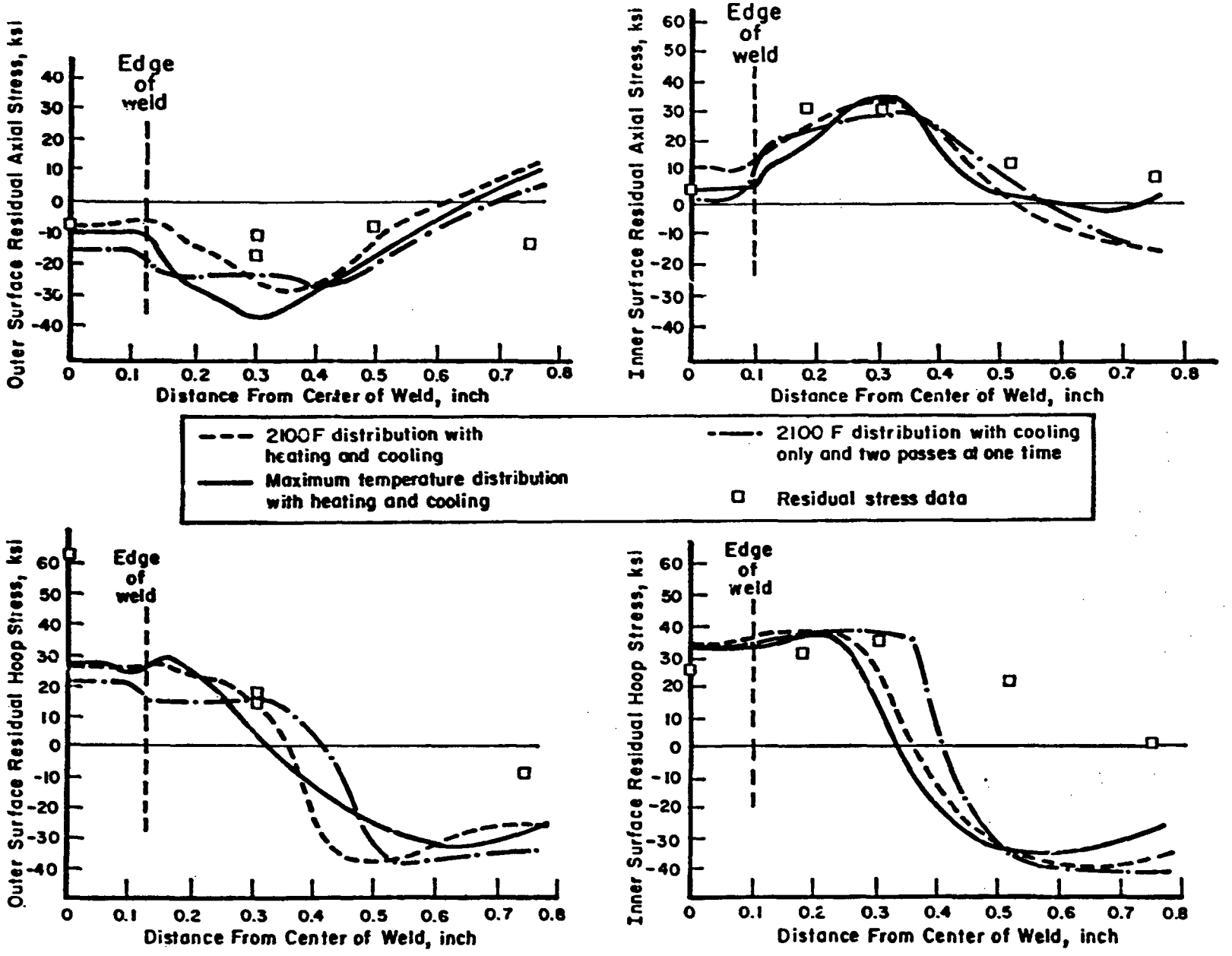

FIGURE 50. COMPARISON OF RESIDUAL STRESS FOR THREE METHODS OF REPRESENTING THE THERMAL LOADING FOR A TWO-PASS WELD

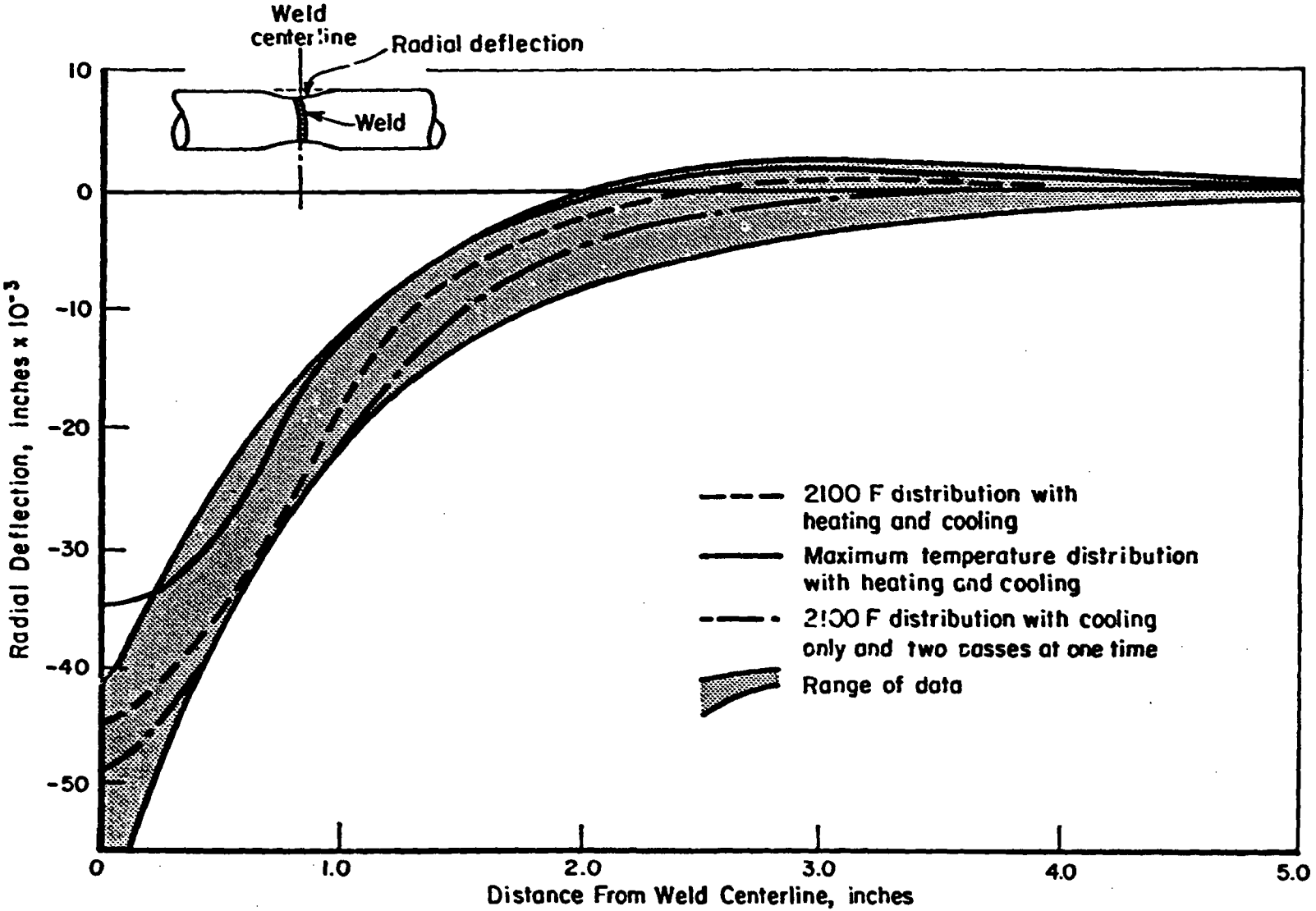

FIGURE 51. COMPARISON OF RESIDUAL DEFLECTION FOR THREE ALTERNATIVE METHODS OF REPRESENTING THE THERMAL LOADING FOR A TWO-PASS WELD

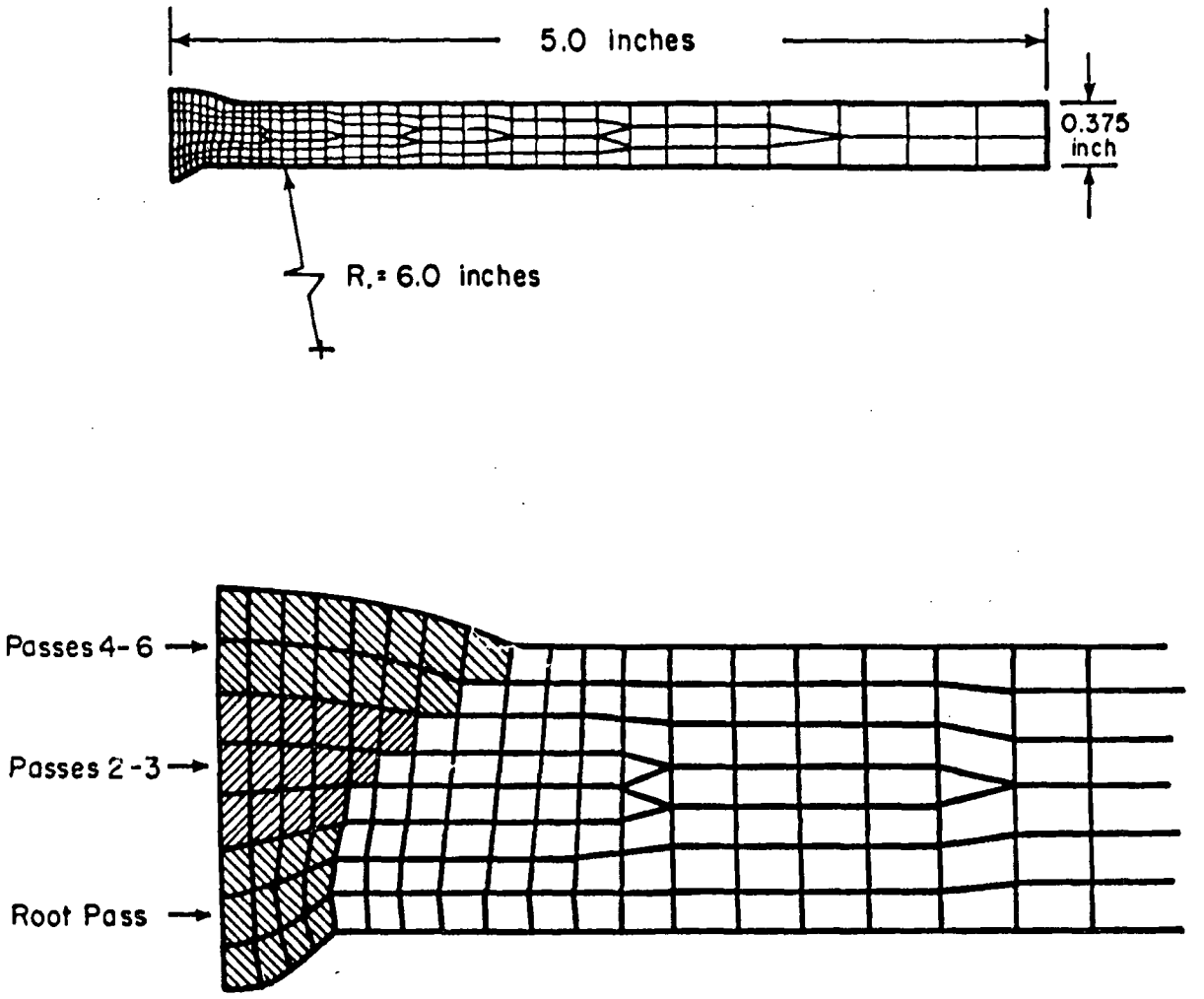

FIGURE 52. SIX-PASS FINITE ELEMENT MODEL FOR BCL MODEL NO. 3

Temperature Calculations

Temperature distributions for the six-pass pipe were modeled based on the maximum temperature profile with the simplified analysis procedure of one cooling phase per pass. The reference temperature for all the weld and pipe material was taken as the same. The welding parameters used for this model are shown in Table 8. The six passes (counting the root pass) were modeled as three layers which were symmetric about the weld centerline. The root pass was modeled as the first layer. The second and third passes were combined to form the second layer. The fourth, fifth, and sixth passes were combined to form the third layer.

Residual Stress Calculations

In Figure 53, the experimentally determined stresses are compared to the calculated values for the inside and outside surfaces of BCL Pipe No. 3. The discrepancy between the open and the solid experimental points is believed to illustrate the effect of the unsymmetrical weld pass geometry. The effect of the centroid of the girth-butt weld being shifted toward the left is seen to be that both the axial and hoop components of stress are larger on the left side than the right side. Another contributing factor to the increase in stress on the left side could be that the last pass was placed on the left side. Since the stresses were calculated under the assumption of symmetry, this effect was not present in the model.

The analysis results for the hoop stress can be seen to start in tension at the weld centerline and then reverse to compression at approximately 0.3 inches. In the measured stress distribution, this reversal in hoop stress occurs at a point further from the weld. Since this discrepancy is larger for the six-pass model than for the two-pass model,* the number of passes is expected to be a contributing factor. The width of the weld on the six-pass pipe is significantly wider than for the two-pass pipe, and the centroids of the individual passes are not on the weld centerline. In the analysis, the weld application was approximated by a point heat source at the centerline centroid of each of the three weld layers. It is believed that a better method of determining temperature, (when the individual passes are combined into layers) would be to assume that

* See Figures 48, 49, and 50.

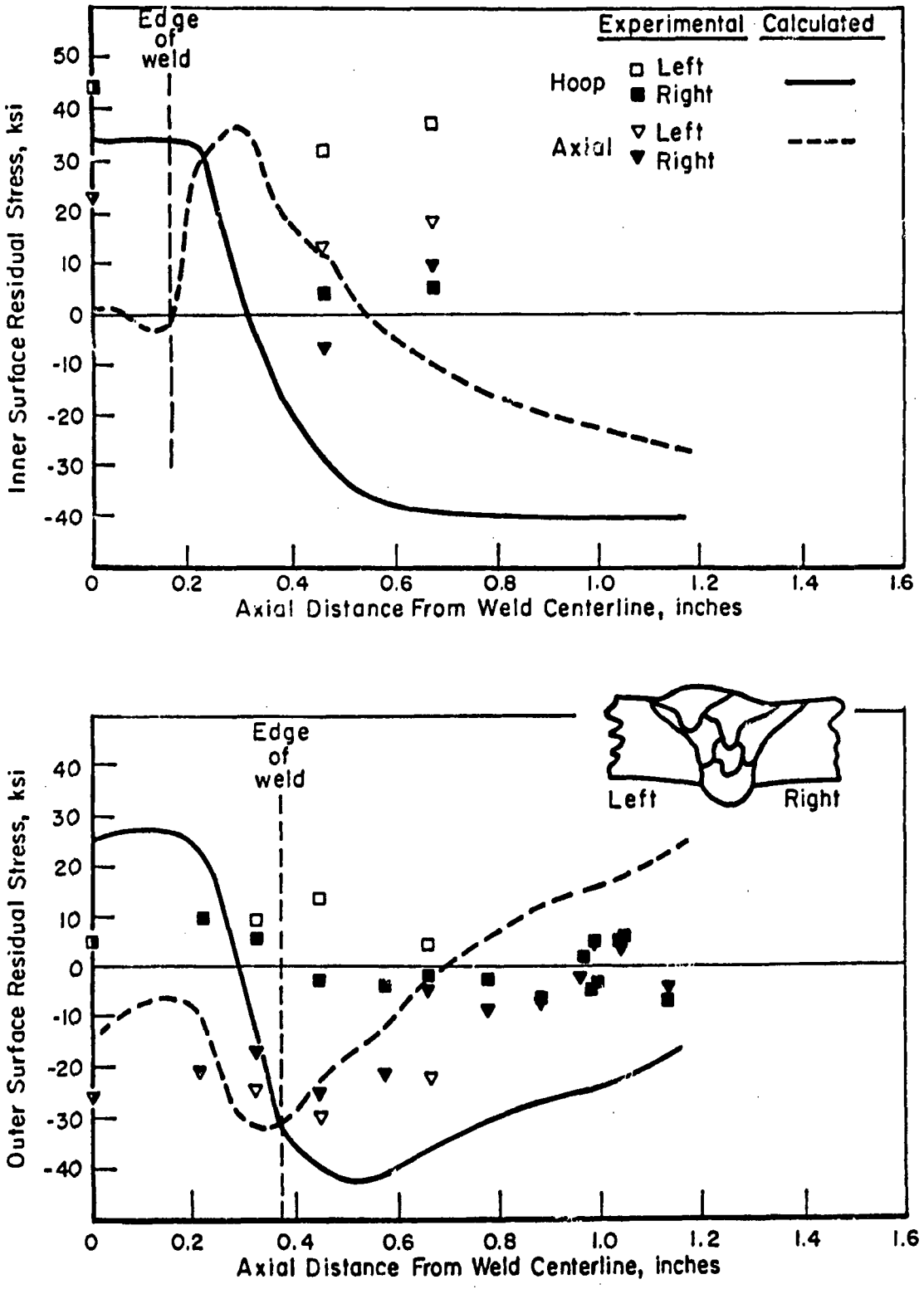

FIGURE 53. COMPARISON OF CALCULATED AND EXPERIMENTALLY DETERMINED RESIDUAL STRESSES FOR BCL EXPERIMENT NO. 3

the heat is being supplied uniformly over the entire weld layer cross section. This would be more realistic and would tend to cause the hoop stress reversal to be shifted further from the weld. In a similar way, this change would also tend to shift the axial stress reversal further from the weld.

The calculated residual displacement at the weld centerline for this model was approximately half of that which was measured experimentally. Based on the results of the two-pass model for the maximum temperature profile (Figure 42), it is likely that this low predicted value of the displacement was at least in part due to the use of the maximum temperature profile. However, it is also believed that this is in part due to the use of the concentrated heat source at the centerline of each layer. If the heat had been applied throughout the weld layer, there would have been more material at a higher temperature with the result being that more radial shrinkage would occur as the weld layer cooled.

Modeling Argonne National Laboratory (ANL) Experiment, Seven-Pass Weld

The data for this girth-butt welded pipe was obtained from measurements taken by ANL. The weldment is denoted by W 27A and was selected because of the relatively small pipe diameter. This pipe is Type 304 stainless steel with an outer diameter of 4.5-inches and a thickness of 0.337 inch. The cross section is shown in Figure 54.

The finite element grid generated for the seven-pass pipe is shown in Figure 55. The model has 314 elements and 350 nodes. The material was 304 stainless steel with the assumed temperature dependent properties shown in Figure 41.

Temperature Calculations

Temperature distributions for the seven-pass weld were modeled based on a representation consisting of four weld layers. The root was the first layer. Passes two and three were combined to form layer two. Passes four and five were combined to form layer three and passes five and six were combined to form layer four. For this pipe, the analysis procedure included one heating phase and one cooling phase. The intermediate temperature distribution corresponded to the time which the weld bead cooled to 2100 F. The reference temperatures for the pipe and the weld bead materials were assumed to be 70 F and 2100 F, respectively.

Welding parameters were based on values reported in References [42] and [43]. Table 8 summarizes the data used to calculate the temperature distributions. The initial temperature for each layer was assumed. Note that a welding efficiency factor is included in the heat input parameters reported in this table. This factor was not given in References [42] or [43], but was determined by fitting the calculated and experimentally measured maximum temperature profiles. The agreement between measured and calculated values is shown in Figure 56.

Residual Stress Calculations

Figure 57 shows a comparison of experimentally determined stresses and values computed from the model for the inside surface of the ANL seven-pass welded pipe. The bars on this figure indicate the effect of taking data at different angular positions about the pipe circumference. The effect of nonsymmetric

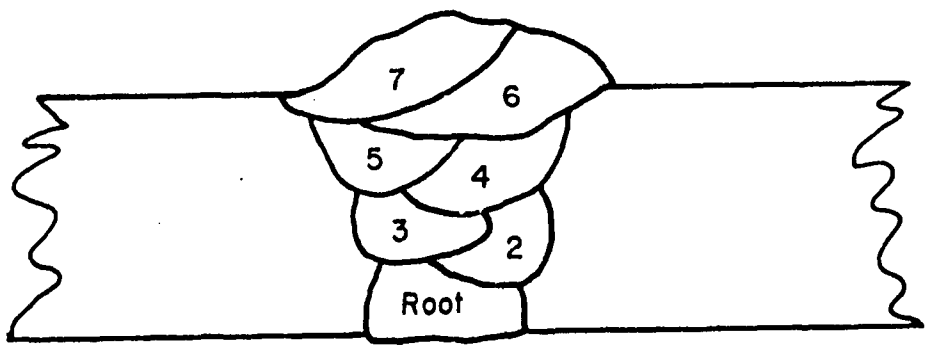

FIGURE 54. CROSS SECTION OF SEVEN-PASS ANL EXPERIMENTAL GIRTH-BUTT WELD W 27A

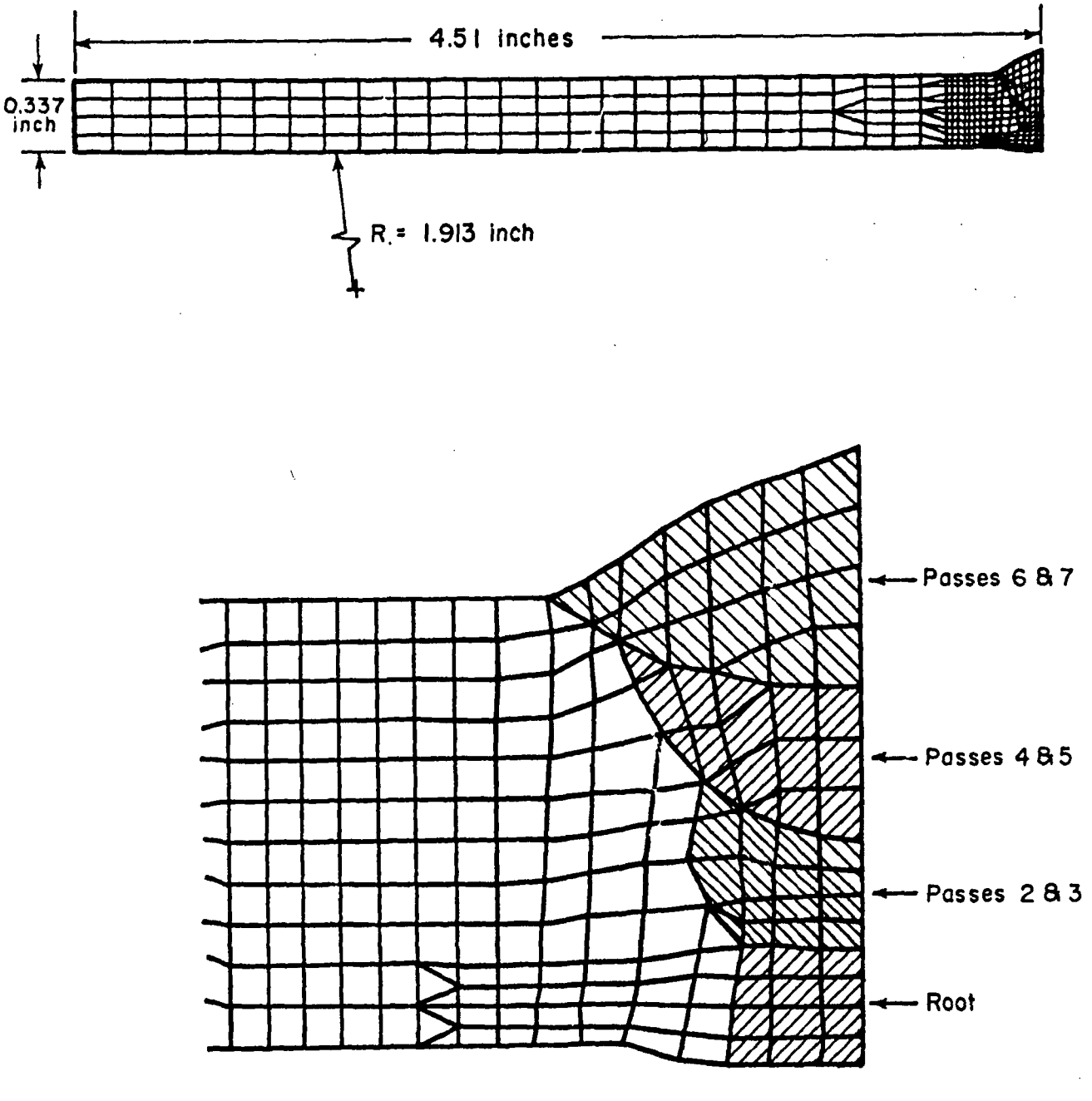

FIGURE 55. SEVEN-PASS FINITE ELEMENT MODEL FOR ANL EXPERIMENT W 27A

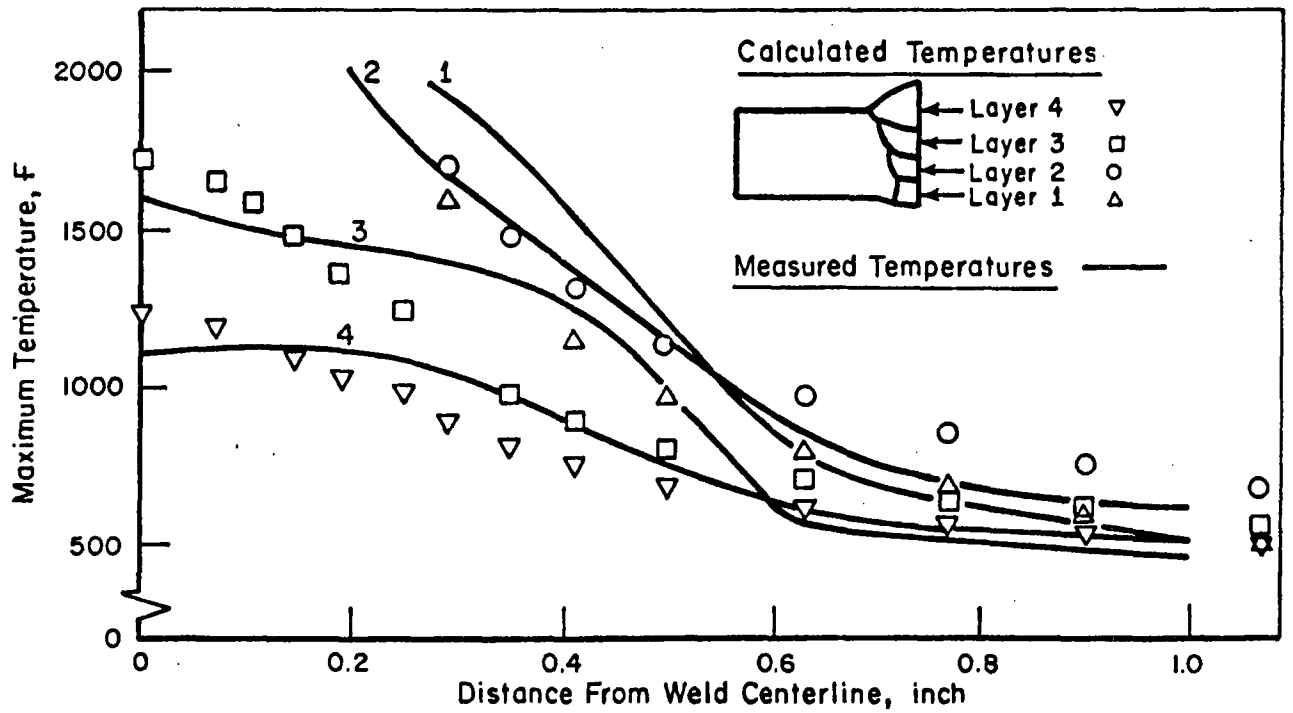

FIGURE 56. COMPARISON OF MEASURED AND CALCULATED MAXIMUM TEMPERATURE PROFILES ALONG INSIDE SURFACE FOR SEVEN-PASS ANL WELD W 27A

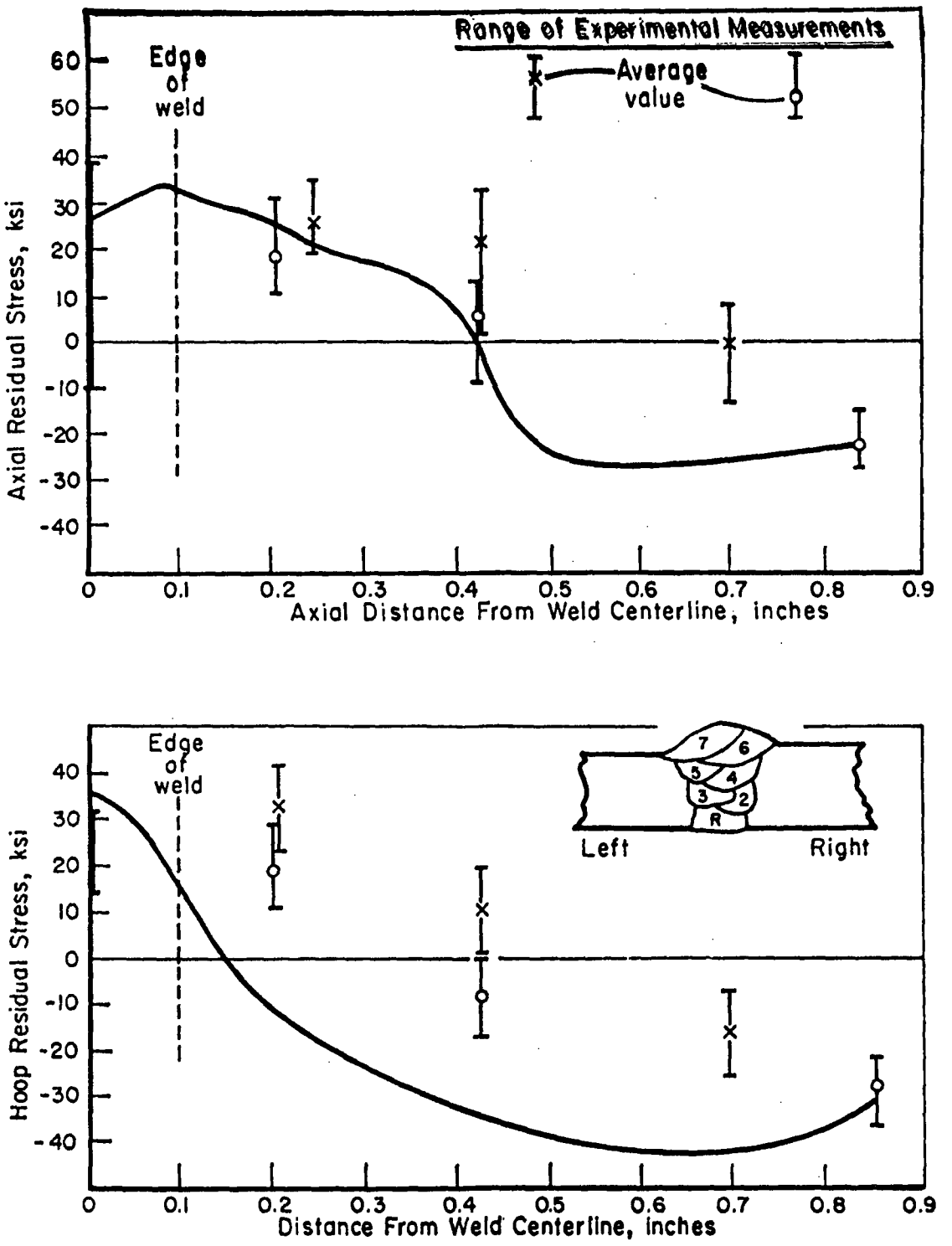

FIGURE 57. COMPARISON OF CALCULATED AND EXPERIMENTAL DETERMINED RESIDUAL STRESSES FOR THE INNER SURFACE OF SEVEN-PASS ANL EXPERIMENT W 27A

behavior about the weld centerline is indicated by the right and lift symbols. Again, the side of the pipe on which the last pass was applied showed the largest experimentally measured stresses.

The seven-pass analysis results are very similar to those of the six-pass analysis in terms of the comparison of analytical predictions and experimental data. In both cases, the axial stress agreement is better than that for the hoop stresses. Also, in both cases, the predicted reversal in the sign of the hoop stress occurs before the location indicated by the experimental data. Since the seven-pass analysis differed from the six-pass analysis in the use of the 2100 F profile rather than the maximum temperature profile and in the use of two reference temperatures rather than one, these two aspects of the analysis are shown to have a secondary effect on this result of the analysis. This agrees with the findings in the sensitivity study with the two-pass weld model.

Two characterisitcs of the seven-pass analysis and the six-pass analysis were similar and are believed to be contributing factors to the similar manner in which the analyses compared with data. One is the way in which the passes were grouped into layers. The other is the way the generated temperature distributions were calculated with the concentrated heat source at the weld centerline. Again, the concept of spreading the heat input over the entire weld layer appears to be an effective representation.

Modeling General Electric Company Experiment, Thirty-Pass Weld

This girth-butt welded pipe was fabricated by GE and selected because of the relatively large number of weld passes. The pipe material is Type 304 stainless steel with an outer diameter of 28 inches and a thickness of 1.3 inches. The cross-sectional geometry of the thirty-pass weld was obtained from Figure 58 which was obtained from the GE report describing the experiment.[41]

The finite element grid for the thirty-pass pipe is shown in Figure 59. The model has 214 elements and 248 nodes. The material properties used with this model are shown in Figure 41.

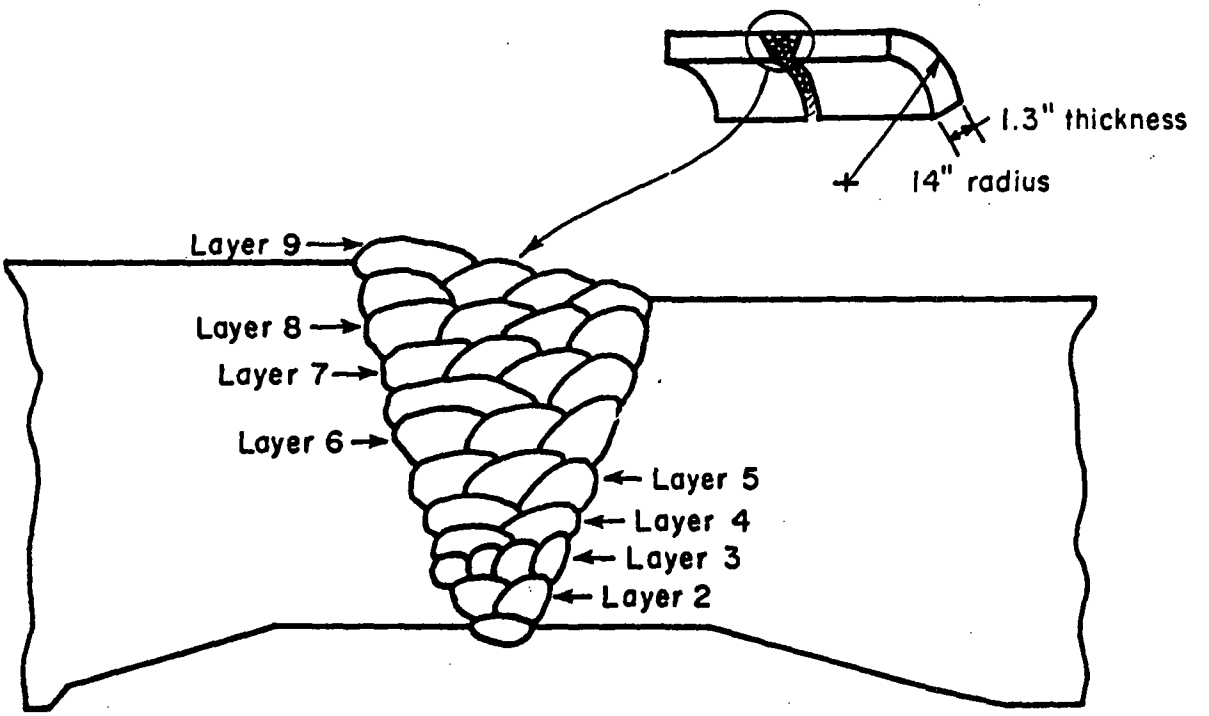

FIGURE 58. CROSS SECTION OF THIRTY-PASS GE EXPERIMENTAL GIRTH-BUTT WELD

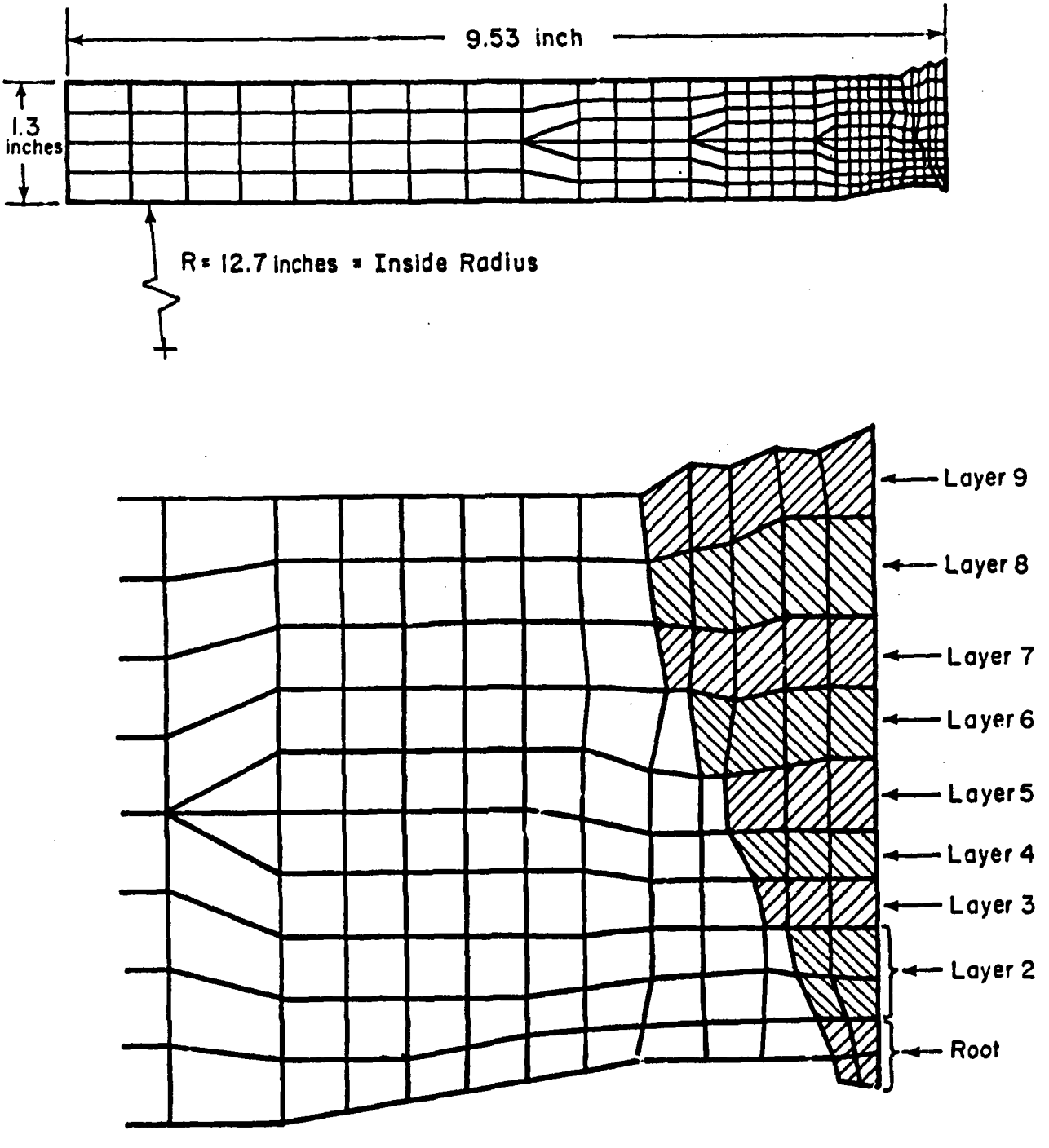

FIGURE 59. FINITE ELEMENT MODEL FOR THIRTY-PASS GE EXPERIMENTAL GIRTH-BUTT WELD

Temperature Calculations

Temperatures for the thirty-pass welded pipe were modeled analytically as having nine weld layers. These layers are shown in Figures 58 and 59.

For this pipe, the analysis procedure was based on one heating phase and one cooling phase with the intermediate temperature distribution corresponding to the time at which the weld bead cooled to 2100 F. The reference temperature for the pipe material was assumed to be a uniform ambient temperature and the reference temperature for the weld bead material was assumed to be 2100 F. The approach used to determine the temperature profiles for each layer of this model was different from that used for the previous models.

In the earlier models, the temperature distribution for each layer was calculated with the heat source located at the centerline of each weld layer. This resulted in temperature distributions which corresponded to the broken line curve of Figure 60. In order to more accurately represent the temperature distribution which occurred between the weld bead and the pipe material of each layer, the assumed temperature distributions used for this model were based on the envelope of the temperature distributions of all the passes contained in the layer. This is illustrated in Figure 60.

The welding parameters used to calculate the temperature distribution are given in Table 1. With the exception of the initial (interpass) temperatures, all of the parameter values are reported in Volume 2 of Reference [41]. The initial temperatures were found by comparing the experimentally measured maximum temperature profiles with the computed values.

Residual Stress Calculations

The computed residual stresses for the inside surface of the thirty-pass model are compared with experimental measurements in Figure 61. The bars on this figure indicate the effect of taking measurements at different angular locations around the pipe circumference. Though experimental measurements were made on both sides of the weld centerline, data points from both sides generally fell within the same range.

The calculated stresses in both the axial and hoop directions agree quite well with the data. Since for this model, the axial stress sign reversal agrees with the experimental values better than for the six and seven-pass pipes, it appears that the method of using the temperature distribution envelope had

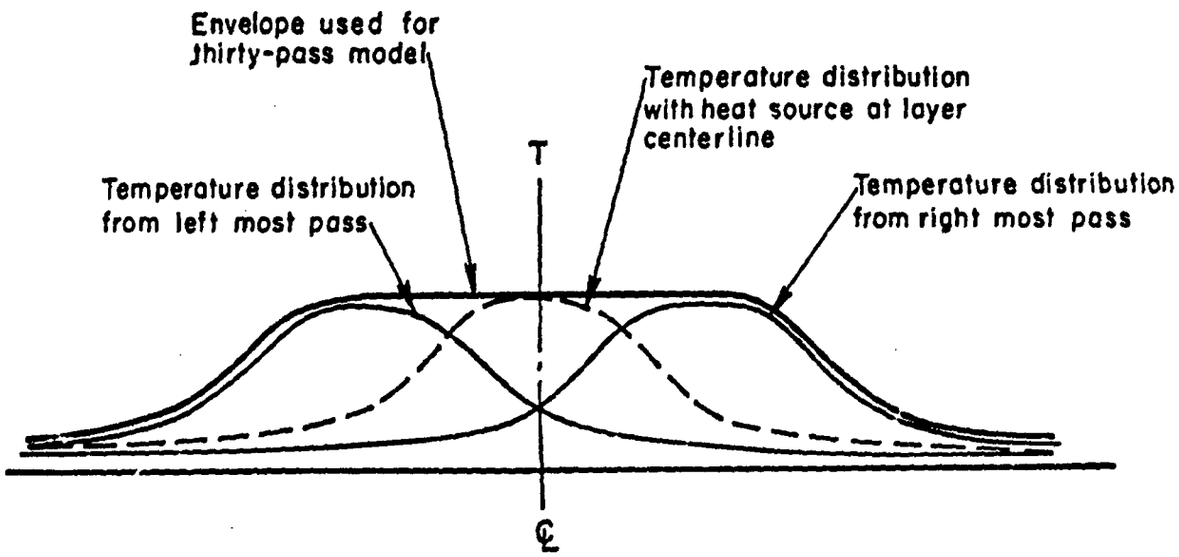

FIGURE 60. METHOD OF TEMPERATURE DISTRIBUTION CALCULATION FOR THIRTY-PASS MODEL

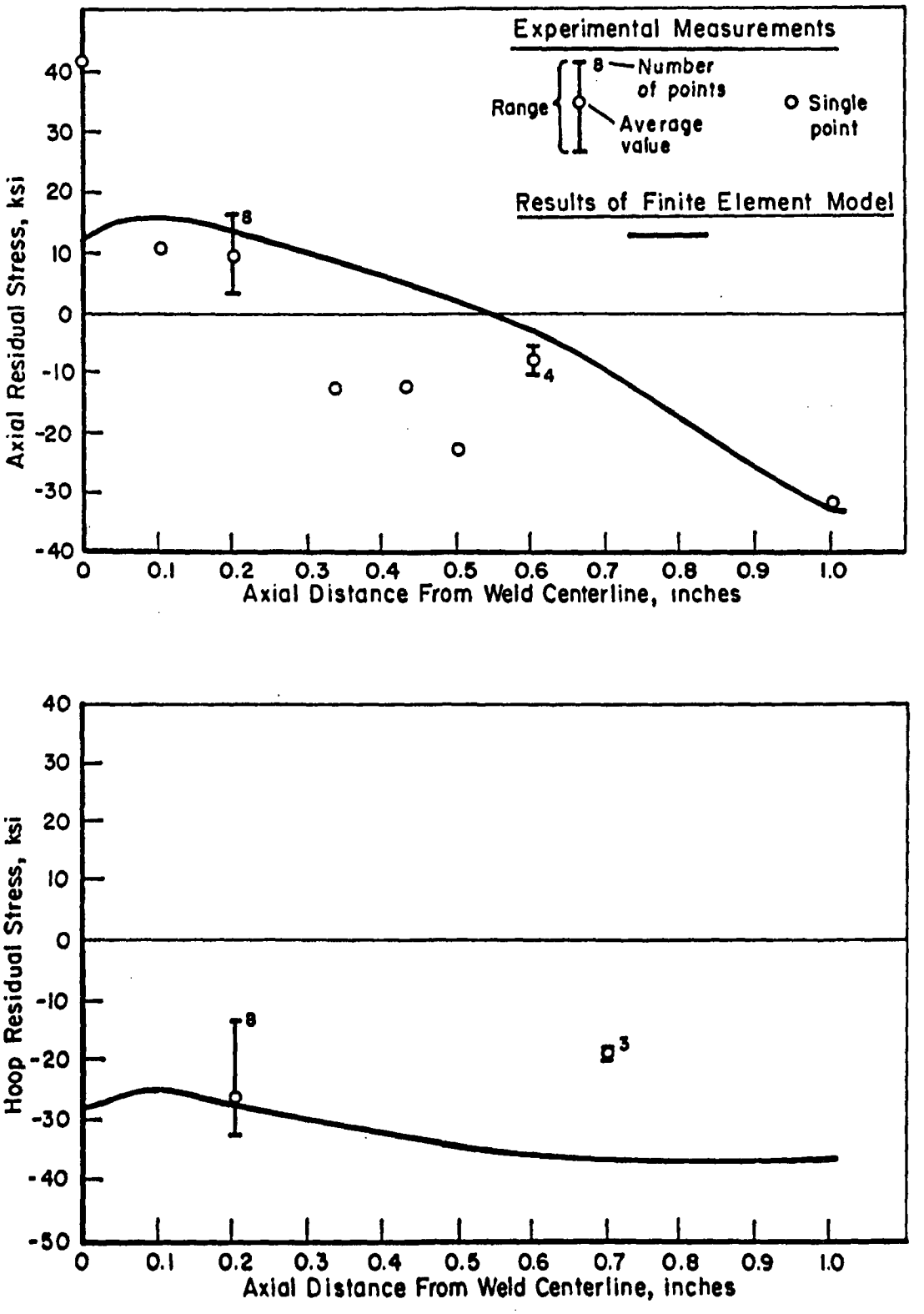

FIGURE 61. COMPARISON OF CALCULATED AND EXPERIMENTALLY DETERMINED RESIDUAL STRESSES FOR THE INNER SURFACE OF THIRTY-PASS GE EXPERIMENT

a beneficial effect on the accuracy of the model. This is especially significant because of the increased number of passes per layer which was used in this pipe as compared to those in the six and seven-pass pipes.

One aspect of the modeling of pipes with large numbers of passes, that was briefly addressed during the study of the thirty-pass pipe, is the possibility of grouping layers of passes in the analysis procedure. In this study, the thirty-pass welded pipe was modeled by grouping the thirty passes into three layers. The results of this model did not agree with the experimental data. Though the method of calculating the temperature distributions did not use the envelope approach, it did tend to distribute the heat input over the entire weld layer region. Therefore, it is believed that the major reason for the three layer representation not giving satisfactory results was that too many passes were put in each layer. At this time, this question of how many passes can be represented by one layer in the model cannot be fully answered. However, results indicate there is merit to the modeling concept of using a layer that contains one row of weld passes.

Preliminary Application of the Residual Stress Model to A Weld Repair of a Pressure Vessel

The residual stress model described here has many potential applications to welds of pressure vessels and pipes. One such application is to understanding the residual stresses resulting from a weld repair of a pressure vessel. It is emphasized that the model, in its present form, would require some extensions before accurately representing several aspects of the problem. Nonetheless, it is of value to apply the model to this problem with the intent of obtaining qualitative results. The following contains a description of the vessel, the weld repair cavity and the model. A comparison of residual stress data and results obtained from the model is also presented.

Description of the Weld Repair

The weld repair of interest was done on the HSST intermediate vessel V-8. The same weld repair procedure was applied to a two foot long prolongation cylinder with comparable dimensions to the cylindrical section of the vessel. The dimensions of the weld cavity and the cylindrical section of the pipe are

shown in Figure 62. The vessel material is ASTM A533, Grade B class 1 carbon steel. The size of each weld bead is about .1 inch by .1 inch. Thus, it is estimated that close to 900 weld passes were required to fill the weld cavity.

Results of Residual Stress Model

The residual stress data for this weld repair was available along a line around the circumference of the cylindrical section of the vessel. The model is not three dimensional and cannot represent the three-dimensional aspects of the weld cavity geometry. A model was selected to represent a section of the vessel in the hoop direction through the center of the weld cavity. Another approximation in the model concerns modeling the large number of weld passes. The total number of filler passes were modeled as a single deposit of material. Because of these approximations in the model, quantitatively accurate results were not expected. However, qualitative comparisons with the data should be attainable because the model does include some aspects of the geometry and the material properties. Figure 63 shows the comparison of results obtained by computations with the model and residual stress data obtained at Oak Ridge National Laboratory. The model exhibits good agreement with the hoop stress data as shown in Figure 63 solid and dotted lines. Hoop and axial stress distributions form the model are on the outer surface of the vessel. The Oak Ridge data were obtained on the outer surface and from points just below the outer surface. Axial stress data is shown at one location and is also in agreement with the results of the analysis. These comparisons are very encouraging and suggest that the model can be a useful tool for residual stresses in weld repair.

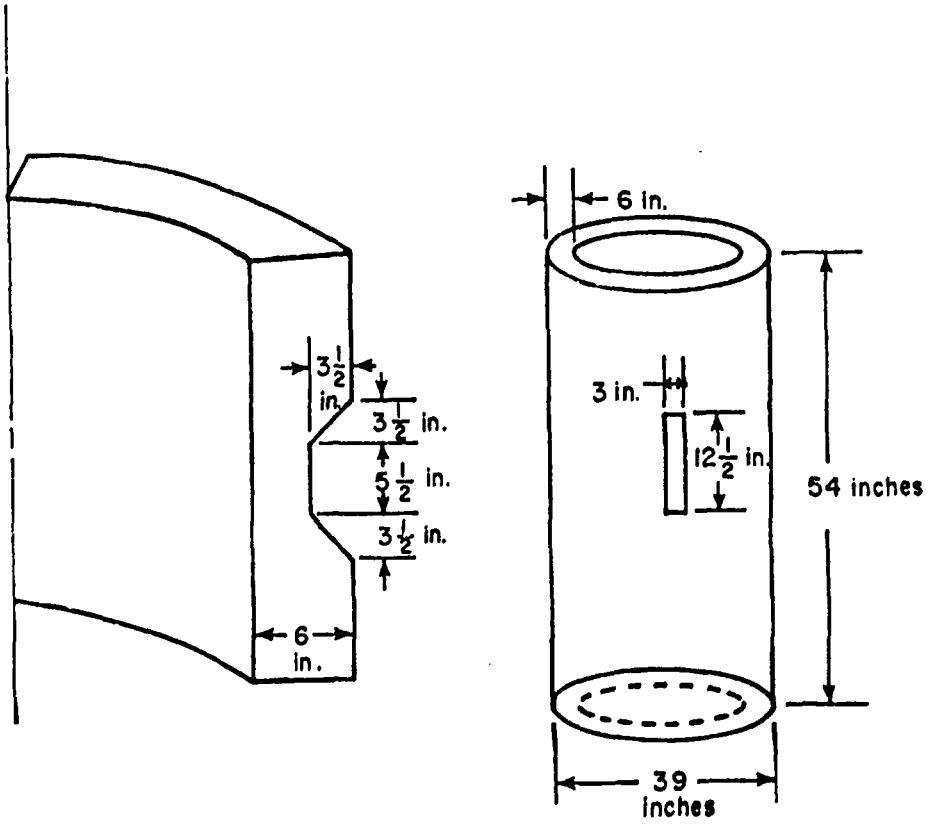

FIGURE 62. ILLUSTRATION OF WELD REPAIR CAVITY IN CYLINDRICAL SECTION OF HSST INTERMEDIATE VESSEL V-8

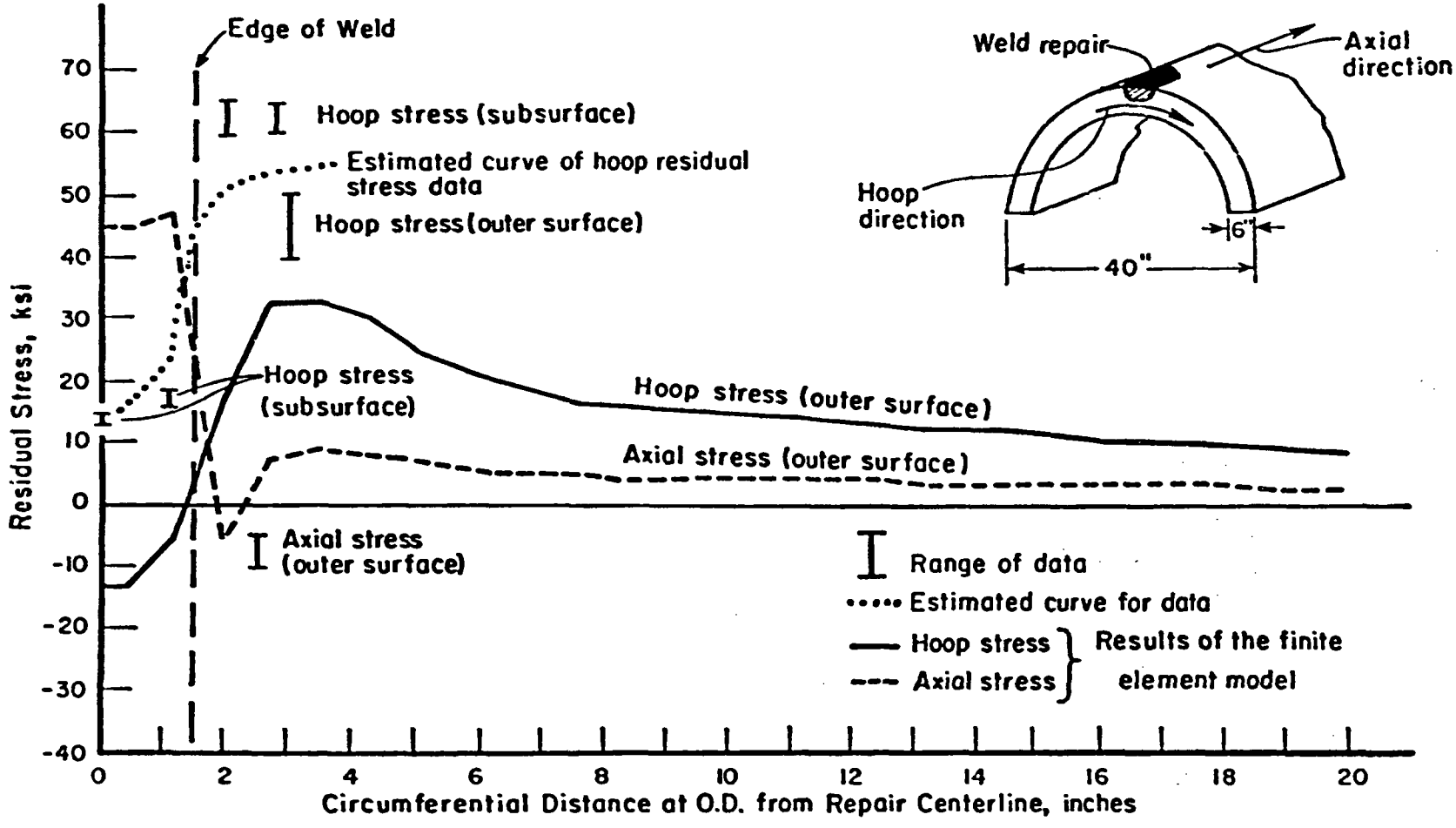

FIGURE 63. COMPARISON OF RESIDUAL STRESS DATA FOR WELD REPAIR OF HSST INTERMEDIATE VESSEL V-8 AND PRELIMINARY COMPUTATIONS BASED ON RESIDUAL STRESS MODEL

VI. SIMPLIFIED MODEL FOR RESIDUAL STRESS IN GIRTH-BUTT WELDS

The models described in the preceding are capable of producing accurate evaluations of residual stresses at girth-butt welds. However, at the present stage of development, the time and cost involved in conducting an analysis with these sophisticated models can be quite high.

It would be desirable to run parametric studies on girth-butt welds to determine optimum conditions to minimize residual stresses and radial displacements. The parameters involved are quite numerous, e.g., heat input (welding voltage and current), weld torch speed, number and size of passes, cooling time between passes, the weld bead material, the pipe diameter, wall thickness, and pipe material. Such parameteric studies would involve many hundreds of individual residual stress calculations and would be very expensive if carried out with a sophisticated model. The purpose of seeking a simplified model is to provide a tool for running parametric studies at reasonable cost.

A simplified model has been proposed by Vaidyanathan, et al.[28] This model makes use of cylindrical shell theory and a simplified method of estimating the maximum temperatures during the welding.

The pipe is assumed to be subjected to uniform distributed hoop-direction stress as seen in Figure 64. Conceptually, these hoop-direction loading stresses arise from the theory of residual stresses at welds between two flat plates. The three regions shown in Figure 64 are quantified by the following relationships:

Distance From Weld, X	Temperature, T	Loading Hoop Stress, σ
$< X_1$	$>(\bar{T} + 2\tau)$	S_y
$> X_1, < X_2$	$<(\bar{T} + 2\tau), > \tau$	$S_y(T - \bar{T} - \tau)/\tau$
$> X_2$	$< \tau$	$- S_y(\bar{T}/\tau)$

In the above, S_y is the yield strength of the pipe material, $\tau = S_y/E\alpha$, where E is the modulus of elasticity and α is the coefficient of thermal expansion of the pipe material. T is the maximum temperature* at a distance X from the weld and is evaluated by the equation:

* Temperatures are actually changes in temperatures from a uniform reference temperature. For comparison with test data, the reference temperature can be considered to be ambient temperature.

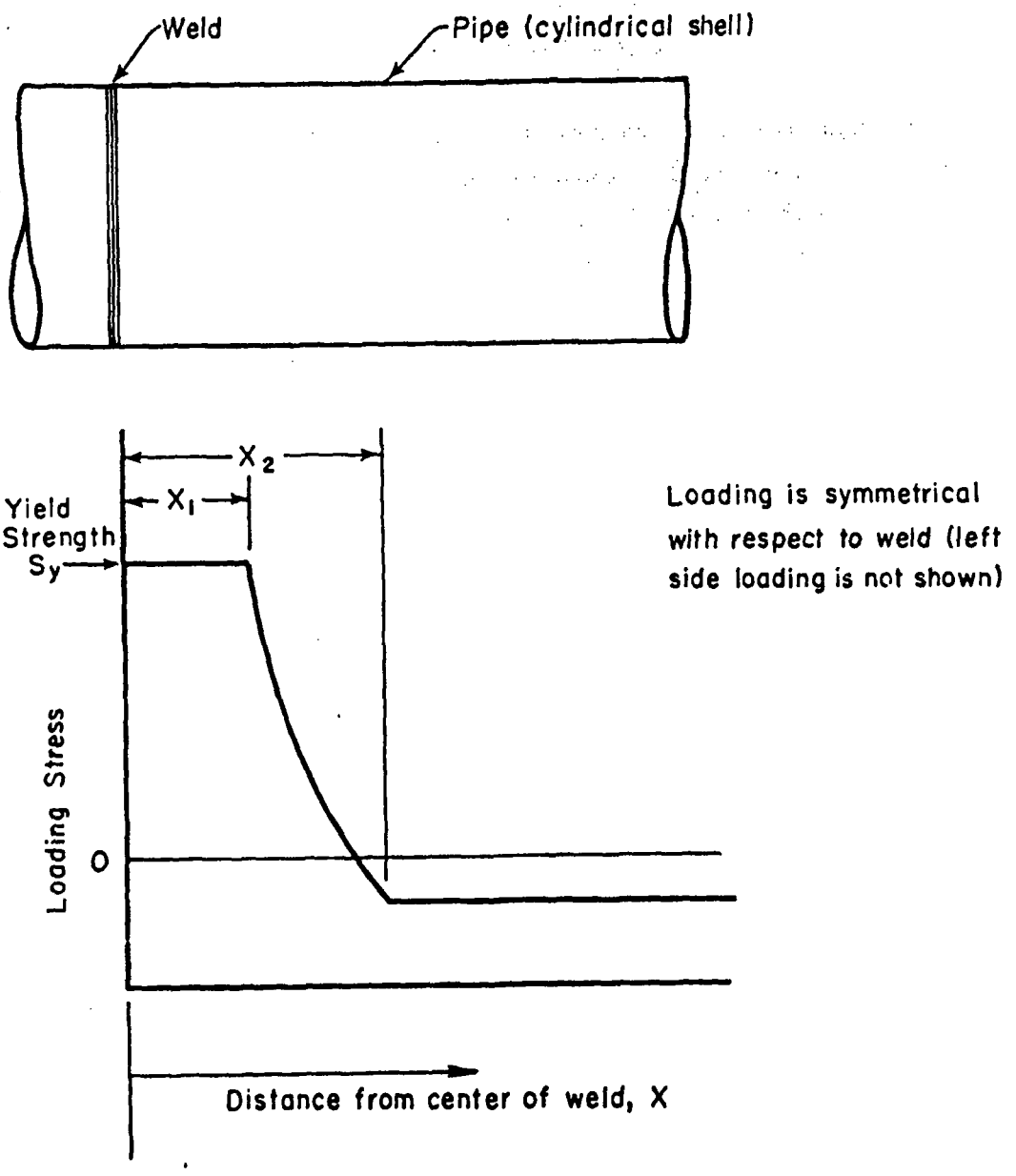

FIGURE 64. LOADING ASSUMPTIONS USED IN SIMPLIFIED MODEL

$$T = Q/[8k(0.2 + VX/2d)] \quad , \qquad (3)$$

where Q = heat input per unit time per unit pipe wall thickness

V = welding travel speed, length per unit time

k = thermal conductivity of pipe material

d = thermal diffusivity of pipe material.

The value of $\bar{T}$ (equilibrum temperature) can be estimated by the equation:

$$\bar{T} = \frac{Q}{2Vc\ W\rho} \quad , \qquad (4)$$

where Q and V are as defined above, and

c = specific heat of pipe material

W = axial length of welded assembly

ρ = density of pipe material.

The value of $\bar{T}$ is subject to considerable uncertainty. However, it appears that the value of $\bar{T}$ is usually between 0 and 40 F and that the stresses and displacements at and near the weld are only slightly changed by $\bar{T}$ within this range.

The theory of Reference [28] covers two cases; when the plastic zone around the weld is small and when the plastic zone is large. The plastic zone is considered small when it extends in the axial direction from the weld not more than $0.47\sqrt{Rt}$, where R = pipe radius, t = pipe wall thickness. In this case, an equivalent concentrated radial load is assumed to act on the weld, leading to a very simple solution. If the plastic zone is large, the solution is more complicated and numerical integration is required. However, even this solution is relatively simple compared to the elastic-plastic, finite element analysis.

The theory of Reference [28] is limited in application to a single pass weld. Reference [28] describes a test in which a girth-butt weld was made to joint two 0.080-inch-thick, 4-inch-radius hemispheres*. The material was 5083-0 aluminum. Welding was done with an electron beam with arc voltage of 65 KV, weld current of 15 mA, welding travel speed of 120 inch/minute. Residual stresses were determined on the outside surface. The calculated and measured residual stresses are shwon in Figures 65 and 66. Reference [28] gives calculated residual

* In the region of the weld, the difference between the spherical shell geometry and cylindrical shell geometry is not significant.

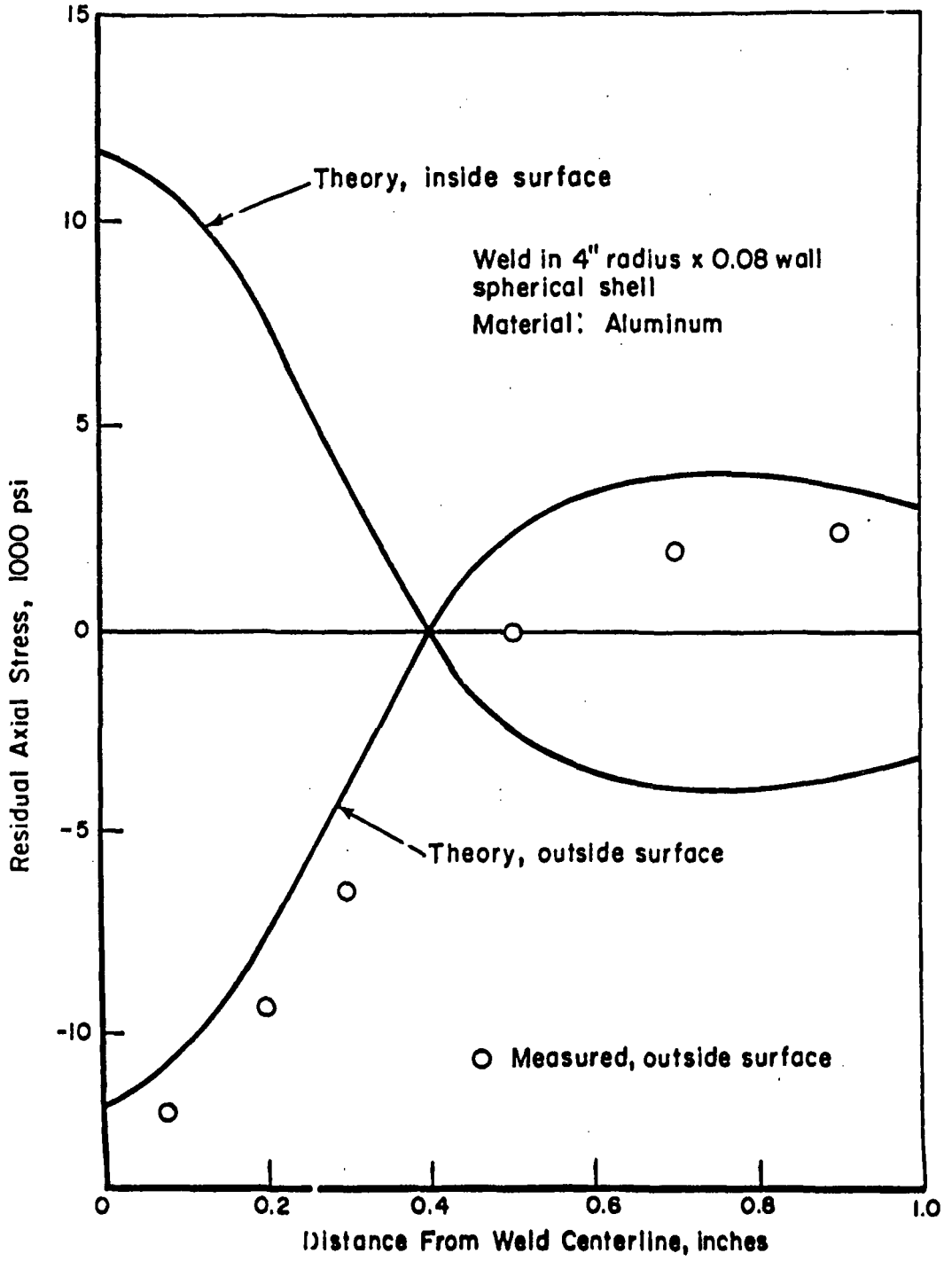

FIGURE 65. COMPARISON OF SIMPLIFIED MODEL THEORY AND TEST DATA[28] FOR RESIDUAL AXIAL STRESSES

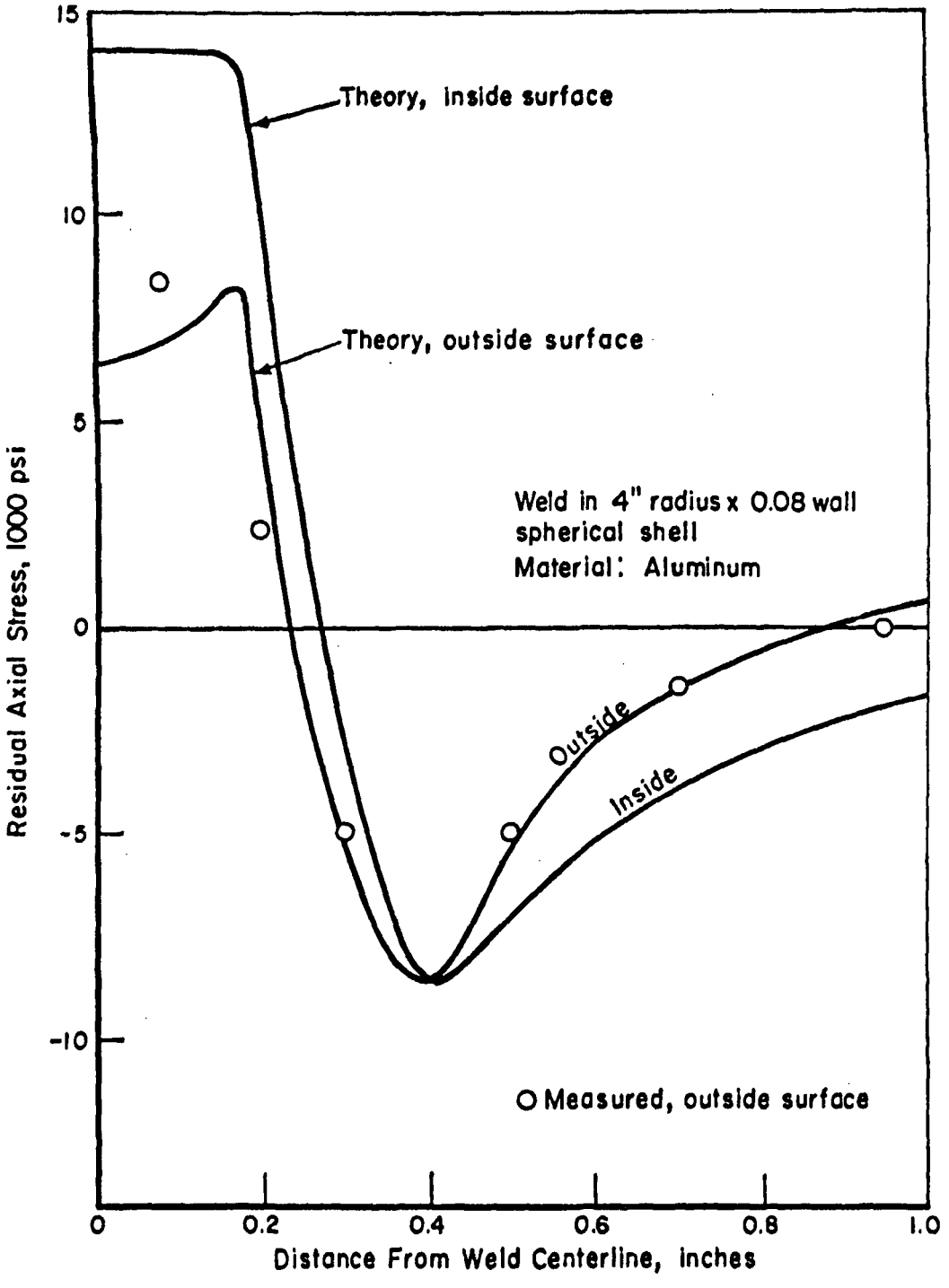

FIGURE 66. COMPARISON OF SIMPLIFIED MODEL THEORY AND TEST DATA[28] FOR RESIDUAL HOOP STRESSES

stresses only for the outside surface; we have calculated residual stresses on both surfaces, using the "large-plastic zone" solution which involves numerical integration. Our results are slightly different than those shown in Reference [28] for the outside surface, possibly due to differences in the numrical integration technique.

It can be seen in Figures 65 and 66 that the calculated and measured stresses are in reasonable agreement with each other. Figure 65 indicates the presence of a high residual tensile stress in the axial direction on the inside surface but, for this particular model, the stress is not as high as the residual hoop stress on the inside surface.

Burdekin[44] gives residual stress measurements at girth-butt welds made in 30-inch outside diameter, 0.438-inch wall thickness, carbon steel pipe. Unfortunately, the welding parameters are not described. Reference [44] only states that: "The circumferential weld was made by the submerged arc process with one run outside, and a manual backing run." Residual stresses after welding were measured on both the outside and inside surface, using the Gunnert gage method. The measured residual stresses from Reference [44] are shown in Figure 67 along with our calculated residual stresses using the simplified model. The calculations are based on estimated welding parameters of 30 volts, 800 amps, 30 in./minute welding travel speed, 50 percent heat input efficiency. As might be expected from the use of the Gunnert gage method, the experimental data (Figure 67) shows wide scatter. However, the calculated residual stresses are generally in rough agreement with the measured residual stresses.

As previously mentioned, the simplified model is applicable to single pass welds. However, if cooling to ambient temperature occurs between passes, we would expect the maximum temperature at a distance x from the weld to be given by Equation (3). Figures 68 and 69 show comparisons between Equation (3) measured temperature and the temperature calculated by Equation (1). It should be noted that Equation (3) is intended to give the maximum temperature; it does not indicate how long it takes to reach that temperature. Accordingly, Equation (3) should form an upper bound to the specific time lines from Equation (1); it can be seen in Figures 68 and 69 that this is approximately true.

Vaidyanathan, et al.,[45] consider the analysis of a multipass weld, using a filler metal different than the base metal and with a partial penetration. Certain of the concepts may be useful in extending the simplified model to cover

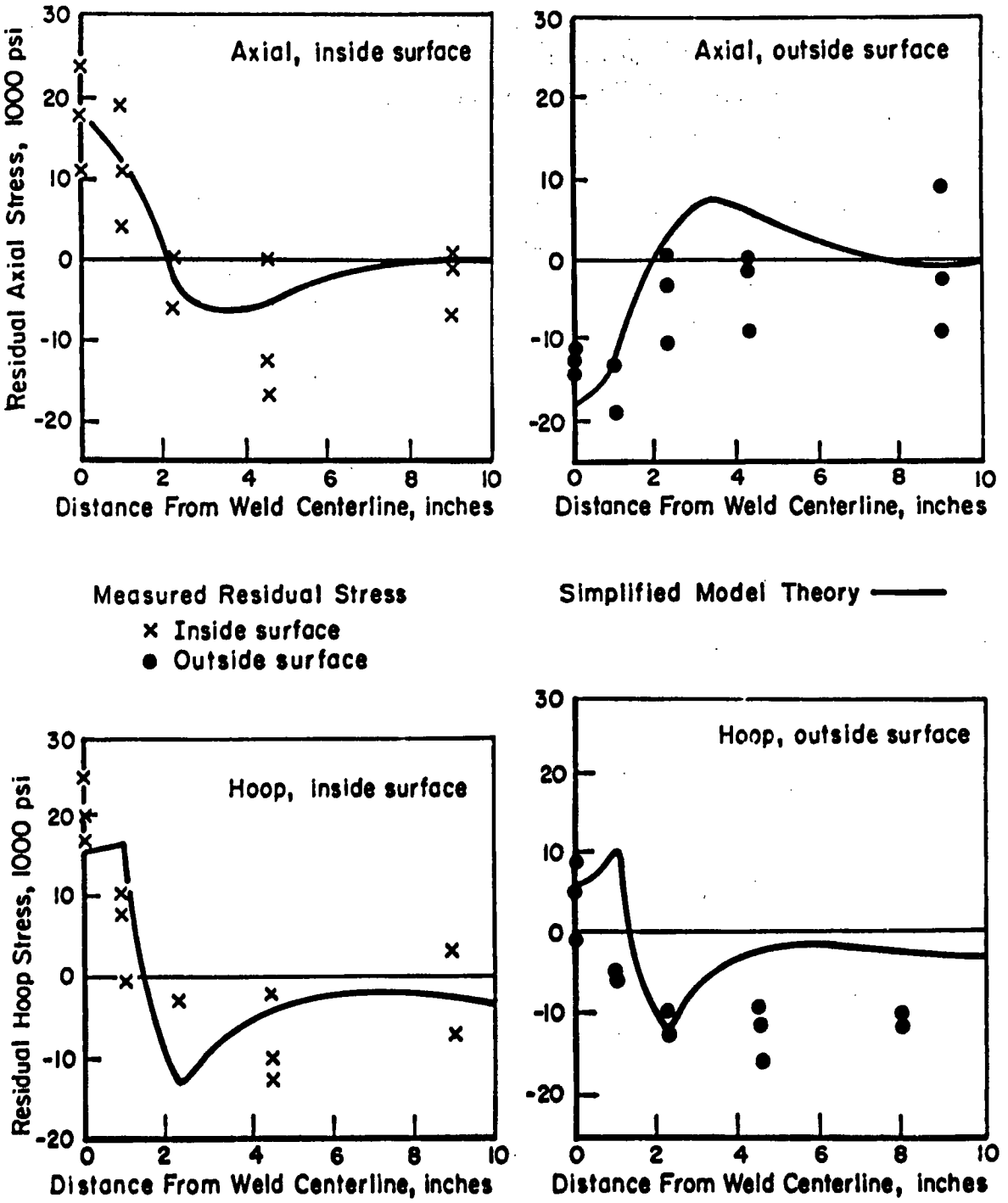

FIGURE 67. COMPARISON OF SIMPLIFIED MODEL THEORY AND TEST DATA[44] GIRTH-BUTT WELD IN 30-INCH DIAMETER, 0.438-INCH WALL THICKNESS, CARBON STEEL PIPE

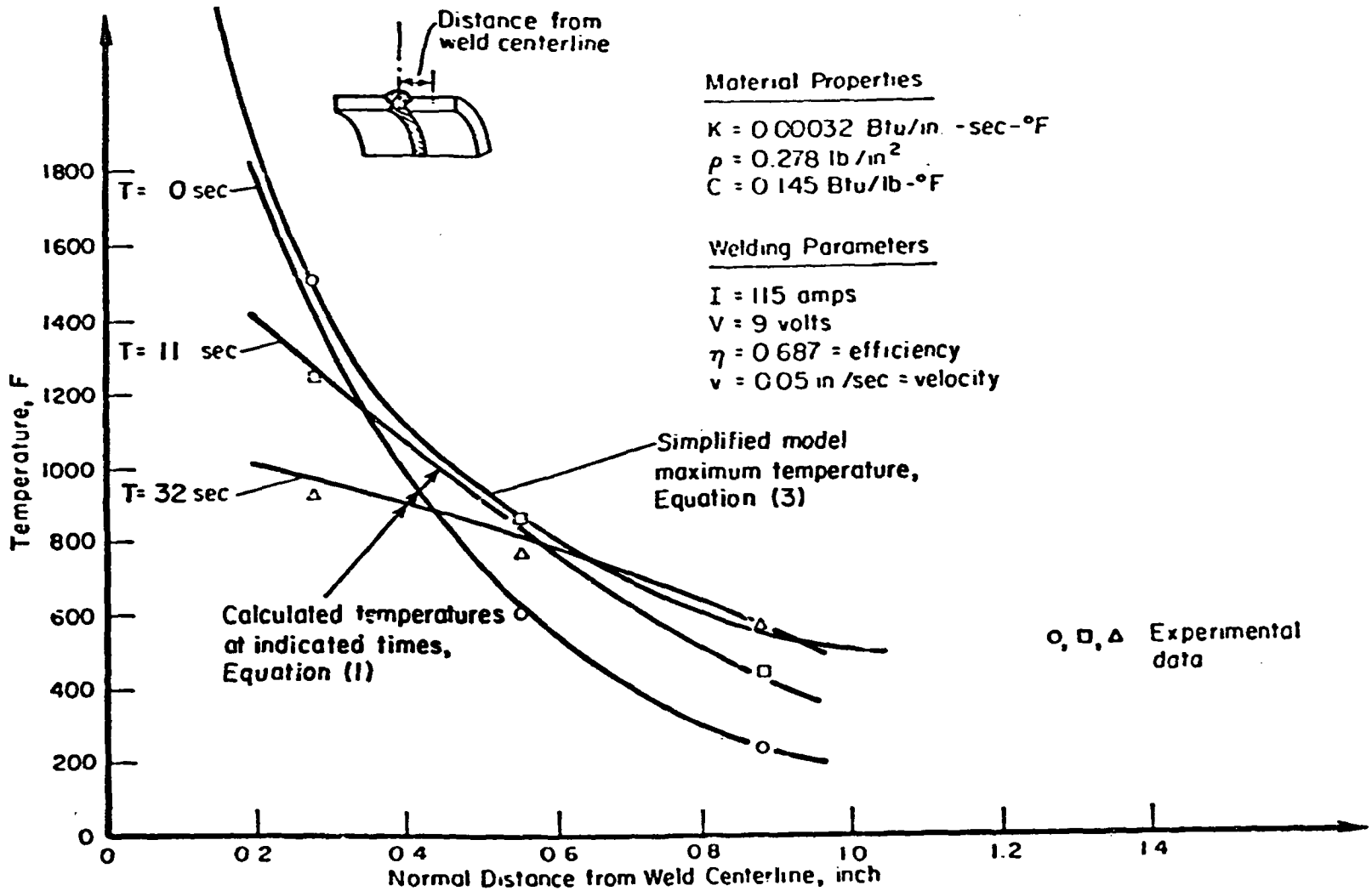

FIGURE 68. COMPARISON OF TEMPERATURE MODEL AND EXPERIMENTAL DATA FOR THE ROOT PASS OF BCL MODEL 2

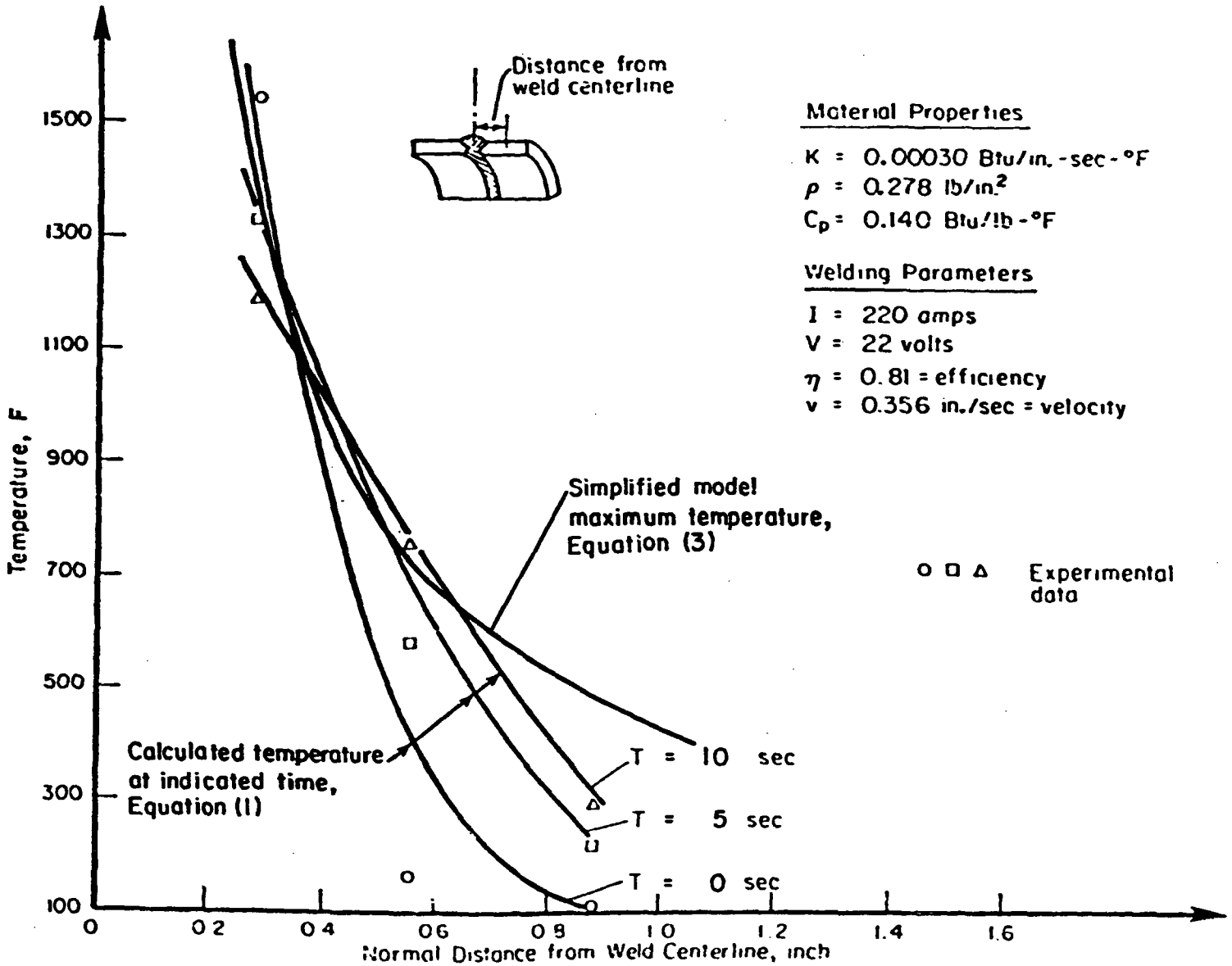

FIGURE 69. CALCULATED TEMPERATURE CURVES AND EXPERIMENTAL DATA POINTS FOR PASS 2 OF BCL MODEL 2 EXPERIMENT

multipass welds; in particular, the use of a more sophisticated temperature evaluation which would account for temperature at the end of successive passes. In addition to the aspects considered in Reference [45], it would appear necessary to consider the pipe as joined by the existing passes at the end of each pass, and the annealing effects of each pass on the preceding passes. This will make the "simplified model" more complex but it still would probably be a very economical tool for parametric studies, as compared to the elastic-plastic, finite element model.

At the present time, extension of the simplified model to represent multipass welds has not been done.

As a kind of "ball-park" comparison, the simplified model has been used to calculate the residual stresses in two-pass girth-butt weld denoted by BCL Model Number 2. The simplified model was based on the following:

(1) Because the second pass is considerably more massive than the root pass, it was assumed that the second pass "anneals-out" the residual stresses due to the first pass.

(2) The work-hardened yield strength of the pipe material is 60,000 psi. This is consistent with the work-hardening aspects encountered in the elastic-plastic finite element analysis where stresses above 60,000 psi were calculated.

(3) The welding parameters (amps, volts, efficiency, and velocity) shown in Figure 69 were used. Also, the thermal conductivity, density and specific heat shown in Figure 69 were used; these are properties of austenitic-stainless steel at 1300 F. The simplified model also uses the modulus of elasticity and coefficient of thermal expansion; these (at 1300 F) are 20.1×10^{6} psi and 12.04×10^{-5}/F, respectively.

Comparison of calculated and measured axial residual stresses are shown in Figure 70. Other than directly at the weld, the agreement between the "ball-park" calculated and measured stresses is encouraging, but needs improvement. It is noted that the axial force is zero, hence, by shell theory, we obtain only linear thru-the-wall bending stresses; the surface stresses must be equal and opposite in sign. It is also noted that the test data does not show this balance, hence there must be either nonlinear variations in stress thru-the-wall or variations in stress around the circumference, or both.

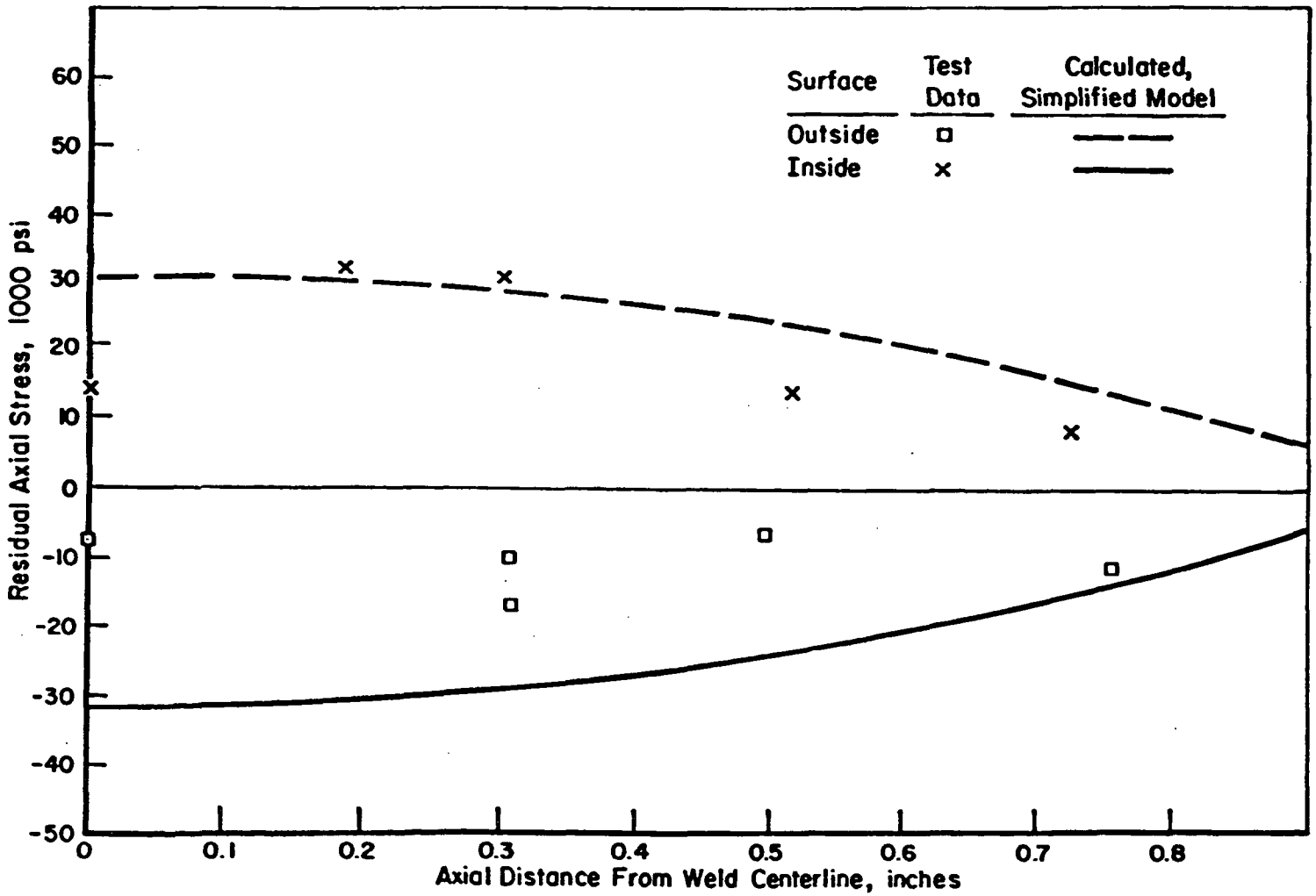

FIGURE 70: COMPARISON OF AXIAL RESIDUAL STRESSES

Comparisons of calculated and measured hoop residual stresses are shown in Figure 71. Again, other than directly at the weld, the agreement is encouraging, but needs improvement.

The measured radial displacement of the pipe surface of BCL Model Number 2 is shown in Figure 72. This consists of an averaging of the data shown in Figure 15 with smoothing out of the "bump" due to the weld reinforcement. The radial weld shrinkage is a significant aspect of girth-butt welds in thin-wall stainless steel pipes. It commonly occurs and has been a source of concern in the Rancho Seco nuclear power plant piping and in piping for the FFTF. The significance and concern arises because this geometrical shape can lead to substantial increases in stress, as compared to welds without the shrinkage, for both pressure loading and bending moment loading. The radial weld shrinkage of BCL Model Number 2 is about 25 percent of the thickness. This is a relatively small shrinkage (shrinkage of up to 100 percent of the wall thickness have been encountered in the field) but even with this small shrinkage, according to Reference [46], the axial stress is increased by 18 percent for pressure loading and by 72 percent for moment loading. Accordingly, a significant aspect of the study of residual stresses in girth-butt welds should include the geometrical effect. Indeed, in the absence of stress corrosion, the geometrical effect is more significant than the residual stresses as such.

Figure 72 also shows radial displacements calculated using the simplified model. For displacements, however, the first pass cannot be ignored because while the second pass may "anneal-out" the residual stresses, the displacements of the first pass will remain, or even increase slightly, due to the second pass. Accordingly, for a "ball-park" estimate, the calculated displacement due to the first pass have been added to those due to the second pass. As can be seen in Figure 72, except at the weld, the agreement is quite good.

A computer program called WELDS has been written to implement the simplified model. A listing of the program is shown in Appendix A. A series of comment cards at the start of the listing gives input instructions and describes the output. The input data consists of title card and cards containing welding parameters, material properties, and pipe radius and wall thickness; a total of 12 numbers. Options are provided for using either the "small plastic zone" or "large plastic zone" method. Options are also provided for the number and spacing of axial locations at which results (radial displacement, stresses, temperature) are printed out. The computer running time (CDC-6400 computer) for print out of 20 locations, is a fraction of a second for the "small plastic zone" method and about 2 seconds for the "large plastic zone" method.

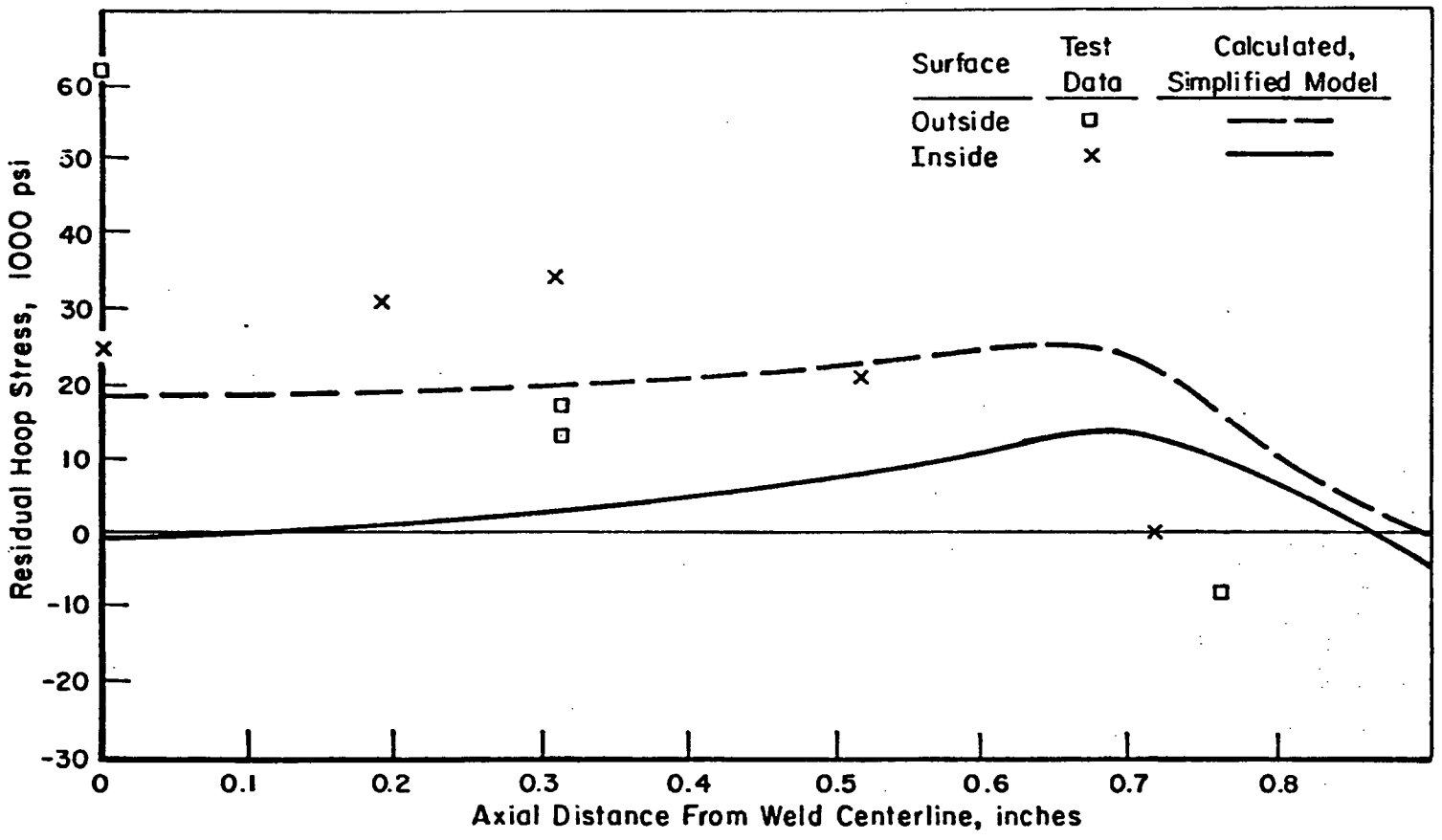

FIGURE 71. COMPARISON OF HOOP RESIDUAL STRESSES

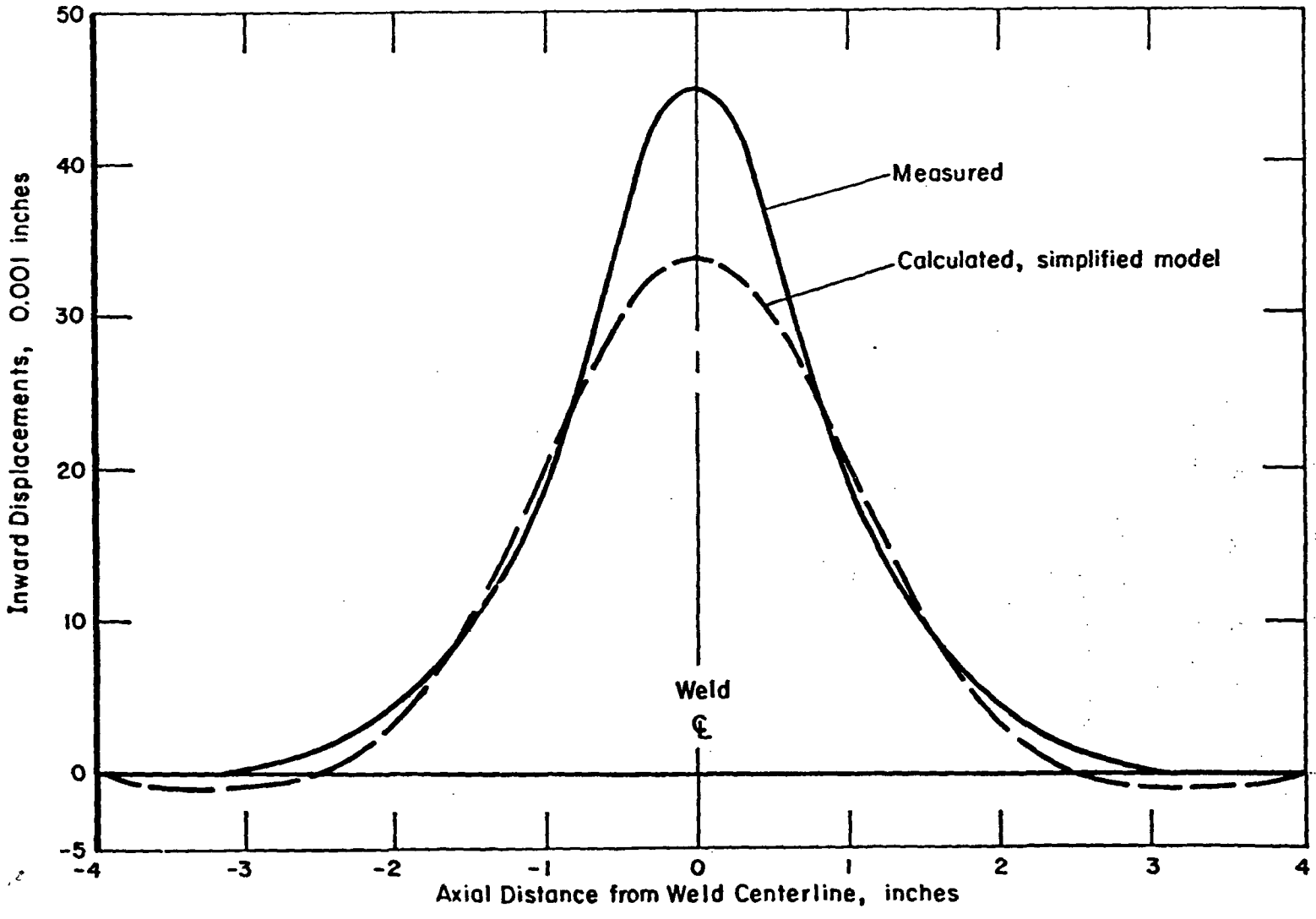

FIGURE 72. COMPARISON OF MEASURED AND CALCULATED RADIAL DISPLACEMENTS

VII. SUMMARY

A research program directed at developing a model or models to predict residual stress distributions due to girth-butt welds in pressure vessels and pipes has been described. The program consisted of three tasks. In Task 1, a critical review of the literature was conducted to obtain relevant information for developing and verifying the residual stress models. The review provided information that was utilized in developing the temperature model and residual stress model. In addition, data on two girth-butt welded pipes was obtained from the literature to provide test cases for the residual models.

The purpose of Task 2 was to provide specific experimental data for the purpose of checking the model capabilities and identifying characteristics of residual stress distributions in girth-butt welds. Two pipes were welded; a two-pass weld and a six-pass weld. Temperature data were taken during the welding procedure for both pipes. Strain measurements were taken during welding on the two-pass weld. Postweld measurements were made to obtain residual stresses and residual deflections of the pipe. Residual stress data were obtained by placing postweld strain gages on the pipe in the vicinity of and on the weld. These gages were removed by a trepanning technique and residual stresses were inferred from the change in strain gage readings. The temperature data during welding, the residual stress data and the residual deformation data were used to test the capabilities of the model.

In Task 3, residual stress models were developed. Because of the thermal nature of the residual stress problem, two models were needed. One was a temperature model to predict the temperature distribution. The other was a stress and deformation analysis model that utilizes the temperatures as input information. The temperature analysis model was developed based on a moving point heat source. It includes parameters of the weld process such as heat input, torch speed, weld pass, location of pipe thickness, and pipe material properties. Good comparisons between results of the model and experimental data for each pass of two-pass and six-pass girth-butt weld were obtained.

The residual stress and deformation model was based on a finite element analysis. The model includes elastic-plastic temperature dependent material behavior for the weld and the pipe, elastic unloading from an elastic-plastic stress state, the effect of geometry changes due to welded distortions,

the number and size of weld passes and the parameters included in the temperature analysis. Good comparisons between experimentally obtained residual stress data and computed values from the finite element model were obtained for the two pipes welded during the program and for two pipes reported in the literature. The number of weld passes in these pipes ranged from two to thirty. A comparison of residual stress data and preliminary results obtained for a weld repair of the HSST-Intermediate Pressure Vessel (ITV-8) indicate that the model can, with modifications, be applied to studying weld repairs.

The feasibility of developing a simplified model was considered and results demonstrated the practicality of doing this. Good comparisons between residual stress data and numerical results of the model were obtained for one- and two-pass girth-butt welds.

All models, except for the weld repair model, were developed for axisymmetric representations. Some discussion of this aspect of the model is in order. Residual stress data taken in the circumferential direction of girth-butt welded pipes have been known to display considerable variations. However, these variations do not seem to follow a consistent pattern. The contention here is that the observed circumferential variation in residual stress is explainable in terms of the bell shaped axial distribution of residual stress. In particular, variations in torch speed, heat input and location of weld pass will change the size and location of the bell shaped distribution. This coupled with the steep gradients found on the bell shaped curves lead to one possible explanation for the circumferential variations in stresses. That is, moving the bell shaped distribution of residual stress just a little to the right or left, (as could easily happen in welding around the pipe circumference) causes noticeable variations in the circumferential distribution of residual stresses. This would lead to circumferential variations in residual stresses, but the axial distributions would still have similar shapes. Thus, it appears that axial distributions of residual stresses are more revealing than circumferential distributions. Therefore, an axisymmetric model can be an important tool for obtaining an understanding of residual stresses at girth-butt welds in pressure vessels and pipes.

REFERENCES

[1] P.S. Myers, D. A. Uyehara, and G. L. Borman, "Fundamentals of Heat Flow in Welding", Welding Research Council Bulletin No. 123, July, 1967.

[2] K. Masubuchi, "Control if Distortion and Shrinkage in Welding", Welding Research Council Bulletin No. 149, April, 1970.

[3] D. Rosenthal, "Mathematical Theory of Heat Distribution During Welding and Cutting", Welding Journal Research Supplement, May, 1941, pp. 220-234.

[4] C.M. Adams, "Cooling Rates and Peak Temperatures in Fusion Welding", Welding Journal Research Supplement, May, 1958, pp. 210-215.

[5] P. Jhaveri, W. G. Moffatt, C. M. Adams, "The Effect of Plate Thickness and Radiation on Heat Flow in Welding and Cutting", Welding Journal Research Supplement, January, 1962, pp. 12-16.

[6] Z. Paley, L. Lynch, C. Adams, "Heat Flow in Welding Heavy Steel Plate", Welding Journal Research Supplement, February, 1964, pp. 71-79.

[7] Z. Paley, and P. Hibbert, "Computation of Temperatures in Actual Weld Designs", Welding Journal Research Supplement, November, 1975, pp. 385-392.

[8] D. Rabkin, "Temperature Distribution through the Weld Pool in the Automatic Welding of Aluminum", British Welding Journal, March, 1959.

[9] V. Makhenko, "Calculation of the Thermal Processes When Depositing Metal on Hollow Cylinders Cooled from Within", Automatic Welding, March, 1963, pp. 23-28.

[10] N. Christensen, L. Davies, K. Gjermundsen, "Distributions of Temperatures in Arc Welding", British Welding Journal, February, 1965, pp. 54-75.

[11] V. Pavelic, "Experimental and Computed Temperature Histories in Gas Tungsten-Arc Welding of Thin Plates", Welding Journal Research Supplement, July, 1969, pp. 295-305.

[12] P. Boughton, "An Analysis of the Thermal Situation in Welding Using An Electrical Analogue", Welding Research International, Vol. 3, No. 4, 1973.

[13] L. Tall, "Residual Stresses in Welded Plates - A Theoretical Study", Welding Journal Research Supplement, January, 1964, pp. 10-23.

[14] D. E. Rodgers, and P. R. Fletcher, "The Determination of Internal Stresses From the Temperature History of a Butt-Welded Pipe", Welding Journal Research Supplement, 1938, pp. 4-7.

[15] K. Masubuchi, F. B. Simmons, and R. E. Monroe, "Analysis of Thermal Stresses and Metal Movement During Welding", Battelle Memorial Institute, RSIC-820, Redstone Scientific Information Center, NAGA-TM-X-61300, N68-37857, July, 1968.

[16] K. Gatovskii, "Determination of Welding Stresses and Strains with Allowance for Structural Transformations of the Metal", Svar. Proiz., No. 11, 1923, pp. 3-6.

[17] V. Makhmenko, V. Shekera, and L. Izbenko, "Special Features of the Distribution of Stresses and Strains Caused by Making Circumferential Welds in Cylindrical Shells", Avt. Svarka., No. 12, 1970, pp. 43-47.

[18] K. Hueber, THE FINITE ELEMENT METHOD FOR ENGINEERS, John Wiley - Interscience, New York, 1975.

[19] P. Marcal, "A Stiffness Method for Elastic-Plastic Shells of Revolution", J. Strain Analysis, 1966, No. 1, p 339.

[20] H. Armen, H. Levine, A. Pilsko, "Plasticity - Theory and Finite Element Applications", Advances in Computational Methods in Structural Mechanics and Design, J. Oden, Editor, University of Alabama, 1972.

[21] Y. Veda, T. Yamakawa, "Thermal Nonlinear Behavior of Structures", Advances in Computational Methods in Structural Mechanics and Design, J. Oden, Editor, U. of Alabama, 1972.

[22] E. Wilson, R. Nickell, "Application of the Finite Element Analysis to Heat Conduction Problems", Nuclear Engineering and Design, No. 4, 1966, pp. 276-286.

[23] V. Sagalevich, and S. Mezentseva, "Calculation of Strains and Stresses in Circular Welds", Svar. Proiz, No. 9, 1974, pp. 7-10.

[24] R. Kamichika, T. Yada, and A. Okamoto, "Internal Stresses in Thick Plates Weld-Overlaid with Austenitic Stainless Steel (Report 2)", Transactions of the Japan Welding Society, Vol. 5, No. 1, April, 1974.

[25] H. Hibbitt, and P. Marcal, "A Numerical Thermo-Mechanical Model for the Welding and Subsequent Loading of a Fabricated Structure", Contract No. N00014-67-A-D191-0006, Brown University, 1972.

[26] R. Nickell, H. Hibbitt, "Thermal and Mechanical Analysis of Welded Structures", Nuclear Engineering and Design, No. 32, 1975, pp. 110-120.

[27] E. Friedman, "Thermomechanical Analysis of the Welding Process Using the Finite Element Method", Journal of Pressure Vessel Technology, August, 1975, pp. 206-213.

[28] S. Vaidyanathan, A. F. Todar, and I. Finne, "Residual Stresses Due to Circumferential Welds", Trans. ASME, Journal of Engineering Materials and Technology, October, 1973, pp. 233-237.

[29] Y. Iwamura, and E. F. Rybicki, "A Transient Elastic-Plastic Thermal Stress Analysis of Flame Forming", ASME Trans. Journal of Engineering for Industry, February, 1973.

[30] N. D. Ghadiali, and E. F. Rybicki, "An Analytical Technique for Evaluating Deformations Due to Welding", Abstract of Paper, Battelle's Columbus Laboratories, August, 1974.

[31] Proceedings of a Workshop on Nondestructive Evaluation of Residual Stress, San Antonio, Texas, August 13-14, 1975.

[32] G. Sachs, "The Determination of Residual Stresses in Rods and Tubes", Zeit. Metallkunde, Vol 19, (1927), p. 352.

[33] H. Buehler, "The Complete Determination of Residual Stresses in Metal Tubes and Rods", Zeit. Metallkunde, Vol. 43 (1952), p. 388.

[34] V. Weiss, "Residual Stresses in Cylinders", S.E.S.A. Proceedings, Vol. 15, No. 2, 1957.

[35] A. Cepolina, and A. Cunonico, "The Measurement of Residual Stress", Welding Journal Research Supplement, March, 1971, pp. 22-30.

[36] N. Nagaraja, and L. Tall, "Residual Stresses in Welded Plates", Welding Journal Research Supplement, October, 1961, pp. 468-480.

[37] N. Prokhorov, "The Dependence of Longitudinal Residual Stress in Butt Welds in Hardenable Steels on Their Initial Structure", Svar. Proiz., No. 3, 1975, pp. 5-6.

[38] T. Muraki, J. Bryan, and K. Masubuchi, "Analysis of Thermal Stresses and Metal Movement During Welding", Journal of Engineering Material and Technology, January, 1975, pp. 81-91.

[39] K. Spiller, "Positional Tig Welding of Aluminum Pipe", Welding and Metal Fabrication, December, 1975, pp. 733-746.

[40] F. Vagner, "Distribution of Residual Stresses and Structural Constituents in Welding with a Pulsating Arc", Svar. Proiz., No. 4, 1975.

[41] H. Klepzer, Et Al., "Investigation of Cause of Cracking in Austenitic Stainless Steel Piping", General Electric Report No. NEDO-21000-1, July, 1975.

[42] C. F. Cheng, W. L. Ellingson, D. S. Kupperman, J. Y. Park, R. B. Poeppel, and K. J. Reiman, "Corrosion Studies of Nuclear Piping in BWR Environments", Quarterly Report, Argonne National Laboratories, June, 1976.

[43] Studies on AISI Types -304, -304L, and -347 Stainless Steels for BWR Applications, NEDO-20985-1, September, 1975.

[44] F. M. Burdekin, "Local Stress Relief of Circumferential Butt Welds in Cylinders", British Welding Journal, 10 (9) 483-490 (1963).

[45] S. Vaidyanathan, H. Weiss, and I. Finnic, "A Further Study of Residual Stresses in Circumferential Welds", Trans. ASME, Journal of Engineering Materials and Technology, October, 1973, 238-242.

[46] E. C. Rodabaugh, and S. E. Moore, "Stress Indices for Girth-Welded Pipe Joints, Including Radial Weld Shrinkage, Mismatch and Tapered-Wall Transitions", Oak Ridge National Laboratory TM-3643, To be published.

APPENDIX A

COMPUTER PROGRAM FOR SIMPLIFIED MODEL

```
      PROGRAM WELDS (INPUT,OUTPUT,TAPE60=INPUT)
C  REVISED 6/3/77
C  RESIDUAL STRESSES IN GIRTH BUTT WELDS IN PIPE
C  Q = HEAT INPUT, BTU / HOUR=(FT OF WALL THICKNESS)
C  Q = 3.4124*VOLTS*AMPS*WELD-EFF.*12/(WALL THICK. IN INCHES)
C  V = WELDING SPEED, FT / HR
C  XK = THERMAL CONDUCTIVITY, BTU / FT-HR-DEG F
C  DEN = DENSITY OF PIPE MATERIAL, LB / CUBIC FT
C  SH = SPECIFIC HEAT , BTU / LB-DEG F
C  SY = MATERIAL YIELD STRENGTH, PSI
C  E = MODULUS OF ELASTICITY, PSI
C  AL = COEFFICIENT OF THERMAL EXPANSION, PER DEG F
C  TBAR = EQUILIBRIUM TEMPERATURE, DEG F
C     ESTIMATE OF TBAR     TBAR = Q/(2.*V*SH*W*DEN), WHERE W = TOTAL AXIAL
C        LENGTH OF WELDED PIPE ASSEMBLY
C  PR = POISSONS RATIO
C  R = PIPE RADIUS, INCH
C  TH = PIPE WALL THICKNESS, INCH
C  X = AXIAL DISTANCE FROM WELD CENTER, INCH (OUTPUT)
C  INK GIVES LENGTH OF STEP, = .02* INK , X STEPS IN INCHES
C  IOPT = 1, SHORT METHOD, IOPT=2, INCLUDES Y3, SA83, IOPT=4, DOES NOT INCLUDE
C  Y3 AND SA83
C  IS = NUMBER OF STEPS OF .02*INK*(IS-1)
C  OUTPUT CONSISTS OF RADIAL DISPLACEMENT (Y), INCH, STRESSES (PSI), AND
C     TEMPERATURE, DEG F, AT X LOCATION SHOWN IN FIRST COLUMN OF PRINTOUT
C  SHM = PORTION OF MEMBRANE HOOP STRESS DUE TO PIPE RESPONSE
C  SAM = AXIAL MEMBRANE STRESS, AXIAL MEMBRANE STRESS = C.G. AXIAL SURFACE
C     STRESSES ARE +SAM, INSIDE, -SAB, OUTSIDE
C  SHMI = MEMBRANE HOOP STRESS
C  SHO = HOOP STRESS ON OUTSIDE SURFACE
C  SHI = HOOP STRESS ON INSIDE SURFACE
C  SHP = PORTION OF HOOP STRESS DUE TO PLATE LOADING, SHMT=SHM+SHP
      COMMON C, XK, V, DUE, R, TBAR, IAU, BETA, IG, IT
      YFUN(F1,F2,F3,F4,F5) = F1*R/(2.*E)* (F2-EXP(-BETA*F3)*COS(BETA*F3)
     1  + F4*EXP(-BETA*F5)*COS(BETA*F5) )
      SFUN(F1,F2,F3,F4,F5) = (TH*BETA**2*R*F1  / (2.*(1.-PR*PR))) *
     1  (F2-.F(-BETA*F3)*SIN(BETA*F3) + F4*EXP(-BETA*F5)*SIN(BETA*F5) )
      PRINT 99
   99 FORMAT (1H1)
    5 READ 7
    7 FORMAT (1CH
     1
     IF(LOF(5) ) 1,2
    2 CONTINUE
      PRINT 7
      PRINT 71
   71 FORMAT (1H0)
      READ  1, Q, V, XK, DEN, SH, SY, E, AL, TBAR, PR, R, TH, INK,IOPT
     1 ,IS
    1 FORMAT (6E12.5/4E10.5,3I5)
      PRINT 19
   19 FORMAT (98H        Q            V            XK          DEN          S
     1H          SY           E            AL          )
      PRINT 4, Q, V, XK, DEN, SH, SY, E, AL
    4 FORMAT (1PE12.3/)
      PRINT 17
```

```
   17 FORMAT (80H    TBAR          PR          R          TH
     1INK      IOPT        IS     )
      PRINT 15, TBAR, PR, R, TH, INK, IOPT, IS
   15 FORMAT (1P4E12.3,3I10///)
      TAU = SY/(E*AL)
      DUF = XK/(DEN*SH)
C  XY, XX, AND XLO ARE CRITICAL LENGTHS IN INCHES
      XY = (Q/(2.*TAU + TBAR) - 1.6*XK) /(.66667*XK*V / (2.*DUF) )
      XX = (Q/TAU - 1.6*XK) /(.66667*XK*V / (2.*DUF) )
      XLO = XY + (XX-XY)/4.
      BETA = (3.*(1. - PR*PR) ) **.25 / SQRT(R*TH)
C     PRINT 9
    9 FORMAT (80H    TAU          DUF          XY          XX          XLO
     1          BETA                    ) )
C     PRINT 6, TAU, DUF, XY, XX, XLO, BETA
    6 FORMAT (1P6E12.3///)
      PRINT 8
    8 FORMAT (118H      X          Y          SHM          SAB          SHM
     1T,          SHO          SHI          SHP          TEMP          )
      DO 3 I=1,IS
      X = (I-1) * .02 * INK
      T = Q / (8.*XK* (.2+.04167*V*X/DUF ) )
      IF (IOPT) 30,30,31
   30 BX = BETA * X
      EX = EXP(-BX)
      CX = COS(BX)
      SX = SIN(BX)
      Y = (BETA*R*SY*XLO / E) *EX * (CX+SX)
      SA1 = (TH*BETA**3*R*SY*XLO / (1.-PR*PR) ) *EX*(CX-SX)
      GO TO 32
   31 CONTINUE
      IF(X.LE.XY) 40,41
   41 Y1 = YFUN(SY, 2., XY+X, -1., XY-X)
      SA31 = SFUN(SY, 1., XY+X, 1., XY-X)
      GO TO 42
   40 Y1 = YFUN(SY,1., XY+X, 1., X-XY)
      SA31 = SFUN(SY, 1., XY+X,-1., X-XY)
   42 CONTINUE
      IF (X.LE.XY) 60,61
   60 IT=IG=1                                                    *
      CALL GAUSS(1,1.5,1.,.01,0., XY-X, XX-X, GINT,ICALC,TEMP1,FU )
      GINT1 = GINT
      IT = 2
      CALL GAUSS(1,1.5,1.,.01,0., XY+X, XX+X, GINT,ICALC,TEMP1,FU )
      Y2 = SY*BETA*R/(2.*E) * (GINT1 + GINT)
      Y = Y1 + Y2
      IT = 1
      IG = 2
      CALL GAUSS(1,1.5,1.,.01,0., XY-X, XX-X, GINT,ICALC,TEMP1,FU )
      GINT1 = GINT
      IT = 2
      CALL GAUSS(1,1.5,1.,.01,0., XY+X, XX+X, GINT,ICALC,TEMP1,FU )
      SA32= (TH*E*TA**3*R*SY/(2.*(1.-PR*PR))) * (GINT1 + GINT)
      SAB = SAB1 + SAB2
      GO TO 62
   61 IF(X.LE.XX) 63,64
```

* GAUSS is a numerical integration subroutine, incorporated in Battelle's computer library. It, in turn, uses the subroutine FEVAL shown on Page A-4. An equivalent numerical integration subroutine, from the user's library, should be substituted.

```
   63 IT=IG=1
      CALL GAUSS(1,1.5,1.,.1,0.,  0. , XX-X, GINT,ICALC,TEMP1,FU )
      GINT1 = GINT
      IT = 3
      CALL GAUSS(1,1.5,1.,.1,0.,  0. , X-XY, GINT,ICALC,TEMP1,FU )
      GINT2 = GINT
      IT = 2
      CALL GAUSS(1,1.5,1.,.1,0., XY+X, XX+X, GINT,ICALC,TEMP1,FU )
      Y2 = SY*BETA*R/(2.*E) * (GINT1 + GINT2 + GINT)
      Y = Y1 + Y2
      IT = 1
      IG = 2
      CALL GAUSS(1,1.5,1.,.1,0.,  0. , XX-X, GINT,ICALC,TEMP1,FU )
      GINT1 = GINT
      IT = 3
      CALL GAUSS(1,1.5,1.,.01,0.,  0. , X-XY, GINT,ICALC,TEMP1,FU )
      GINT2 = GINT
      IT = 2
      CALL GAUSS(1,1.5,1.,.01,0., XY+X, XX+X, GINT,ICALC,TEMP1,FU )
      SAB2= (TH*BETA**3*R*SY/(2.*(1.-PR*PR))) * (GINT1 + GINT2 + GINT)
      SAB = SAB1 + SAB2
      GO TO 62
   64 IT = 3
      IG = 1
      CALL GAUSS(1,1.5,1.,.1,0., X-XX,X-XY , GINT,ICALC,TEMP1,FU )
      GINT1 = GINT
      IT = 2
      CALL GAUSS(1,1.5,1.,.1,0., X+XY,X+XX , GINT,ICALC,TEMP1,FU )
      Y2 = SY*BETA*R/(2.*E) * (GINT1 + GINT)
      Y = Y1 + Y2
      IT = 3
      IG = 2
      CALL GAUSS(1,1.5,1.,.01,0., X-XX,X-XY , GINT,ICALC,TEMP1,FU )
      GINT1 = GINT
      IT = 2
      CALL GAUSS(1,1.5,1.,.01,0., X+XY,X+XX , GINT,ICALC,TEMP1,FU )
      SAB2= (TH*BETA**3*R*SY/(2.*(1.-PR*PR))) * (GINT1 + GINT)
      SAB = SAB1 + SAB2
   62 CONTINUE
      IF(ICPT-3) 53,53,54
   53 CONTINUE
      IF(X.LE.XX) 50,51
   50 SYS = -SY*TBAR/TAU
      Y3 = YFUN(SYS,0., 8.*XX-X,  1., XX-X)
      SAB3 = SFUN(SYS,-1., 8.*XX-X, 1., XX-X)
      GO TO 52
   51 SYS = -SY*TBAR/TAU
      Y3 = YFUN(SYS, 2., 8.*XX-X, -1., X-XX)
      SAB3 = SFUN(SYS, -1., 8.*XX-X, -1., X-XX)
   52 Y = Y + Y3
      SAB = SAB + SAB3
   54 CONTINUE
   32 CONTINUE
      SHM = -E*Y/R
      IF(X.LE.XX) 10,11
   10 SHP = SY
```

```
      SHMT = SY + SHM
      GO TO 14
   11 IF (X.LE.XK) 12,13
   12 SHP = SY * (T - TBAR - TAU) / TAU
      SHMT = SHP + SHM
      GO TO 14
   13 SHP = -SY * TBAR / TAU
      SHMT = SHP + SHM
   14 SHO = SHMT - PR * SAB
      SHI = SHMT + PR * SAB
      PRINT 20, X, Y, SHM, SAB, SHMT, SHO, SHI, SHP,T
   20 FORMAT (1P 9L12.3/)
    3 CONTINUE
      PRINT 99
      GO TO 5
  100 CALL EXIT
      END
      SUBROUTINE FEVAL (U, FU, JF, ICALC)*
      COMMON Q, XK, V, DUF, X, TBAR, TAU, BETA, IG, IT
      GO TO (1,2,3) IT
    1 T = Q / (8.*XK*(.2+.04167*V/DUF   * (U+X) ) )
      GO TO 4
    2 T = Q / (8.*XK*(.2+.04167*V/DUF   * (U-X) ) )
      GO TO 4
    3 T = Q / (8.*XK*(.2+.04167*V/DUF   * (X-U) ) )
    4 GO TO (5,6) IG
    5 FU = (T-TBAR-TAU)/TAU * EXP(-BETA*U) * (COS(BETA*U) + SIN(BETA*U))
      GO TO 7
    6 FU = (T-TBAR-TAU)/TAU * EXP(-BETA*U) * (COS(BETA*U) - SIN(BETA*U))
    7 RETURN
      END
```

* See footnote on p A 2.

NRC FORM 335 (7-77) U.S. NUCLEAR REGULATORY COMMISSION

BIBLIOGRAPHIC DATA SHEET

1. REPORT NUMBER (Assigned by DDC): NUREG-0376

4. TITLE AND SUBTITLE (Add Volume No., if appropriate): Residual Stresses at Girth-Butt Welds in Pipes and Pressure Vessels

2. (Leave blank)

3. RECIPIENT'S ACCESSION NO.: PB-273947

7. AUTHOR(S): E. F. Rybicki and others

5. DATE REPORT COMPLETED: MONTH August, YEAR 1977

9. PERFORMING ORGANIZATION NAME AND MAILING ADDRESS (Include Zip Code):
Battelle Columbus Laboratories
505 King Avenue
Columbus, OH 43201

DATE REPORT ISSUED: MONTH November, YEAR 1977

6. (Leave blank)

8. (Leave blank)

12. SPONSORING ORGANIZATION NAME AND MAILING ADDRESS (Include Zip Code):
Office of Nuclear Regulatory Research
Division of Nuclear Safety Research
U.S. Nuclear Regulatory Commission
Washington, D.C. 20555

10. PROJECT/TASK/WORK UNIT NO.

11. CONTRACT NO.: AT(49-24)-0293

13. TYPE OF REPORT: Technical Report

PERIOD COVERED (Inclusive dates):

15. SUPPLEMENTARY NOTES

14. (Leave blank)

16. ABSTRACT (200 words or less)

The objective of this research program is to develop mathematical models for calculating the magnitude, direction, and distribution of residual stresses at girth-butt welds. Models developed are to include parameters of the welding process and are to be evaluated by comparing experimental data with numerical computations obtained using the models. Only axisymmetric models are to be considered in this study.

A residual stress model for girth-butt welds in pressure vessels and pipes was developed and verified for welds ranging from 2 to 30 passes. The model also accurately predicts residual deformations. Results indicate that the model can be extended to represent weld repairs in pressure vessels. In addition, preliminary results directed at developing a simplified model of girth-butt welds show good agreement with data for one and two-pass welds.

17. KEY WORDS AND DOCUMENT ANALYSIS

17a. DESCRIPTORS

17b. IDENTIFIERS/OPEN-ENDED TERMS

18. AVAILABILITY STATEMENT: Unlimited availability.

19. SECURITY CLASS (This report)

20. SECURITY CLASS (This page)

21. NO. OF PAGES: 154

22. PRICE: PC A08 A01

NRC FORM 335 (7-77)